

THE ELECTRICAL CHARACTERISTICS OF ANTENNAS IN THEIR  
OPERATIONAL ENVIRONMENT

A THESIS SUBMITTED TO  
THE GRADUATE SCHOOL OF NATURAL AND APPLIED SCIENCES  
OF  
MIDDLE EAST TECHNICAL UNIVERSITY

BY

GÖNENÇ AFACAN

IN PARTIAL FULFILLMENT OF THE REQUIREMENTS  
FOR  
THE DEGREE OF MASTER OF SCIENCE  
IN  
ELECTRICAL AND ELECTRONICS ENGINEERING

DECEMBER 2007

Approval of the thesis:

**THE ELECTRICAL CHARACTERISTICS OF ANTENNAS IN THEIR  
OPERATIONAL ENVIRONMENT**

submitted by **GÖNENÇ AFACAN** in partial fulfillment of the requirements for  
the degree of **Master of Science in Electrical and Electronics Engineering  
Department, Middle East Technical University** by,

Prof. Dr. Canan Özgen  
Dean, Graduate School of **Natural and Applied Sciences**

\_\_\_\_\_

Prof. Dr. İsmet Erkmn  
Head of Department, **Electrical and Electronics Engineering**

\_\_\_\_\_

Prof. Dr. Tuncay Birand  
Supervisor, **Electrical and Electronics Dept., METU**

\_\_\_\_\_

**Examining Committee Members:**

Prof. Dr. Gülbin Dural  
Electrical and Electronics Engineering Dept., METU

\_\_\_\_\_

Prof. Dr. Tuncay Birand  
Electrical and Electronics Engineering Dept., METU

\_\_\_\_\_

Assoc. Prof. Dr. Sencer Koç  
Electrical and Electronics Engineering Dept., METU

\_\_\_\_\_

Assoc. Prof. Dr. Özlem Aydın Çivi  
Electrical and Electronics Engineering Dept., METU

\_\_\_\_\_

M.Sc. Şakir KARAN  
ASELSAN AŞ

\_\_\_\_\_

**Date:** 06/12/2007

**I hereby declare that all information in this document has been obtained and presented in accordance with academic rules and ethical conduct. I also declare that, as required by these rules and conduct, I have fully cited and referenced all material and results that are not original to this work.**

Gönenç Afacan

## **ABSTRACT**

# **THE ELECTRICAL CHARACTERISTICS OF ANTENNAS IN THEIR OPERATIONAL ENVIRONMENT**

Afacan, Gönenc

M.Sc., Department of Electrical and Electronics Engineering

Supervisor: Prof. Dr. Tuncay Birand

December 2007, 119 pages

This thesis investigates the variations of electrical properties of linear antennas mounted on certain platforms, depending on the physical properties of that platform. In this respect, related basic antenna simulations, electromagnetic simulations from primitive to complex models of airframes, and scale model measurements were used.

Firstly, electrical properties of monopoles at known environment were examined and basic analyses were performed via an electromagnetic simulation tool, named CST Microwave Studio<sup>®</sup>. In addition, important aspects of simulation tool were investigated.

Then, an F-4 aircraft model was used to observe the electrical characteristics of antennas mounted on it. Using 3D model of F-4 aircraft, realistic antenna placement points were assigned and monopoles were attached to those points.

Alternatively, a simplified F-4 model was also used and for two different models, identical simulations were done, followed by accuracy and performance analysis between the results obtained from simplified and exact models. As the outcome of these simulations, certain parameters like impedance, antenna-to-antenna coupling and radiation pattern values were examined. Additionally, change in antennas' electrical characteristics due to their position over the airframe was investigated.

In addition, a 1:10 down-scaled and copper-plated F-4 aircraft model was obtained and equipped with identical antennas. By using the measurements done on this scale model, antenna-to-antenna coupling results of MWS<sup>®</sup> were verified by measurements. Finally, advantages and disadvantages of using electromagnetic simulation tools and scale model measurements for such antenna studies were discussed.

Keywords: Finite Integration Technique (FIT), scale model measurements, antenna-to-antenna coupling.

# ÖZ

## ANTENLERİN ÇALIŞMA ORTAMLARINDAKİ ELEKTRİKİ ÖZELLİKLERİ

Afacan, Gönenç

Yüksek Lisans, Elektrik ve Elektronik Mühendisliği Bölümü

Tez Yöneticisi: Prof. Dr. Tuncay Birand

Aralık 2007, 119 sayfa

Bu tezde, belli platformlar üzerine yerleştirilen doğrusal antenlerin, yerleştirildikleri platformun yapısına bağlı olarak, elektriksel özelliklerinin değişimi incelenmiştir. Bu hususta, belirli temel anten simülasyonları, basitten karmaşığa doğru modellenen hava araçları ile yapılan simülasyonlar ve ölçekli model ölçümleri kullanılmıştır.

İlk olarak, bilinen ortamlarda yer alan monopol antenlerin elektriksel özellikleri incelenmiş ve CST Microwave Studio® adlı elektromanyetik simülasyon aracı kullanılarak temel analizler gerçekleştirilmiştir. Ayrıca bu simülasyon aracının önemli özellikleri incelenmiştir.

Ardından, üzerine yerleştirilen antenlerin elektriksel özelliklerini incelemek amacıyla bir F-4 uçak modeli kullanılmıştır. 3 boyutlu F-4 modeli üzerinde gerçekçi anten yerleşimi noktaları belirlenmiş ve bu noktalarda monopol antenler

modellenmiştir. Buna ek olarak, sadeleştirilmiş bir F-4 modeli de kullanılmış ve her iki model üzerinde eş simülasyonlar yapılmıştır. Bu iki modelden elde edilen sonuçlar karşılaştırılarak, hassasiyet ve performans analizi yapılmıştır.

Bunlara ek olarak, 1:10 oranında ölçeklendirilmiş ve bakırla kaplanmış bir F-4 maketi temin edilmiş ve benzer şekilde antenler ile donatılmıştır. Bu ölçekli model üzerinde yapılan ölçümler yardımı ile, Microwave Studio® ile yapılan simülasyonlarda elde edilen antenden antene bağlaşım sonuçları doğrulanmıştır.

Sonuç olarak, bu tip anten çalışmalarında elektromanyetik simülasyon araçları ve ölçekli model ölçümlerinin kullanımının avantaj ve dezavantajları tartışılmıştır.

Anahtar kelimeler: Finite integration technique-FIT (sonlu integral tekniği), ölçekli model ölçümleri, antenden antene bağlaşım.

## ACKNOWLEDGEMENTS

I would like to express my gratitude to my supervisor Prof. Dr. Tuncay Birand, for his guidance, support, understanding and tolerance throughout this study.

I wish to thank Prof. Dr. Altuncan Hızal, for his contribution to determining the content of my simulation studies.

I wish to tender my thanks to Dr. Uğur Dalli, the former project manager of F-4 Modernization Program in ASELSAN-MGEO Division; for encouraging me to get involved in such a platform level antenna study and helping me procure the 1:10 scaled F-4 model.

I am also grateful for my directors in ASELSAN-MGEO Division, for allowing me to use all relevant facilities, such as measurement equipment and simulation tool.

I also wish to thank my colleague Mustafa Ural, for helping me with laborious antenna measurements.

Finally, I am indebted to my family and friends, who never let me lose my motivation and energy, regardless of any circumstance.

# TABLE OF CONTENTS

PLAGIARISM .....	iii
ABSTRACT.....	iv
ÖZ.....	vi
ACKNOWLEDGEMENTS .....	viii
TABLE OF CONTENTS.....	ix
LIST OF TABLES.....	xi
LIST OF FIGURES .....	xii
1. INTRODUCTION.....	1
2. A CLOSER LOOK AT ELECTROMAGNETIC SIMULATION TOOLS .....	4
2.1. Introduction .....	4
2.2. Common Numerical Methods.....	5
2.3. CST Microwave Studio - MWS®.....	6
2.3.1. Introduction .....	6
2.3.2. Solvers in MWS® .....	6
2.3.3. Finite Integration Technique – FIT .....	7
2.3.4. Excitation – Port Selection .....	13
2.3.5. Sequence of Actions in a Simulation Run .....	15
2.4. Verification of MWS®.....	16
2.4.1. Defining the Geometry and Port.....	22
2.4.2. Convergence Criteria for Transient Solver.....	35
2.4.3. Local Mesh Settings .....	39
2.4.3.1. Port Length .....	40
2.4.3.2. Local Mesh Refinement Settings.....	41
3. ANTENNA SIMULATIONS ON F-4 AIRCRAFT .....	47

3.1.	<i>Analysis of Dipoles in Free Space</i> .....	47
3.2.	<i>Analysis on Hand-Made F-4 Model</i> .....	49
3.3.	<i>Analysis on Actual F-4 Model</i> .....	50
3.4.	<i>Comparison of Antenna-to-Antenna Coupling</i> .....	51
3.4.1.	Coupling between Existing Antennas and New Antenna at Position #4 .....	51
3.4.2.	Coupling between Existing Antennas and New Antenna at Position #5 .....	53
3.4.3.	Coupling between Existing Antennas and New Antenna at Position #5 .....	55
3.4.4.	Interpretation of Coupling Results .....	57
3.5.	<i>Comparison of Radiation Patterns</i> .....	59
3.5.1.	Comparison of Radiation Pattern Plots for Hand-made & Actual F-4 Model (Existing Antennas).....	61
3.5.2.	Comparison of Radiation Pattern Plots of New Antenna at 3 Different Positions 65	
4.	<b>SCALE MODEL MEASUREMENTS</b> .....	68
4.1.	<i>Reasons for Using Scale Models in Electromagnetics</i> .....	68
4.2.	<i>Rules of Scale Modeling</i> .....	71
4.3.	<i>1:10 Scaled F-4 Aircraft Model</i> .....	73
4.4.	<i>Measurement Environment</i> .....	78
4.5.	<i>Measurement Setup &amp; Procedure</i> .....	80
4.6.	<i>Measurement Results</i> .....	82
4.6.1.	Return Loss Measurements .....	82
4.6.2.	Transmission Loss (Coupling) Measurements .....	86
4.6.2.1.	Antenna #4 vs. Existing Antennas .....	87
4.6.2.2.	Antenna #5 vs. Existing Antennas .....	89
4.6.2.3.	Antenna #9 vs. Existing Antennas .....	91
4.6.3.	Comparison of Antenna-to-Antenna Interactions for Different Positions of “New” Antenna 93	
4.6.4.	Interpretation of Results .....	98
5.	<b>CONCLUSION AND FUTURE WORK</b> .....	101

## LIST OF TABLES

Table 2-1 Input impedance of 0,5" diameter monopole elements on an 8 ft. diameter ground plane (comparison of measurements, MoM & FIT) .....	20
Table 2-2 Comparison of Results obtained from Discrete and Waveguide Port Excitations .....	33
Table 2-3 Effects of Transient Solver Accuracy on Simulation Results.....	39
Table 2-4 Effect of port length on impedance (Discrete port) .....	41
Table 2-5 Effects of Local Mesh Refinement on Impedance & Radiation Pattern	45
Table 3-1 Coupling scenarios between existing and new antennas .....	51
Table 3-2 Comparison of three different simulation models .....	58
Table 3-3 Performance comparison for “actual” and “hand-made” F-4 models ...	59
Table 4-1 Rules of modifying electrical parameters due to scaling factor “n” .....	72
Table 4-2 Main features of measurement equipment [22] .....	82
Table 4-3 List of S-parameters to be measured.....	87
Table 4-4 Comparison of average coupling differences between simulation and measurement results in 2,4-3 GHz band .....	100

## LIST OF FIGURES

Figure 2-1 Illustration of dual mesh grid in MWS <sup>®</sup> .....	8
Figure 2-2 Spatial allocation of a cell and its dual cell .....	9
Figure 2-3 Faraday's Law applied on a unit cell.....	9
Figure 2-4 Illustration of Gauss's Law for magnetism, over a unit cell [3].....	10
Figure 2-5 Discrete divergence matrix for magnetic fluxes.....	11
Figure 2-6 Illustration of leap-frog scheme for FIT.....	12
Figure 2-7 Input resistance vs. ground plane radius (measurement-MoM-FIT)....	21
Figure 2-8 Input reactance vs. ground plane radius (measurement-MoM-FIT) ....	21
Figure 2-9 Planar antenna fed by a discrete port.....	23
Figure 2-10 Planar antenna fed by a waveguide port.....	24
Figure 2-11 Monopole Over Ground Plane of Normalized Radius, $k.a = 4$ .....	25
Figure 2-12 Detailed view of discrete port.....	25
Figure 2-13 A general mesh view (discrete port).....	26
Figure 2-14 Top view of monopole-ground plane junction .....	27
Figure 2-15 Detailed view of coaxial feed section (bottom view).....	28
Figure 2-16 Detailed mesh view of coaxially fed monopole .....	29
Figure 2-17 Return loss of monopole fed by discrete port.....	30
Figure 2-18 Return loss of monopole fed by waveguide port.....	30
Figure 2-19 Directivity ( $\theta, \phi=0^\circ$ ) for discrete port excitation.....	31
Figure 2-20 Directivity ( $\theta, \phi=0^\circ$ ) for waveguide port excitation.....	32
Figure 2-21 Energy vs. time graph for a non-resonating (a) and resonating (b) structures .....	37
Figure 2-22 Effects of solver accuracy on return loss.....	38
Figure 2-23 Effect of mesh density on time step [7].....	42

Figure 2-24 Calculated input impedance for cylindrical center-fed dipoles with length-to-diameter of 60 and 2000 as a function of $l/\lambda$ [15].....	44
Figure 3-1 Two dipoles in free space, with distance “d” in horizontal plane, “h” in echelon .....	48
Figure 3-2 Side view of “hand-made” F-4 model .....	49
Figure 3-3 Side view of “actual” F-4 model .....	50
Figure 3-4 Coupling between antenna #6 and new antenna at position #4.....	52
Figure 3-5 Coupling between antenna #7 and new antenna at position #4.....	52
Figure 3-6 Coupling between antenna #10 and new antenna at position #4.....	53
Figure 3-7 Coupling between antenna #6 and new antenna at position #5.....	54
Figure 3-8 Coupling between antenna #7 and new antenna at position #5.....	54
Figure 3-9 Coupling between antenna #10 and new antenna at position #5.....	55
Figure 3-10 Coupling between antenna #6 and new antenna at position #9.....	56
Figure 3-11 Coupling between antenna #7 and new antenna at position #9.....	56
Figure 3-12 Coupling between antenna #10 and new antenna at position #9.....	57
Figure 3-13 Combination of $\phi=90^\circ$ and $\phi=270^\circ$ planes for elevation plane.....	60
Figure 3-14 Orientation of F-4 aircraft model in cartesian & spherical coordinates .....	61
Figure 3-15 Directivity in azimuth plane - antenna #6 (actual vs. hand-made F-4) .....	62
Figure 3-16 Directivity in elevation plane - antenna #6 (actual vs. hand-made F-4) .....	62
Figure 3-17 Directivity in azimuth plane - antenna #7 (actual vs. hand-made F-4) .....	63
Figure 3-18 Directivity in elevation plane - antenna #7 (actual vs. hand-made F-4) .....	63
Figure 3-19 Directivity in azimuth plane - antenna #10 (actual vs. hand-made F-4) .....	64
Figure 3-20 Directivity in elevation plane - antenna#10 (actual vs. hand-made F-4) .....	64
Figure 3-21 Directivity of new antenna for three positions (azimuth plane).....	66

Figure 3-22 Directivity of new antenna at three positions (elevation plane).....	66
Figure 4-1 Overall view of model cabling (top cover removed).....	75
Figure 4-2 Detailed view of coaxial cables inside the fuselage (top cover opened) .....	76
Figure 4-3 SMA (female) connectors assembled on bottom face.....	76
Figure 4-4 Detailed view of a monopole over the fuselage .....	77
Figure 4-5 Scaled F-4 model, placed on wooden masts in hangar (side view).....	80
Figure 4-6 Antennas involved in S-parameter measurements .....	81
Figure 4-7 Return loss (dB) vs. frequency (MHz) for antenna #4 .....	83
Figure 4-8 Return loss (dB) vs. frequency (MHz) for antenna #5 .....	84
Figure 4-9 Return loss (dB) vs. frequency (MHz) for antenna #6 .....	84
Figure 4-10 Return loss (dB) vs. frequency (MHz) for antenna #7 .....	85
Figure 4-11 Return loss (dB) vs. frequency (MHz) for antenna #9 .....	85
Figure 4-12 Return loss (dB) vs. frequency (MHz) for antenna #10 .....	86
Figure 4-13 $S_{64}$ vs. Frequency.....	88
Figure 4-14 $S_{74}$ vs. Frequency.....	88
Figure 4-15 $S_{104}$ vs. Frequency .....	89
Figure 4-16 $S_{65}$ vs. Frequency.....	90
Figure 4-17 $S_{75}$ vs. Frequency.....	90
Figure 4-18 $S_{105}$ vs. Frequency .....	91
Figure 4-19 $S_{69}$ vs. Frequency.....	92
Figure 4-20 $S_{79}$ vs. Frequency.....	92
Figure 4-21 $S_{109}$ vs. Frequency .....	93
Figure 4-22 Comparison of coupling values between “antenna #6” and “new” antenna, for three different positions – simulation.....	95
Figure 4-23 Comparison of coupling values between “antenna #6” and “new” antenna, for three different positions – measurement .....	95
Figure 4-24 Comparison of coupling values between “antenna #7” and “new” antenna, for three different positions – simulation.....	96
Figure 4-25 Comparison of coupling values between “antenna #7” and “new” antenna, for three different positions – measurement .....	96

Figure 4-26 Comparison of coupling values between “antenna #10” and “new” antenna, for three different positions – simulation.....	97
Figure 4-27 Comparison of coupling values between “antenna #10” and “new” antenna, for three different positions – measurement .....	97

# CHAPTER I

## INTRODUCTION

In avionics, communication and navigation systems have a major role in system design. All air-based platforms are equipped with numerous communication and navigation sub-systems, all of which serve for a specific mission. In this respect, RF transmission and reception characteristics of these sub-systems take importance.

A typical aircraft is equipped with several transmitter and receiver units, which have particular type of antennas, placed over the fuselage. Types of radiating and receiving antennas are determined, depending on system specifications and operational performance criteria, as well as the properties of platform itself. Here comes the concept of appropriate selection and placement of antennas on the platform. Therefore, performance of antennas mounted on airframes is an important factor in design of airborne radio systems, and it should be considered at an early stage in the study of system requirements for any particular aircraft [1].

This thesis investigates the effects of airframe on certain electrical properties of antennas mounted on it, such as impedance, antenna-to-antenna coupling and radiation pattern. The effects are investigated via using an electromagnetic simulation software, named CST Microwave Studio<sup>®</sup>.

This thesis covers three main parts, all of which follow one another in continual and complementary manner. In the first part, use of simulation tools for general purpose antenna analysis was discussed. Then, the simulation tool used throughout the study, “Microwave Studio<sup>®</sup> - MWS”, was introduced. The numerical method (Finite Integration Technique, which MWS<sup>®</sup> uses) was briefly explained and also a rough comparison between other methods used by different simulation tools was given. After a brief introduction to MWS<sup>®</sup>, main specifications of MWS<sup>®</sup> were interpreted to the reader, via doing simple case studies about well-known antenna analyses. These studies aim to introduce the specific features of MWS<sup>®</sup> to the reader and point out key features of the software. Besides, effects of these specific features were examined and validity of results obtained from these simulations is discussed.

In the second part, after determining key settings of MWS<sup>®</sup>, antenna simulations were done on a real airframe, namely F-4 aircraft. Based on an initial realistic antenna placement, a series of analyses on an F-4 aircraft was performed. This study covered simulation models from simple to complicated, using a primitive representation of antenna placement, a simplified model of F-4 aircraft and an actual CAD model of F-4 aircraft, with each and every geometrical detail introduced. Depending on different antenna positions, performances of antennas were investigated and reasons of change in antenna characteristics were ascertained. Then, differences of S-parameter and radiation pattern results between different simulation models were discussed in detail.

The third part covers verification of simulation results via measurements done on a 1:10 down-scaled model of the airframe. First, use of scale models in electromagnetic analysis was discussed. Important aspects of scale model measurements were stated and related methods of measurements were discussed.

A 1:10 down-scaled F-4 mock-up was constructed, plated with copper sheet and equipped with identical antennas, as close as possible to an actual antenna

placement of that aircraft. Then, a measurement environment was obtained for doing reliable S-parameter measurements. Measurements were repeated for different antenna positions and results were compared with the ones of related simulations. Main reasons of discrepancies were examined. With this study, it was aimed to see whether such simulation tools provide accurate and reliable results about this type of electromagnetic problems; thus such problems can totally be handled by simulations, rather than doing laborious on-site or scaled-down measurements.

In last part, all conclusions obtained at each subsection were summarized and further studies which can be done using a similar approach were discussed.

## **CHAPTER II**

### **A CLOSER LOOK AT ELECTROMAGNETIC SIMULATION TOOLS**

In this chapter, use of electromagnetic simulation tools on antenna placement analyses was discussed, together with more detailed information of CST Microwave Studio<sup>®</sup>, which was used throughout simulation studies.

#### **2.1. Introduction**

As computers evolve and capability of performing large numerical computations increase, tools using numerical methods better serve for doing complex electromagnetic calculations. Use of digital computers for solution of boundary value problems using integral equations has substantially increased in 1960s. Nowadays, the computational resources, by great evolution of digital computers, are much higher; thus today's available simulation tools are much faster and of higher performance, as compared to their predecessors. Therefore, by the help of this development, numerical electromagnetic problems with much higher degree of complexity can easily be handled.

## 2.2. Common Numerical Methods

In the market, there are various simulation tools, each of which uses various simulation tools, developed for solving certain numerical electromagnetic problems. Most commonly used methods are Method of Moments (MoM), Finite Element Method (FEM), Finite Difference Time Domain (FDTD), Finite Integration Technique (FIT), Uniform Theory of Diffraction (UTD), etc. There are also hybrid techniques which combine two distinct methods for covering both low and high frequency problems. Each method has its own approach in constructing the electromagnetic problem; formulizing and solving it.

All these methods rely on space discretization of the structure, defining the excitation, writing Maxwell's equations in appropriate form and obtaining the unknowns via certain post-processing features. Some tools work in frequency domain, i.e. they yield solution at only a specific frequency (such as MoM, FEM and UTD), whereas some work in time domain, i.e. they output a full-band result with a single run (such as FIT and FDTD). From another point of view, some methods use different type of space discretization, such as wire grid model (surface), tetrahedral grids (surface), hexahedral grids (volume), etc. This is related to how the method handles the equations to be solved.

One of main distinctions between different electromagnetic methods is the domain at which method works, i.e. time domain or frequency domain. Well-known methods like MoM and FEM, which yield exact solution of Maxwell's Equations, as well as UTD, which uses ray diffraction – an approximate high frequency method, work in frequency domain, where the solution is obtained for only a single frequency. Whereas, methods like FIT and FDTD are time domain techniques, which yield broadband solution within a single simulation run.

## **2.3. CST Microwave Studio - MWS<sup>®</sup>**

### **2.3.1. Introduction**

MWS<sup>®</sup> is a numerical electromagnetic tool for 3D electromagnetic simulation of high frequency problems. MWS<sup>®</sup> is equipped with different solvers for different electromagnetic applications.

MWS<sup>®</sup> is able to import 2D and 3D CAD data at various formats such as IGES, STEP, ProE, DXF, GDSII, et cetera; and convert them to its ACIS based parametric solid modeling front-end. By using built-in shape creation tools, the user can create basic shapes like traces, 2D surfaces, 3D volumes (brick, sphere, cylinder, cone, toroid, etc.) and do geometric manipulations on those shapes. Finally, these created shapes can be combined with the imported file and the desired geometry can be constructed. After the geometry is modeled, a fully automatic mesh generation is applied on the structure, depending on solver settings.

### **2.3.2. Solvers in MWS<sup>®</sup>**

In MWS<sup>®</sup>, there are three different solvers, namely transient solver, frequency domain solver and eigenmode solver. Depending on the application, each of them has certain advantages and benefits. Since only transient solver license is available, the entire study was done using it.

Briefly, transient solver is a tool which obtains the entire frequency behavior of the simulated device from a single simulation run. Transient solver uses hexahedral grids and it is efficient for most high frequency applications such as transmission lines, filters, antennas and so forth.

Frequency domain solver is a more appropriate tool for narrowband problems such as filters or simulation of electrically small structures which are much smaller than a wavelength.

MWS<sup>®</sup> also offers eigenmode solver, which is used for calculating a finite number of modal field distributions in a closed device. This solver also uses hexahedral grids.

Main advantage of transient solver over frequency domain and eigenmode solvers is that it uses a time domain technique, named as FIT – Finite Integration Technique, and yields broadband result of an electromagnetic problem with a single simulation. Considering the scope of this study, both frequency domain and transient solvers serve for the needs. However, as stated above, the available license only supports transient solver; therefore, all simulations are done using that solver.

### **2.3.3. Finite Integration Technique – FIT**

MWS<sup>®</sup> is based on the Finite Integration Technique (FIT), first proposed by Weiland in 1976/1977 [2]. This numerical method provides a universal spatial discretization scheme, which is applicable to various electromagnetic problems ranging from static field calculations to high frequency applications, in time or frequency domain. In the following section, the main aspects of this procedure are explained and extended to specialized forms concerning the different solver types.

Unlike most numerical methods, FIT discretizes the following integral form of Maxwell's equations rather than the differential ones:

$$\oint_{\partial A} \vec{E} \cdot d\vec{S} = - \int_A \frac{\partial \vec{B}}{\partial t} \cdot d\vec{A} \quad (2-1)$$

$$\oint_{\partial V} \vec{D} \cdot d\vec{A} = \int_V \rho \cdot dV \quad (2-2)$$

$$\oint_{\partial A} \vec{H} \cdot d\vec{S} = - \int_A \left( \frac{\partial \vec{D}}{\partial t} + \vec{J} \right) \cdot d\vec{A} \quad (2-3)$$

$$\oint_{\partial V} \vec{B} \cdot d\vec{A} = 0 \quad (2-4)$$

In order to solve these equations numerically, a finite calculation domain is defined. Depending on solver settings and geometrical considerations, automatic mesh generation is applied and the calculation domain is divided into finite number of hexahedral segments. Although the mesh view shows a single grid structure on overall calculation domain, actually two orthogonal mesh structures are defined.

Figure 2-1 illustrates how calculation domain is segmented into small grids and how dual grid representation is defined.

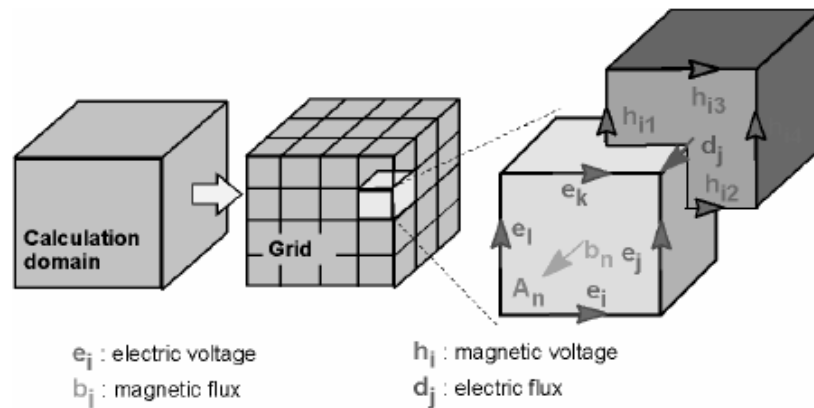


Figure 2-1 Illustration of dual mesh grid in MWS®

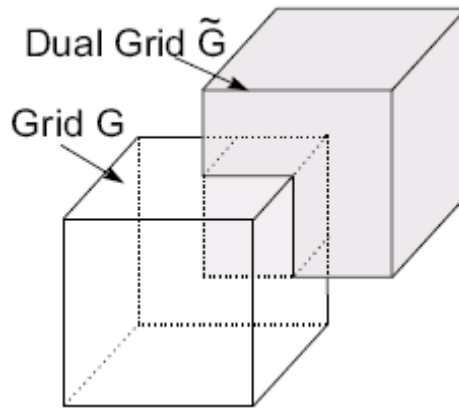


Figure 2-2 Spatial allocation of a cell and its dual cell

In dual grid structure, one grid involves electric voltages ( $e_i$ ) on edges of hexagons and magnetic fluxes ( $b_i$ ) normal to each face; and the other grid involves magnetic voltages ( $h_i$ ) on edges of hexagons and electric fluxes ( $d_i$ ) normal to each face. For each cell, Maxwell's equations are formulated as demonstrated in

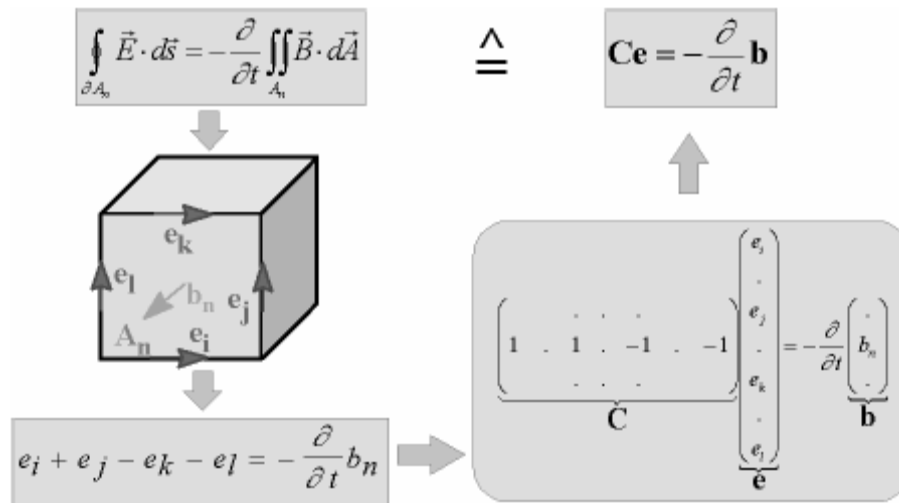


Figure 2-3 Faraday's Law applied on a unit cell

Using Faraday’s Law in integral form, the equation given in Figure 2-3 is written as the sum of four electrical grid voltages; the right hand side of that equation represents the time derivative of total magnetic flux within that facet. Then, “matrix C - topological matrix” is introduced as the discrete equivalent of analytical curl operator.

On the dual grid, similarly, same procedure is applied on Ampere’s Law in integral form (Formula 2.3) and the corresponding dual discrete curl operator is defined. Coming to the divergence equation (Formula 2.4), which describes the non-existence of a magnetic charge, the surface integral given in that formula is evaluated over each cell as shown in Figure 2-4. The double bar over discrete magnetic fluxes is used to represent that these are defined over the dual grid structure (denoted as  $\hat{G}$ ), rather than the original one (denoted as G).

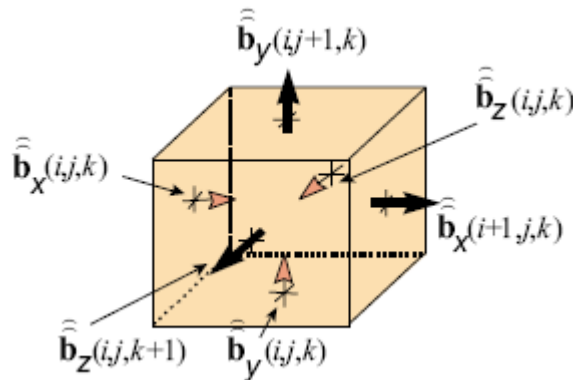


Figure 2-4 Illustration of Gauss’s Law for magnetism, over a unit cell [3]

This turns out to be a sum of fluxes evaluated over each facet of a unit cell, as written in the form given below,

$$\begin{aligned}
& -\overline{b}_x(i, j, k) + \overline{b}_x(i+1, j, k) - \overline{b}_y(i, j, k) + \overline{b}_y(i, j+1, k) \\
& -\overline{b}_z(i, j, k) + \overline{b}_z(i, j, k+1) = 0
\end{aligned} \tag{2-5}$$

Similarly, this relation is expanded to the entire grid structure, and written in matrix form, as shown in Figure 2-5 below.

$$\underbrace{\begin{pmatrix} \dots & \dots & \dots & \dots & \dots & \dots \\ \dots & -1 & 1 & -1 & 1 & -1 & 1 & \dots \\ \dots & \dots & \dots & \dots & \dots & \dots & \dots & \dots \end{pmatrix}}_{\mathbf{S}} \underbrace{\begin{pmatrix} \vdots \\ \overline{b}_{m1} \\ \overline{b}_{m2} \\ \overline{b}_{m3} \\ \overline{b}_{m4} \\ \overline{b}_{m5} \\ \overline{b}_{m6} \\ \vdots \end{pmatrix}}_{\mathbf{\overline{b}}} = 0$$

Figure 2-5 Discrete divergence matrix for magnetic fluxes

Similarly, the same procedure is applied on Gauss's Law (Formula 2.2) and it introduces another discrete divergence operator  $\hat{S}$ , which is also consists of topological information as elements 0, -1 or +1. Finally, the complete discrete set of Maxwell's grid equations is obtained as follows:

$$C_e = -\frac{d}{dt} b \tag{2-6}$$

$$\tilde{C}h = \frac{d}{dt} d + j \tag{2-7}$$

$$\tilde{S}d = q \tag{2-8}$$

$$Sb = 0 \tag{2-9}$$

Material relations, which are approximated over grid edges and cell areas, are introduced using the formulas given below;

$$\vec{D} = \varepsilon \cdot \vec{E} \Rightarrow d = M_\varepsilon e \quad (2-10)$$

$$\vec{B} = \mu \cdot \vec{H} \Rightarrow b = M_\mu h \quad (2-11)$$

$$\vec{J} = \sigma \cdot \vec{E} + \vec{J}_s \Rightarrow j = M_\sigma e + j_s \quad (2-12)$$

Finally, the time derivatives are substituted by central differences and the following explicit update formulation is obtained;

$$e^{n+\frac{1}{2}} = e^{n-\frac{1}{2}} + \Delta t \cdot M_\varepsilon^{-1} [\tilde{C} \cdot M_\mu^{-1} \cdot b^n + j_s^n] \quad (2-13)$$

$$b^{n+1} = b^n - \Delta t \cdot C \cdot e^{n+\frac{1}{2}} \quad (2-14)$$

where n denotes n<sup>th</sup> cell in the overall grid structure. As seen in the formulas above, electric voltages and magnetic fluxes are defined for separate dual grid structures and they represent a leap-frog type algorithm [4] which is illustrated in Figure 2-6.

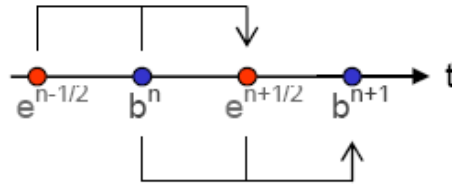


Figure 2-6 Illustration of leap-frog scheme for FIT

According to the leap-frog scheme shown in Figure 2-6, magnetic flux density (at any facet of any grid) at time instant of  $t = (n+1).\Delta t$  ( $\Delta t$  is the time step, which is mentioned later in this chapter) is computed using the magnetic flux at previous time step  $t = n.\Delta t$ , and the electric voltage half a time step before at  $t = (n+1/2).\Delta t$ . Similar sequence is followed for computing the electric voltage at iterative time steps. The time step ( $\Delta t$ ) is determined to be less than a certain time, which is specified by Courant–Friedrichs–Lewy criterion [5], where the time step is a function of grid cell size and maximum electromagnetic wave propagation velocity. This condition states that, in order to have sufficiently dense time sampling, time step shall be smaller than time of propagation of electromagnetic wave within any cell, yielding the following formula;

$$\Delta t_{\max} \leq \frac{\Delta d_{\min}}{v_{\max}} \quad (2-15)$$

$$\Delta d_{\min} = \sqrt{\Delta x_{\min}^2 + \Delta y_{\min}^2 + \Delta z_{\min}^2} \quad (2-16)$$

The minimum time step is calculated in order to satisfy this condition for each and every mesh cell; and as will be explained in the following sections of this chapter, it is one of the predominant items for simulation run time.

To sum up, a brief overview of finite integration technique is given and the detailed theory behind this technique is left to the reader.

#### **2.3.4. Excitation – Port Selection**

Within the technique used in MWS<sup>®</sup>, one of the most determining factors is excitation of geometry. MWS<sup>®</sup> uses two different types of excitation ports, waveguide and discrete port, respectively.

Discrete port is in the form of a lumped circuit element, which is composed of an internal resistor and a current source in parallel [6]. This port consists of a single lumped element in the middle and two perfectly electric conducting wires connecting the port to the structure. A certain voltage/current relation is then introduced along the lumped element, and the S-parameters are calculated based on the element's current and voltage. Discrete port is simply attached between two metallic parts of the system, i.e. monopole and ground plane or between two segments of a dipole.

Since a discrete port is not an exact realization of a feed system (such as a coaxial or ladder line, or a waveguide), there is an improper match between the port and the structure. Thus, some fringing effects may take place due to the difference between the geometry of structure's feed line and that of discrete port [7]. This yields slightly worse impedance characteristics, as compared to waveguide port excitation.

On the other hand, more accurate results can be obtained by using waveguide ports. This kind of port simulates an infinitely long waveguide connected to the structure. Waveguide port is suitably used to excite homogenous/inhomogeneous waveguides of any cross section, planar structures such as microstrips, transmission lines, etc. Applying a waveguide port on an empty waveguide or a coaxial line is straightforward. Only the electrically conducting boundaries are selected and the port is parametrically defined on those boundaries. However, there are some other considerations while exciting microstrip lines with waveguide port; such as port size, other port modes or modeling the proximity of excitation region. These concepts are critical mainly for microstrip structures; however they are not within the scope of this study, thus are only given here for information purpose.

### 2.3.5. Sequence of Actions in a Simulation Run

Below, are the items which follow during a simulation run, using transient solver of MWS<sup>®</sup>;

- Start with a suitable working template
- Create/import the geometry
- Do automatic and/or manual healing on the imported geometry (if necessary)
- Create additional geometric features such as antennas, mechanical parts, etc., using shape creation tools (if necessary)
- Define background material of calculation domain
- Define ports (waveguide or discrete port)
- Define frequency band of simulation
- Define mesh type (tetrahedral or hexahedral)
- Adjust general and local mesh settings
- Define outputs of simulation
- Apply field/voltage monitors (if necessary)
- Adjust transient solver settings
- Start the simulation
- Check convergence (readjust parameters and restart the simulation, if necessary)
- Interpret the results

All these steps are listed for information purpose only; and some of these steps are described in more detail, in related parts of this chapter.

## 2.4. Verification of MWS<sup>®</sup>

There are many electromagnetic simulation tools available, each of which uses different methods for solving different types of electromagnetic problems. Each simulation tool is specialized to achieve the most accurate result by using certain electromagnetic techniques and settings of its own. As every simulation tool does, MWS<sup>®</sup> also requires the user to properly adjust the simulation settings to obtain reliable and accurate results.

The user is recommended to learn the theory behind the computation technique – FIT, and also the specific features of the simulation tool. Using these features determines the difference between the simulation tools which use the same computation method.

Main differences between different simulation tools can be listed as follows;

- Importing / creating geometry
- Manipulating geometry
- Mesh settings
- Simulation settings
- Outputs of simulation / post processing features

It is user's responsibility to digest the meaning of each setting in a simulation tool and use appropriate settings according to the needs. The main concern about the simulation settings is the point which determines the size and complexity of the problem to be solved. Basically, a small size problem requires small amount of memory and computation effort. For such a case, increasing the complexity does not cost much of resources of hardware or computation time. However, mainly for electrically large problems where the simulation tool pushes the limits of hardware resources, the user must carefully work on simulation settings and decide on

accuracy requirement and computation complexity. In certain cases, the problem may go beyond the limits of available resources, in terms of physical memory. Then, the user may prefer to readjust the simulation settings and try to solve the problem at the expense of reduced accuracy and reliability. At this point, the user must be able to make an estimate of loss of accuracy.

Depending on type of problem (either simulation of a small and simple microwave component or an electrically large system with considerable structural complexity), major simulation settings shall be maintained. These settings are decided upon according to the main requirements of the method to be used, which are covered in instructions given in tutorials of the related simulation tool to be used. Furthermore, some cases may require special treatment on geometrical adjustments. It can be concluded that, questioning the validity of a simulation tool requires good knowledge of the tool and the method being used.

Within the scope of this thesis, preliminary work was carried out to determine proper simulation settings for a system with certain antennas mounted on it. The main purpose of this preliminary work is to find optimum simulation settings using simple and well known electromagnetic problems, such as “monopole over a finite size ground plane”.

In literature, there are many studies done on antennas mounted on ground planes of different finite size. Most of these studies cover certain type of monopoles like rod, conical, sleeve, etc., mounted on a circular ground plane having finite radius. In this thesis, the reason why “monopole over finite ground plane” was chosen as a basis for the verification of MWS<sup>®</sup> is that; there is a strong similarity between the structure modeled for primary verification of MWS<sup>®</sup> and the actual case study (F-4 aircraft) which was handled within the scope of this thesis. F-4 aircraft is also equipped with monopoles of different length, mounted on different positions over its fuselage. The fuselage acts as a finite size ground plane (with a rather abrupt shape) and the geometrical variation around the feed of each antenna causes the

electrical properties of that specific antenna to differ from the ones of an ideal monopole mounted on a ground plane of infinite extent. Therefore, this preliminary study also gives an intuition about how the characteristics of a monopole change as the ground plane size and shape varies.

Within the scope of this preliminary study, effects of some critical settings of MWS<sup>®</sup> were examined via the given examples, below. Although there are many simulation parameters embedded in MWS<sup>®</sup>, only most dominant and critical ones were taken into consideration. The items listed below, are the major points which strongly affect accuracy and performance of simulations done by MWS<sup>®</sup>. These are,

- Defining the geometry and excitation port
- Convergence criteria & solver accuracy
- General & local mesh settings

In the following section, all critical settings of MWS<sup>®</sup> were explained by using the results of similar studies found in literature, and depicted by examining results of sample simulations. Thus, effects of each simulation setting were more closely investigated by comparing the results by those found in literature, which consist of measurement and simulation results of an identical structure.

For verification purposes, a study done by Melvin M. Weiner was examined and adopted to MWS<sup>®</sup>. Weiner [8], in his study of monopoles mounted over finite size ground planes, computed the input impedance of several monopoles of finite thickness, which are mounted on a circular ground plane of finite extent. His study covers resistance and reactance results of both simulation and measurement.

In Weiner's study, the simulation results were obtained by using Method of Moments, and the measurements were done in The VHF Antenna Range in MITRE [8]. The measurement setup consists of a circular ground plane of fixed

radius, set of monopoles of different lengths, all of which having finite and equal diameter. For various frequencies, thus for various electrical dimensions of both monopole length and ground plane diameter, input impedance of each monopole was measured. Resistance and reactance values were measured at 17 distinct sizes of antennas with normalized ground plane radii differing between 0,766 and 6,5. Normalized ground plane radius was defined as “ $k*a$ ”, where “ $k$ ” equals wave number, i.e.  $2\pi/\lambda$  and “ $a$ ” equals actual ground plane radius. The length of each monopole was selected to be resonant (purely resistive) when mounted on a ground plane of infinite extent [9]. Looking at the results of this study, the input reactance is expected to asymptotically decay to zero, as normalized ground plane radius extends towards infinity. In addition, the length (denoted as “ $h$ ”) and thickness (denoted as “ $b$ ”) of monopoles were also described in terms of wavelength, hence the normalized monopole lengths ( $h/\lambda$ ) were varying around 0,23 to 0,24. Monopole thickness ( $b$ ) was fixed for each case and equals quarter of an inch; hence the normalized element radii ( $b/\lambda*10^{-4}$ ) varied between 6,35 and 53,69.

This study was reproduced and similar structures were simulated via MWS<sup>®</sup>. Using different simulation settings, several simulations were done and these settings were optimized in terms of accuracy and computational complexity. Then, the impedance results were compared with the ones obtained in Weiner’s study, and the validity of these results and simulation settings were investigated.

Table 2-1, below shows the resistance and reactance values measured by MITRE, predicted by Method of Moments and computed by FIT. As seen on the graphs, there is a good agreement between impedance values, with maximum variation of approximately 10%, which was found to be acceptable. Since the antennas were adjusted to be near resonance, the reactance values were distributed around zero, and again it was seen that both simulation and measurement results followed a similar pattern. Since the values were around zero, the similarity between simulation and measurement results were given in terms of difference, instead of

percentage. Maximum difference between Weiner's measurement results and FIT results was shown to be  $9\Omega$ , where normalized ground plane radius was equal to 6.

Table 2-1 Input impedance of 0,5" diameter monopole elements on an 8 ft. diameter ground plane (comparison of measurements, MoM & FIT)

Frequency (MHz)	Normalized Groundplane Radius (k*a)	Normalized Element Radius (b/λ*10 <sup>-4</sup> )	Normalized Element Length (h/λ)	R <sub>in</sub> (Ω) Meas.	R <sub>in</sub> (Ω) MoM	R <sub>in</sub> (Ω) FIT	X <sub>in</sub> (Ω) Meas.	X <sub>in</sub> (Ω) MoM	X <sub>in</sub> (Ω) FIT
30	0,766	6,35	0,2396	17,6	17,7	19,6	-30,9	-36,0	-30,0
36	0,919	7,63	0,2396	18,6	18,3	19,1	-13,6	-25,5	-18,9
43	1,097	9,11	0,2385	19,1	18,7	19,5	-16,4	-19,3	-13,9
54	1,379	11,43	0,2382	20,2	19,9	20,0	-5,9	-12,1	-3,6
62,4	1,593	13,21	0,2379	22,8	20,8	21,0	-0,5	-4,7	2,5
75	1,915	15,89	0,2374	23,2	22,9	23,6	1,6	-0,4	10,1
86	2,197	18,22	0,2366	27,6	25,3	27,3	7,4	3,3	14,8
89,7	2,3	19	0,2366	28,2	26,6	28,8	-1,0	5,0	16,1
97,5	2,5	20,65	0,2363	31,2	29,4	33,2	11,1	7,3	19,2
117	3	24,78	0,2355	40,5	39,3	45,8	15,2	8,3	18,1
136,5	3,5	28,91	0,2352	46,2	45,8	50,8	7,2	0,8	6,8
156	4	33,04	0,2346	38,6	40,4	43,3	-1,1	-8,2	0,6
175,5	4,5	37,17	0,2344	30,9	34,0	37,4	-1,9	-7,5	3,2
195	5	41,3	0,2335	28,6	30,5	34,8	0,5	-4,4	7,4
214,5	5,5	45,44	0,233	28,3	30,3	36,0	4,9	-0,2	12,0
234	6	49,56	0,2328	31,4	33,7	40,9	5,6	3,6	14,6
253,5	6,5	53,69	0,2335	41,1	40,2	46,0	6,6	3,9	12,0

In the following figures below, in order to see the variation of resistance and reactance values given in Table 2-1 with respect to ground plane size, all values were given in graphical form. Here, it is more easily seen that all resistance and reactance values follow a similar pattern among themselves.

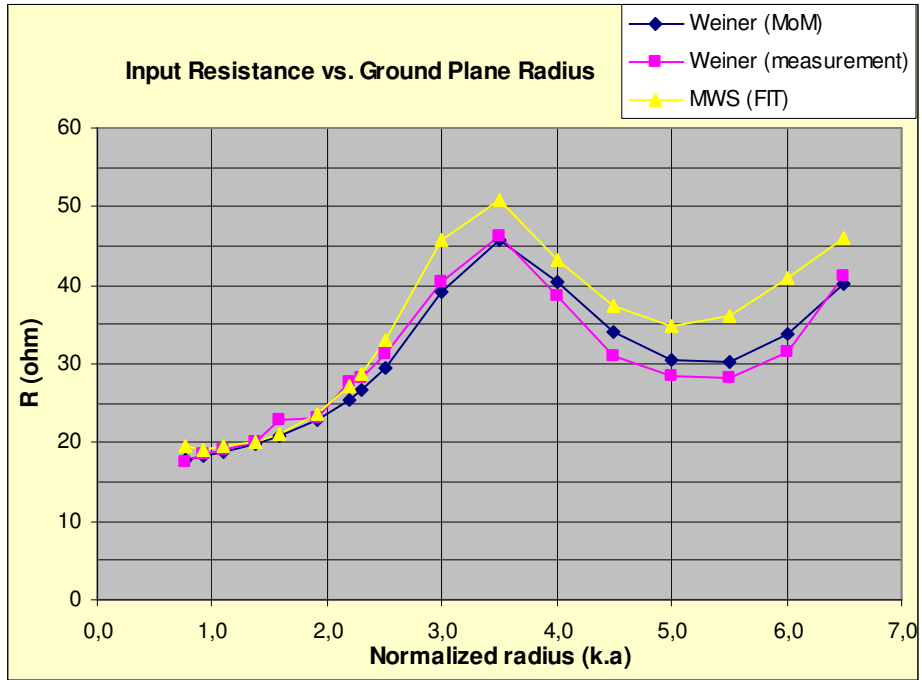


Figure 2-7 Input resistance vs. ground plane radius (measurement-MoM-FIT)

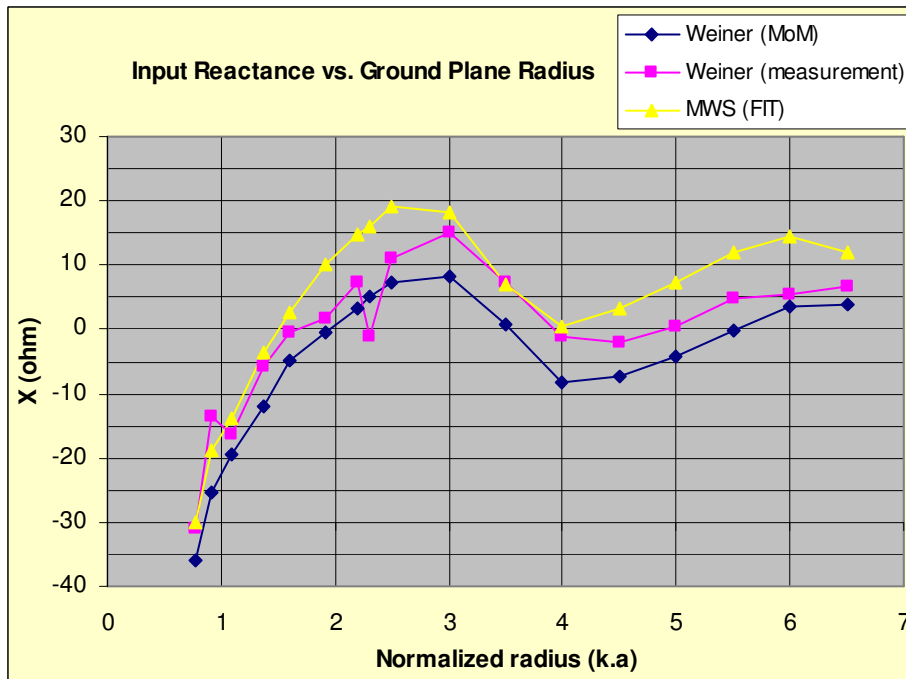


Figure 2-8 Input reactance vs. ground plane radius (measurement-MoM-FIT)

Relying on the results given in Table 2-1, it was deduced that using such settings were sufficient for achieving accurate enough impedance values. Therefore, these results were used as a basis for the oncoming simulations covered in this thesis.

#### **2.4.1. Defining the Geometry and Port**

MWS<sup>®</sup> is able to import many different formats of 2D and 3D CAD data, such as SAT, IGES, STEP, ProE, DXF, GDSII, etc. and convert them to its ACIS based parametric solid modeling front end. Additionally, by using shape creation tools, the user can create basic shapes like linear traces, 2D surfaces, 3D volumes (brick, sphere, cylinder, cone, toroid, etc.) and do geometric manipulations on those shapes. Finally, these created shapes can be combined with the imported file and the desired geometry can be constructed.

Once the desired geometry has been constructed, a suitable port for exciting the geometry is defined. This can be either any type of antenna or any microwave component to be excited. MWS<sup>®</sup> uses two different types of ports, namely waveguide and discrete ports; both of which are used for exciting certain types of structures, respectively.

In Figure 2-9, a square shaped planar antenna mounted over a square shaped ground plane, which is simply fed by a discrete port, is shown. Discrete port consists of a single lumped element, which represents a current source with an internal resistance, and two perfectly electric conducting wires, through which the port is attached to the structure. This approach delivers accurate far field results but may yield S-parameters which are not directly comparable to the measurements [10]. Discrete port, at the expense of impedance accuracy, is the most practical way of defining an excitation in MWS<sup>®</sup>.

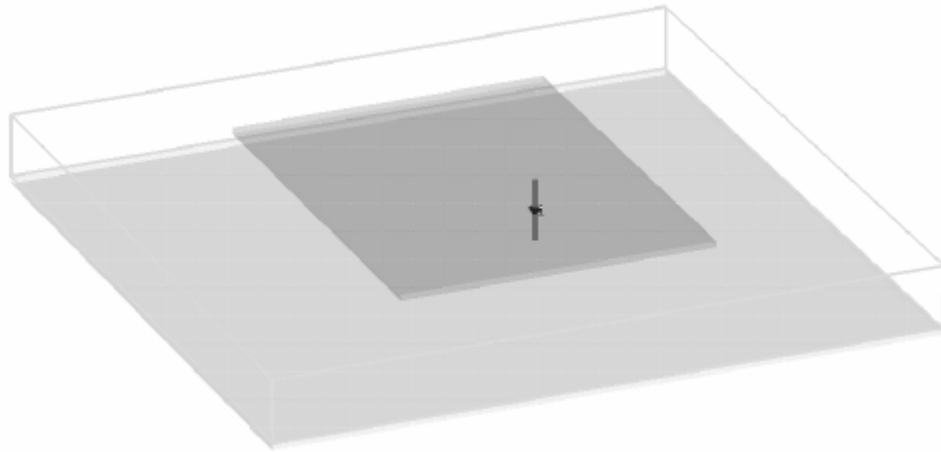


Figure 2-9 Planar antenna fed by a discrete port

In Figure 2-10, the same planar antenna was fed by a coaxial line (similar to a realistic case). Waveguide port normally provides very low reflection and it is appropriate whenever high impedance accuracy is desired. Waveguide port is conveniently used to excite waveguides of any cross section, coaxial lines, microstrips, coplanar lines, etc. At this particular case, the expense is having too many mesh cells, especially around the feed section, which is modeled as a coaxial cable formed by relatively thin layers of materials like inner/outer conductors and dielectric in between. The negative effects of having many details within the overall structure are explained below.

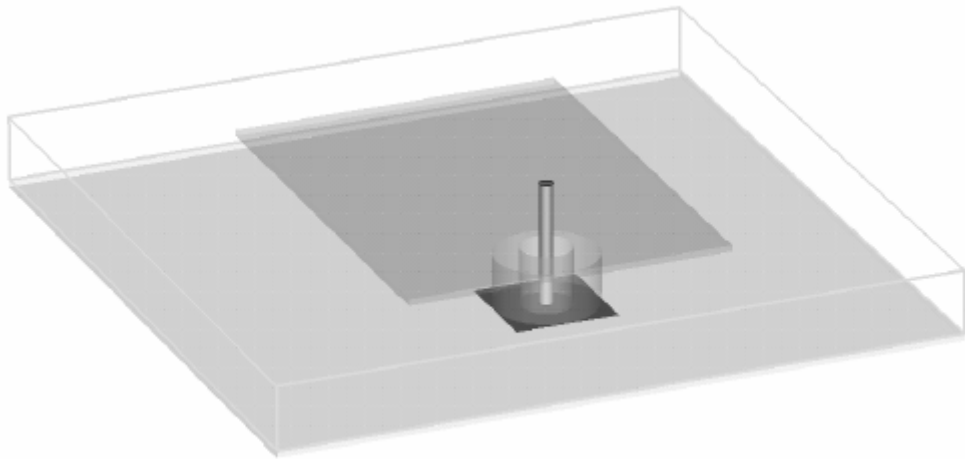


Figure 2-10 Planar antenna fed by a waveguide port

In order to see the effects of using different ports and to compare the performance of two cases, a set of results among Weiner's study was used and similar cases were simulated via MWS<sup>®</sup>, for both applying discrete and waveguide ports.

As an example, the set of results of Weiner, where the normalized ground plane radius equals 4, were used. Firstly, the monopole was fed by a discrete port. The geometry is depicted in Figure 2-11 and discrete port section is shown in detail in Figure 2-12. In Figure 2-13 below, the overall mesh view of the structure is given.

The geometry is defined as follows:

- $f = 156 \text{ MHz}$  ( $\lambda = 75,66''$ )
- monopole length :  $17,75''$
- monopole diameter :  $0.5''$
- ground plane diameter :  $8 \text{ ft.}$  ( $= 4\lambda / 2\pi$ )
- material of antenna and ground plane : PEC

Below are the results which were observed:

- Impedance at 156 MHz
- Polar radiation pattern in elevation plane at 156 MHz
- Total number of mesh cells
- Total simulation time (mm:ss)

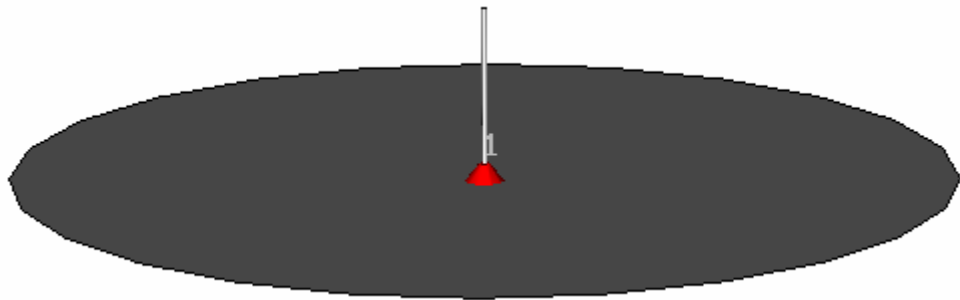


Figure 2-11 Monopole Over Ground Plane of Normalized Radius,  $k.a = 4$

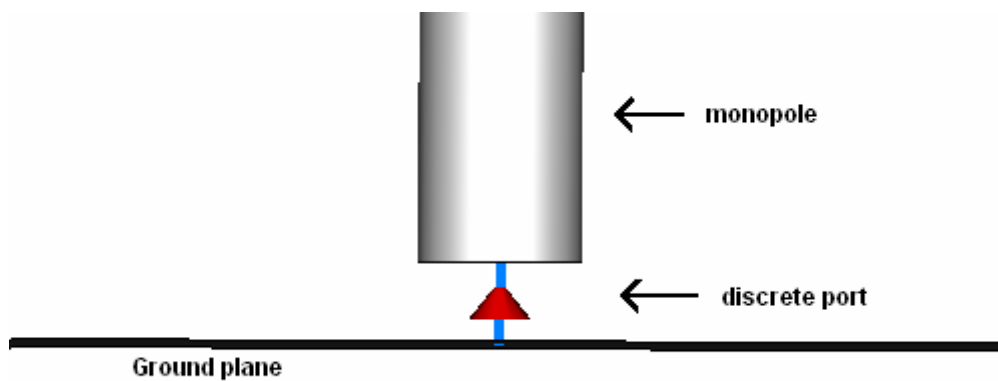


Figure 2-12 Detailed view of discrete port

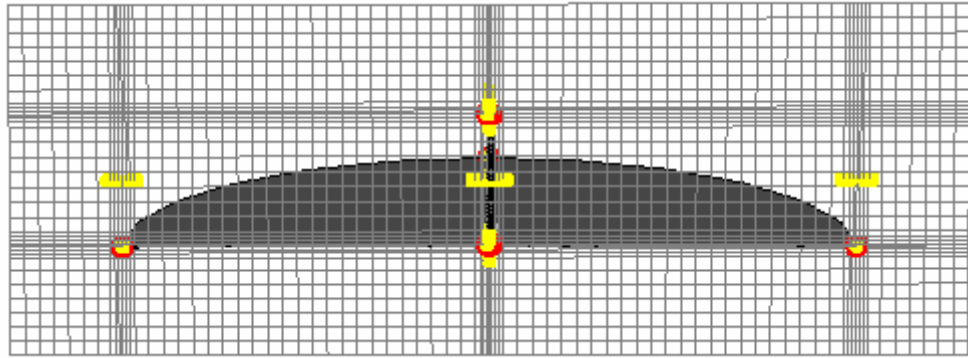


Figure 2-13 A general mesh view (discrete port)

In order to see the difference between the results obtained from discrete port and waveguide port, the same monopole was excited with waveguide port and an identical simulation was run. In order to be able to excite the monopole with waveguide port, a short coaxial line segment was added to the structure. The outer conductor of the coaxial line was attached to the ground plane, onto its lower surface. The dielectric layer and inner conductor passed through the center of ground plane, and the monopole was designed as the extension of the center conductor above the upper side of ground plane. Figure 2-14 shows the top view of the antenna-ground plane junction, where the antenna is fed by a coaxial cable. In the related figure, the ground plane is seen in dark grey, antenna in light gray and dielectric layer in green.

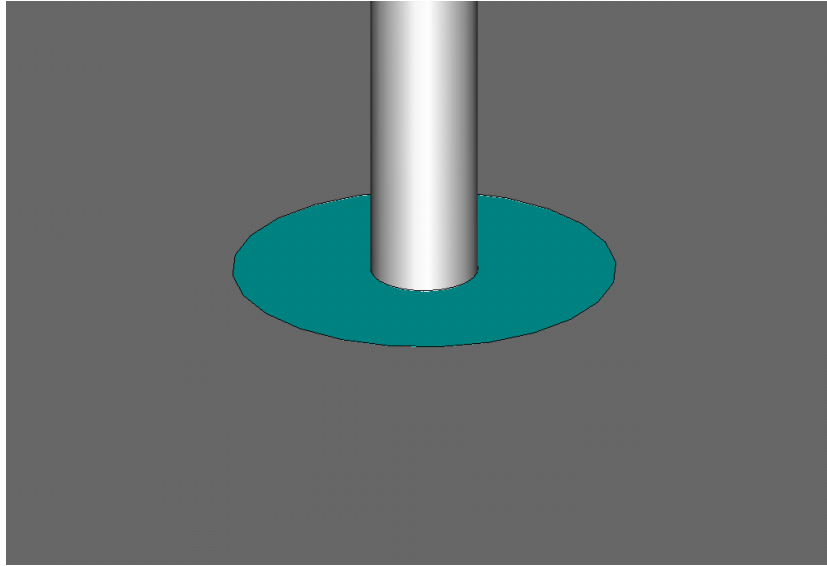


Figure 2-14 Top view of monopole-ground plane junction

Here, the coaxial cable extension was selected to be 2" long and its dimensions and material properties were adjusted so that its characteristic impedance was exactly 50  $\Omega$ . The formula below gives the characteristic impedance of a coaxial cable.

$$Z_0 = \frac{60}{\sqrt{\epsilon_R}} \ln\left(\frac{D_2}{D_1}\right) \quad (2-17)$$

where,

$Z_0$ : Characteristic impedance of coaxial cable

$\epsilon_R$ : Relative permittivity of dielectric layer between inner and outer conductor

ln: Natural logarithm function

$D_1$ : Outer diameter of inner conductor

$D_2$ : Inner diameter of outer conductor

For the inner conductor thickness ( $D_1$ ), the same diameter of the monopole itself, 0,5" was selected. For the dielectric layer, a typical relative permittivity of 2 was assigned. To achieve the characteristic impedance of 50  $\Omega$ ,  $D_2$  was calculated to be

3,25 times  $D_1$ , which is 1,625". Assigning a thickness of 0.1" mm to the outer conductor, the outer diameter of outer conductor was found to be 1,725". The length of coaxial cable measured from its tip to the junction point at the bottom face of ground plane was selected to be 2". In order the waveguide port to yield accurate results, there must be at least three mesh lines along the coaxial or waveguide structure [10]. By using these dimensions and proper mesh settings, this condition was automatically satisfied, so there was no need to modify the local mesh properties.

Below, Figure 2-15 depicts the cross sectional view of the coaxial feed. The diameters of inner ( $D_1$ ) and outer ( $D_2$ ) conductor and layers are marked on the figure.

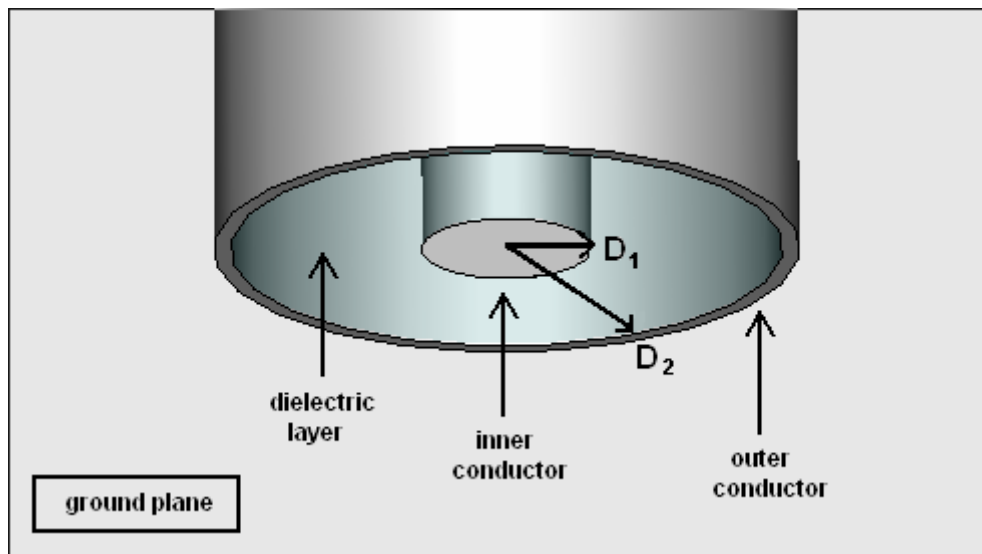


Figure 2-15 Detailed view of coaxial feed section (bottom view)

In order to match the thicknesses of monopole and inner conductor of coaxial cable, and thus keep mesh density as close as possible to the case of discrete port excitation, the dimensions of coaxial cable were a little bit exaggerated. Here, the

critical additional detail is that the outer conductor was selected to be very thin (0,05") in terms of wavelength (approximately 0,6%). In order not to use very small mesh cells and increase computational complexity, the outer conductor was represented by a single mesh line passing along it. Although it is not a feasible illustration of hexahedral discretization, this is achieved by “Thin Sheet Technique™” embedded in MWS®, which is explained in more detail, in following sections. Finally, a mesh view as seen Figure 2-16 was achieved.

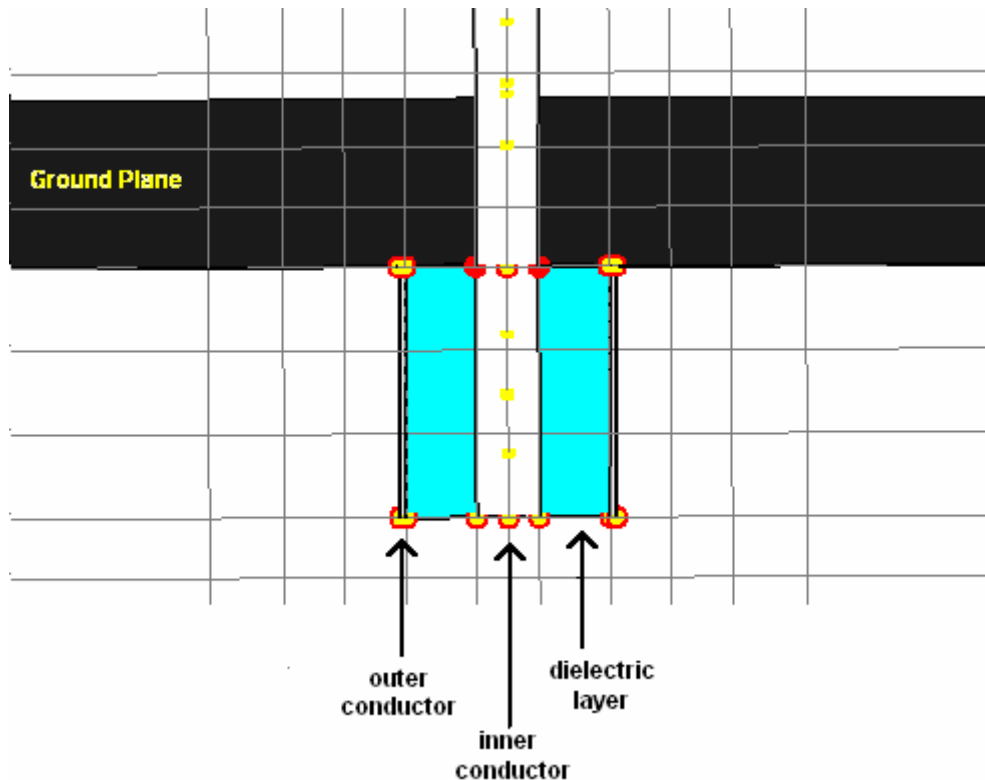


Figure 2-16 Detailed mesh view of coaxially fed monopole

Coming to the results obtained by two different excitation techniques, the return losses ( $S_{11}$ ) and radiation patterns were found to be close to each other. In Figure 2-17 and Figure 2-18, return losses of two cases are given, respectively. On both figures, the marker was placed at 156 MHz.

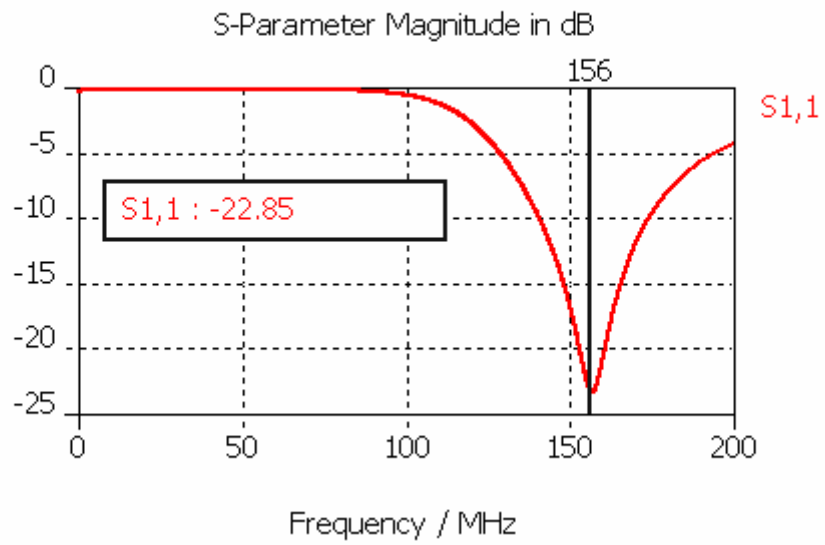


Figure 2-17 Return loss of monopole fed by discrete port

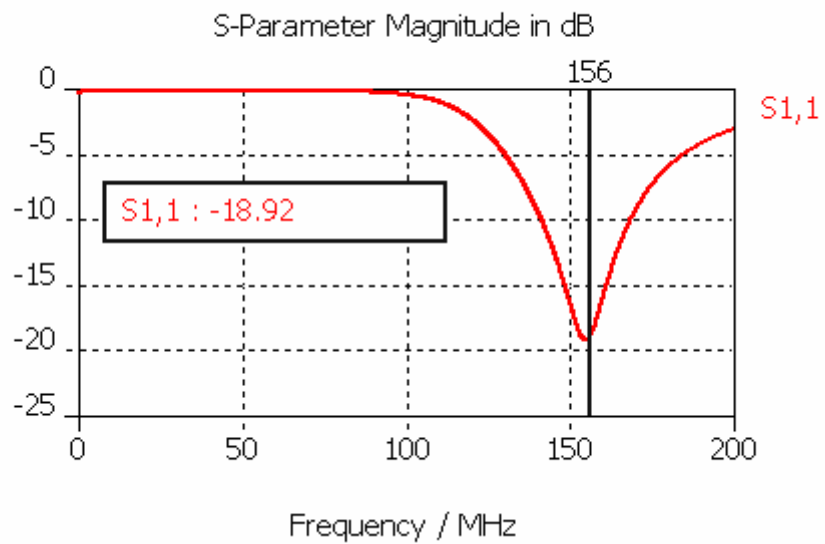


Figure 2-18 Return loss of monopole fed by waveguide port

As seen on figures above, the frequencies where return losses have the minimum value are very close to each other, whereas the minimum values of  $S_{11}$  vary about 4 dB.

Coming to the radiation pattern, both discrete and waveguide port excitation yields almost same results, showing that very slight impedance difference yields very small difference in radiation efficiency (less than 1%), thus both directivities (in dB) are identical.

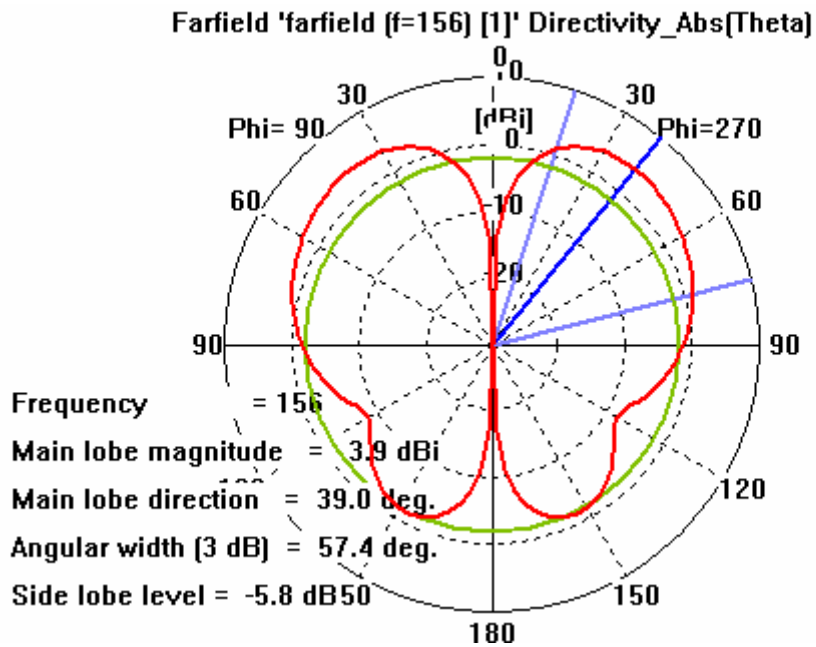


Figure 2-19 Directivity ( $\theta$ ,  $\phi=0^\circ$ ) for discrete port excitation

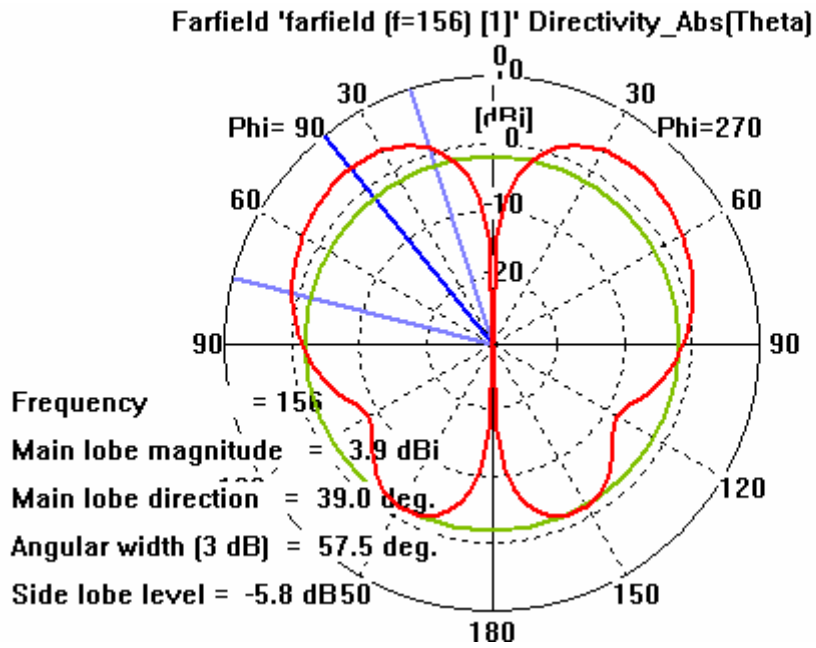


Figure 2-20 Directivity ( $\theta$ ,  $\phi=0^\circ$ ) for waveguide port excitation

Table 2-2 gives a comparison of results obtained from discrete and waveguide port excitation, respectively. Additionally, radiation pattern results were compared with the ones listed in Weiner's study, where directivity results were obtained from simulating a "thin" monopole via Method of Moments.

Table 2-2 Comparison of Results obtained from Discrete and Waveguide Port Excitations

	<b>Discrete Port (FIT)</b>	<b>Waveguide Port (FIT)</b>	<b>Weiner's Results (meas.)</b>	<b>Weiner's Results (MoM)</b>
Frequency (MHz)	156	156	156	156
Normalized ground plane radius (k.a)	4	4	4	4
Normalized element length (h/λ)	0,2346	0,2346	0,2346	0,2346
Normalized element radius (b/λ*10 <sup>-4</sup> )	33,04	33,04	33,04	<1
Input impedance (R+jX)	43,3+j0,6	41,7-j4,8	40,4-j8,2	38,6-j1,1
Return loss (dB)	-22,8	-19,6	-17,1	-17,8
Mismatch loss (dB)	-0,02	-0,05	-0,08	-0,07
Peak directivity (dBi)	3,9	3,9	N/A	3,9
Directivity on horizon (dBi)	-1,4	-1,4	N/A	-1,5
Elevation angle of peak directivity (θ°)	39	39	N/A	39
Total # of meshcells	218.000	249.000	N/A	N/A
Simulation run time (mm:ss)	02:35	02:55	N/A	N/A

As a result, the impedances obtained from simulations containing discrete and waveguide ports respectively, were quite similar, and also in good agreement with Weiner's measurement and simulation results. Input variation (with respect to frequency) of a thin antenna is much faster than that of a thicker antenna [11], and this effect reveals itself for reactance values, which show considerable variations from case to case. This variation is tolerable in a sense that mismatch loss of all four antennas are very close to each other. Thus, this does not yield considerable difference to impedance matching and radiation efficiency.

Considering radiation results, both port types yield almost identical results and they well agree with Weiner's results [8], which cover a much thinner monopole. Thus, both excitation types yield equally good results in terms of radiation characteristics.

Comparing two simulations in terms of total number of mesh cells and simulation time, it is seen that both cases require similar amount of physical memory and run time. For waveguide port excitation, slight increase in simulation run time is a result of increased number of mesh cells. For a relatively simple problem, this does not cost much to the user. However, considering a case where the monopole is much thinner, applying waveguide port would yield difficulties because of structural considerations related to dimensions around feed section. Modeling a much thinner coaxial feed for the monopole would require much denser mesh lines, thus would yield great increase in computation complexity. Then, using a waveguide port would definitely be disadvantageous.

Another difficulty for the application of waveguide port is that, it is not possible to perfectly mechanically align and excite a waveguide port inside any closed PEC (perfectly electric conductor) shape, such as an imported aircraft or ship, which is composed of several hundreds of flat or curved shells, attached to each other. Over such curved and closed geometries, it is harder to adopt waveguide port excitation. Instead, discrete port requires only a single contact point to be attached to platform. Looking back to the problem stated in previous paragraph, it becomes much more difficult to represent the waveguide port's feed section over an electrically large structure. At such a case, regardless of the frequency limitation, the feed region itself would require much denser mesh lines than the overall mesh settings impose; thus this would result in great increase in memory requirement and total simulation time.

In conclusion, referring to antenna simulations done on an 18 meter long F-4 aircraft, it is more feasible to use discrete ports for exciting monopoles mounted on the fuselage of aircraft. Due to the reasons stated above, discrete ports are found to be more convenient than waveguide ports; in terms of accuracy, simplicity, run-time and memory requirements.

## 2.4.2. Convergence Criteria for Transient Solver

As mentioned in previous sections, MWS<sup>®</sup> uses transient solver, which works in time domain and provides broadband S-parameter results in a single simulation run. For transient solver, there are two criteria for convergence, which determine the accuracy level reached. These conditions are "solver accuracy, in dB" and "maximum number of time steps".

Transient solver accuracy determines the convergence of the simulation in a way that, simulation stops when the total remaining electromagnetic energy within the three dimensional calculation domain drops a certain value (in dB) below the maximum energy of the excitation signal energy [7]. Since it is a time domain solver, the energy is also calculated in time and at the instant where the total remaining energy within the computation domain drops below the specified value, the simulation is said to be "converged" and it stops. The energy decay within the computation domain is caused by

- resistive/dielectric losses in lossy material
- signals coupled to any port
- absorption at boundaries (whenever specified as "open" boundary, where a fictitious reflection coefficient at the boundary of calculation domain is defined).

Due to these absorption mechanisms, as time progresses, the propagating electromagnetic energy decays gradually within the computation domain.

The default value for transient solver accuracy is -30 dB, which yields sufficiently accurate results for antenna structures. However, to obtain more accurate results, accuracy value can be decreased down to -40 to -50 dB [10]. Transient solver accuracy can be varied between -20 dB down to -80 dB. There is also a "no check"

option, where the remaining energy is not taken into account. For highly resonating cases, where the energy in the system mostly goes back and forth and does not decay, another parameter determines the termination of simulation; that is the total excitation duration.

For certain cases, regardless of accuracy setting, the simulation does not end within favorable time duration. This can be observed as the non-decaying behavior of port signals or energy in computation domain. In order to prevent the solver from running for a very long period of time, the simulation is made to stop after a certain period. This period is defined in terms of duration of excitation signal, i.e. "pulse length", which is somewhat related to the frequency band of interest (determined by start and stop frequencies). The default setting is 20 pulse lengths, where the simulation stops when run time reaches 20 times the excitation pulse duration [7]. This is actually a forced way of terminating the simulation, thus depending on the application; it may yield loss of accuracy.

The "pulse length" condition dominates "solver accuracy" setting. When predefined number of time steps is calculated, solver stops regardless of the amount of energy remained. At that instance, there still may remain considerable amount of energy within the computation domain, thus port signals may not sufficiently vanish. Then, a "truncation error" appears, which yields ripples on S-parameter plots but does not change much the overall pattern (i.e. maxima or minima) of S-parameters. In order to avoid truncation error without compromising accuracy, either total number of time steps can be increased and solver is let run for a longer period; or "Auto-Regressive Filtering" can be applied, which is out of the scope of this study and not explained in detail.

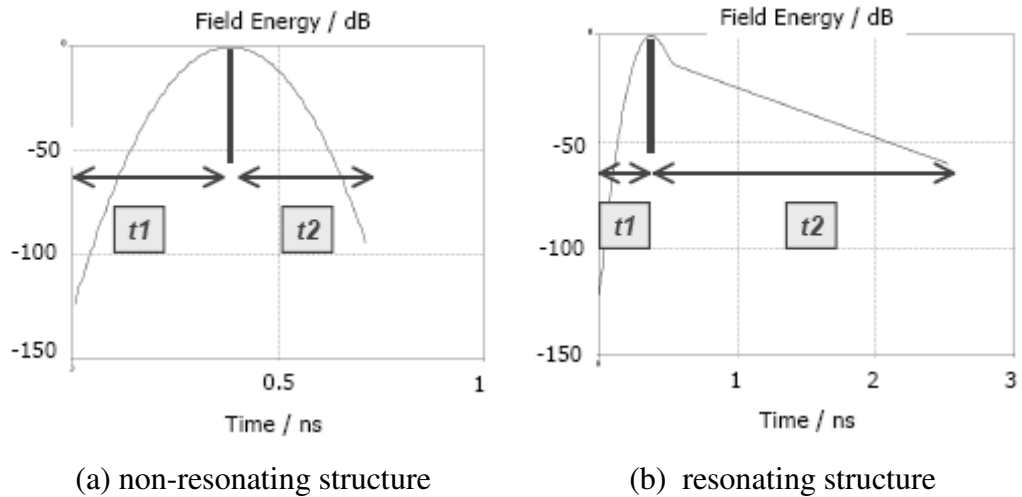


Figure 2-21 Energy vs. time graph for a non-resonating (a) and resonating (b) structures

In Figure 2-21 above, two “total energy vs. time” plots are given for a non-resonating and resonating structure, respectively. The frequency range of both simulations is identical, thus duration of excitation pulse ( $t_1$ , energy rise time) is identical for both, and equals approximately 0,4 nanoseconds. This parameter is independent of the structure and is only determined by the frequency band of simulation. However, energy decays much slower in the resonating case, thus  $t_2$  (energy fall time to the desired dB level) is much longer, as compared to the one in non-resonating case.

For verification purpose, the same monopole studied in Paragraph 2.4 was simulated by using different solver accuracy levels. There is no complexity in the model, nor is the problem electrically large. So the default solver accuracy (-30 dB) was easily achieved within default allowed run time (duration of 20 pulse lengths).

In addition to the default accuracy setting, three different values were assigned, “-50 dB”, “-60 dB” and “no check”, respectively. When “no check” option was

selected, the simulation ran along 20 pulse lengths and the solver reached an accuracy level of approximately -86 dB. For cases where accuracy was -50 dB or below, the results were found to be identical (maximum difference of 0,05 dB). For accuracy level of -30 dB, the return loss was slightly different from that of others (maximum difference of 0,6 dB). Thus, it was deduced that a solver accuracy level of -50 dB is acceptable for such radiation problems. Figure 2-22 shows return loss values obtained by using four different accuracy levels (-30, -50, -60 dB and "no check", respectively). Since the differences among each plot were very small, the graph was zoomed between 156-158 MHz in horizontal axis and -22 to -24 dB in vertical axis, where the maximum difference between each plot can be observed. It is clearly seen that results obtained from -50 dB, -60 dB and "no check" cases are almost equal to each other. However, default setting of -30 dB yields a maximum difference of 0,6 dB, as compared to higher accuracy settings.

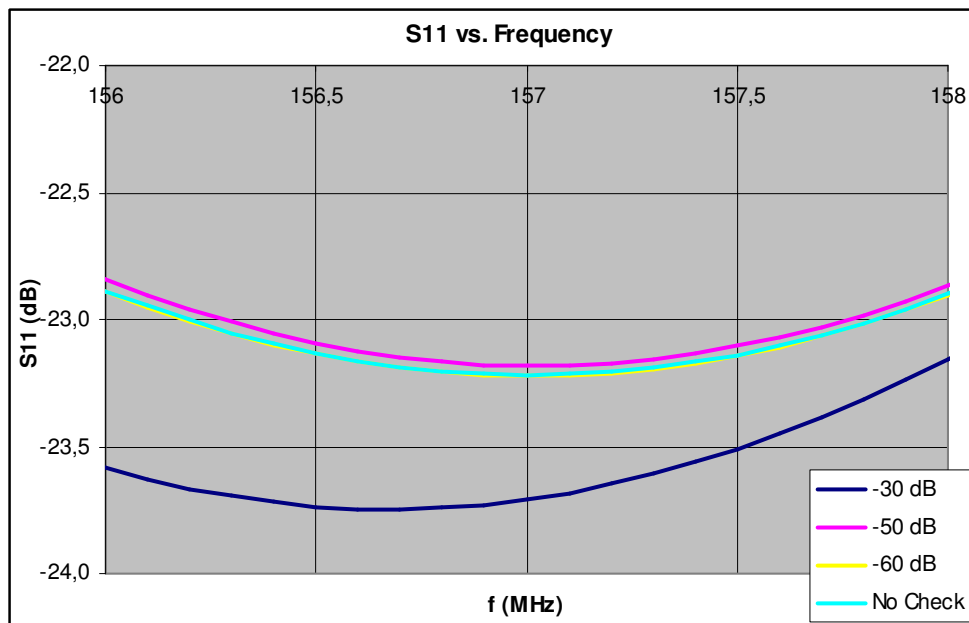


Figure 2-22 Effects of solver accuracy on return loss

Considering performance criteria, simulation run times were compared in Table 2-3 below. Here, both impedance and radiation pattern results were computed and listed for 156 MHz. Expectedly, as transient solver accuracy is increased, simulation time gradually increases; however, after a certain value (here it was found to be -50 dB), it does not yield any further gain in accuracy for radiation or impedance results.

Table 2-3 Effects of Transient Solver Accuracy on Simulation Results

Accuracy level (dB)	-30	-50	-60	No Check (-85,7)
Input impedance (R+jX)	44+j1,6	43,3+j0,6	43,3+j0,65	43,3+j0,65
Return Loss (dB)	-23,6	-22,8	-22,9	-22,9
Peak directivity (dBi)	4	3,9	3,9	3,9
Directivity on horizon (dBi)	-1,5	-1,4	-1,4	-1,4
Elevation angle of peak directivity ( $\theta^\circ$ )	39	39	39	39
Simulation run time (mm:ss)	02:12	02:35	03:13	12:56

### 2.4.3. Local Mesh Settings

One of the basic rules of doing numerical electromagnetic computation is correctly determining mesh settings. In MWS<sup>®</sup>, there are two main mesh settings, namely global and local ones. As the name implies, global mesh settings act on entire computation domain and define the mesh accordingly; whereas local mesh settings are defined only for any selected part of the geometry and redefine mesh properties for that particular section only.

Considering the same example with monopole mounted on a finite size ground plane, accurate representation of antenna and source are two major critical issues. Thus, the following issues are examined and the results are interpreted.

- Port length
- Mesh density around transverse plane of monopole
- Mesh density along longitudinal axis of monopole

#### **2.4.3.1. Port Length**

The study on determining the source type for monopole excitation shows that discrete port is a convenient way which yields accurate results without introducing much complexity. Two main parameters are specified for a discrete port; its impedance and length. Since  $50 \Omega$  is the common basis for many RF applications, only port length is the point to be determined.

For a realistic case where a monopole on a ground plane is simply fed by a coaxial line, no source length is defined. For such a case, the outer conductor is attached to the ground plane, and the antenna is directly attached to the inner conductor of the coaxial section. At this point, depending on difference of thicknesses of antenna and inner conductor of coaxial line, some suitable kind of tapering is applied. Due to shape of tapering, base reactance shall be taken into consideration. If antenna is relatively thick, a conical section is introduced at the cable-antenna junction, in order to reduce shunt capacitance at the gap [12]. For considering simulations with discrete port excitation, the user needs to define a certain port length, which affects the overall current distribution and thus antenna impedance. In MWS<sup>®</sup>, in order not to lose accuracy, discrete port length shall not exceed  $\lambda/10$ , which is equal to the maximum size allowed for any mesh cell [13].

Using the same monopole with the one in previous sections, three sets of simulations were done for determining a proper port length. The default simulation setting consisted of a source length 0,25" ( $\lambda/300$ ), whereas the subsequent simulations consisted of source lengths 0,5" ( $\lambda/150$ ) and 0,75" ( $\lambda/100$ ), respectively. These lengths are much shorter than the maximum allowed value

( $\lambda/10$ ). Below, Table 2-4 lists different impedance values, in comparison with Weiner's simulation and measurement results.

Table 2-4 Effect of port length on impedance (Discrete port)

	MWS	MWS	MWS	MWS	Weiner-measurement	Weiner-MoM
Port length (inch)	0,25 ( $\lambda/300$ )	0,5 ( $\lambda/150$ )	0,75 ( $\lambda/100$ )	1,00 ( $\lambda/75$ )	N/A	N/A
Resistance (ohm)	43,3	43,3	43,4	43,4	38,6	40,4
Reactance (ohm)	0,6	3,5	6,0	8,6	-1,1	-8,2

In order to keep the overall monopole length fixed, solid section of monopole is shortened the same amount. What happens as port length varies is that the base of monopole gets away from the ground plane, which mainly influences reactance. The data in Table 2-4 show that, near first resonance frequency of monopole, as port length increases, resistance changes very slightly, whereas reactance shows more deviation. It was also observed that, for considerably small variation of source length, the radiation characteristics do not change significantly. Additionally, since no change occurs in number of mesh cells, and a minor change in smallest mesh size (which is located in source section), simulation time is almost same for three cases. As a result, port length is kept as short as possible, till mesh settings put a limit on smallest mesh step size.

#### 2.4.3.2. Local Mesh Refinement Settings

MWS<sup>®</sup> offers local mesh refinement settings, which can be applied on any subsection of the total geometry; and affects mesh settings of that subsection and/or its surrounding. For any antenna, most critical points which need to be represented in more detail are the regions with higher current density. Especially

for a monopole or dipole, which is operated at or below its first resonance frequency, current maxima occurs near feed region; thus refining the mesh structure around feed region yields better spatial representation of current distribution.

The important point is meshing the antenna itself. For cases where monopole is rather thin (i.e. diameter smaller than  $\lambda/100$ ), by using the default mesh settings, the automatic mesh generator produces fix points on the center of top and bottom faces of monopole (which was designed as cylindrical solid) and on tip points of discrete port, connected to the monopole. So, only a single mesh line passes through the centre axis of monopole. This representation is achieved by the PBA – Perfect Boundary Approximation, which allows discretization of thin wires without using the mesh step for wire radius [7]. Thus, the user does not need to apply very dense meshing on a thin antenna. Having very dense meshing is not desired because very small mesh size requires very small time step, which yields considerable increase in numerical effort, hence total simulation time.

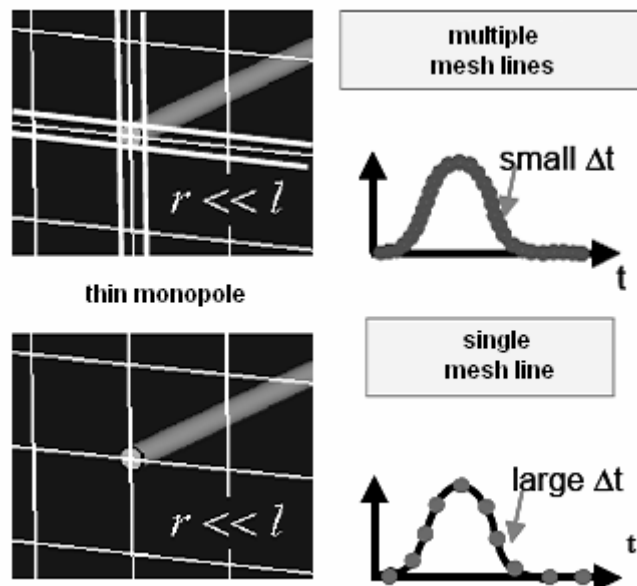


Figure 2-23 Effect of mesh density on time step [7]

Figure 2-23 [7] better illustrates the effect of having too small mesh size around thin segments. The structure of a thin monopole requires fine meshing to be represented in three-dimensional cylindrical form. However, PBA removes the necessity of densely meshing thin structures. This feature is helpful for analyzing relatively thin monopoles, which can be approximated by a thin line. However, while working with monopoles with considerable thickness, especially near even resonances (where length  $l$  is an even multiple of half a wavelength) both resistance and reactance are critically affected by thickness. So, especially around those electrical lengths of any linear antenna, "thin line" approximation is no more valid. This fact is illustrated in Figure 2-24, where the input impedance of dipoles with length-to-diameter ratios ( $l/a$ ) of 60 and 2000, for varying dipole length (in terms of  $\lambda$ ) are plotted, respectively [14]. As seen in the figure, as antenna thickness increases, both resistance and reactance values tend to increase; and it is also observed that, impedance varies more rapidly near even resonances. Near odd resonances, input resistance is almost independent of antenna thickness [15]. Near first odd resonance ( $l$  equals about  $0,24\lambda$ ), the dashed and straight lines fairly agree; meaning that, antenna thickness does not affect resistance; and it has less impact on reactance, as compared to the case of even resonances.

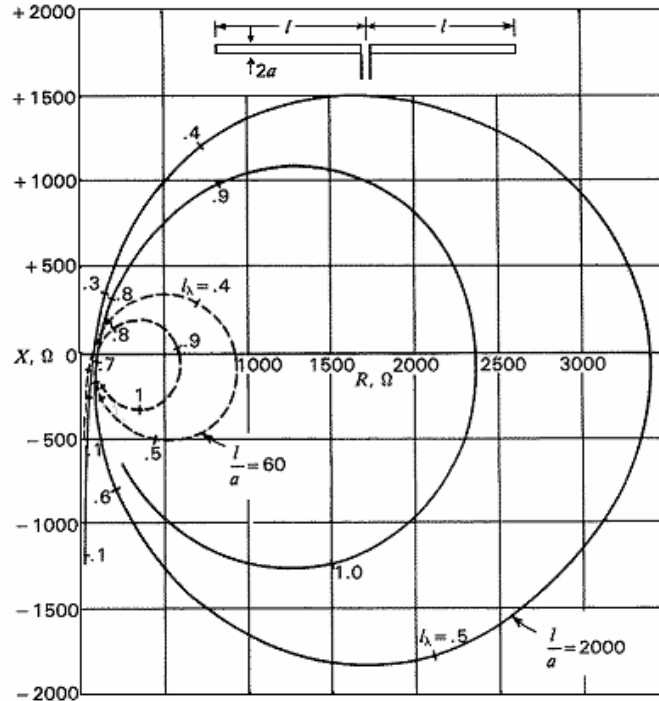


Figure 2-24 Calculated input impedance for cylindrical center-fed dipoles with length-to-diameter of 60 and 2000 as a function of  $l/\lambda$  [15]

In order to see the effects of local mesh refinement on and around monopole, a set of simulations were done on the same example, which has been used throughout Paragraph 2.4. The effects of following simulation settings were investigated;

- Edge refinement factor
- Mesh density along longitudinal axis

The results which were compared are listed below;

- impedance at 156 MHz
- Peak directivity
- directivity on horizon
- Elevation angle of peak directivity

The results were tabulated in Table 2-5, along with six different mesh settings, which were adjusted to achieve the desired mesh structure. These six settings are explained below;

Sim #1: Basic mesh (monopole thickness is not represented in mesh view)

Sim#2: Basic mesh (monopole thickness is represented in mesh view)

Sim #3: Mesh density along longitudinal axis increased

Sim #4: Edge refinement factor increased

Sim #5: Optimized mesh settings

Sim #6: Over-meshed case

Table 2-5 Effects of Local Mesh Refinement on Impedance & Radiation Pattern

	Sim #1	Sim #2	Sim #3	Sim #4	Sim #5	Sim #6
Lines per wavelength	20	20	20	20	30	40
Edge refinement factor	1	1	1	4	4	4
# of segments along z-direction	6	6	9	12	13	16
Total # of mesh cells	30.000	32.000	38.000	91.000	217.000	410.000
Impedance (R+jX)	55,7+j1,5	53,8-j10,7	52,7-j8,9	44,5+j1,7	43,3+j0,6	42,7-j0,1
Max. directivity (dBi)	3,8	3,8	3,9	3,9	3,9	3,9
Directivity on horizon (dBi)	-1,25	-1,25	-1,3	-1,35	-1,4	-1,4
Elevation angle of peak dir. (degree)	40	40	40	40	40	40

The results show that, introducing antenna thickness for the mesh view is essential for the analysis of linear antennas of considerable thickness. Additionally, increasing mesh density along longitudinal axis or increasing edge refinement

factor (which directly affects mesh density around tip points and edges of circular ground plane, where we have greater current density and discontinuity) yields results more close to the ones for over-meshed case. Coming to radiation characteristics, it was seen that any moderate or high level of meshing yields almost identical results. Thus, advanced mesh tuning does not bring much of accuracy in terms of radiation characteristics. As a consequence, it was deduced that main settings (named as "Sim #5" in Table 2-5) yield a good compromise between accuracy and numerical effort.

## CHAPTER III

### ANTENNA SIMULATIONS ON F-4 AIRCRAFT

This chapter contains antenna placement analyses done on F-4 aircraft. The simulations follow an order from simple case to complicated one, and relying on the comparison of results, a general performance and accuracy analysis is done.

Firstly, a simple representation of monopoles over the fuselage was done using identical dipoles placed in free space. Then, the problem was put one step further and a similar antenna placement analysis was done on a “hand-made” F-4 model, which was constructed in MWS<sup>®</sup>. Finally, the desired antenna placement analysis was done on the exact F-4 aircraft model, which had been prepared using mechanical CAD tools (in \*.prt format) and was imported into MWS<sup>®</sup>.

Finally, all simulation results were compared and an overall performance analysis was done for these three different models.

#### 3.1. Analysis of Dipoles in Free Space

As the starting point, dipoles in free space were used as the simplest representation of analyzing coupling between monopoles mounted on an aircraft fuselage. In order to keep the overall geometry similar, thus to have a good representation of actual antenna placement, position of antennas were kept identical, within the absence of aircraft fuselage (which acts as ground plane for monopoles). In

addition, antenna dimensions (thickness, port length) were also kept unchanged. However, relying on image theory, monopole length was doubled; i.e. each monopole of length  $l$  ( $l$  equals  $\lambda/4$  at upper most frequency of band of interest, i.e. 300MHz) was represented by a dipole of length  $2l$ . Finally, a simple representation of monopoles along the aircraft fuselage was achieved via dipoles in free space. Figure 3-1 shows a simple illustration of two parallel dipoles in free space, one moved in echelon.

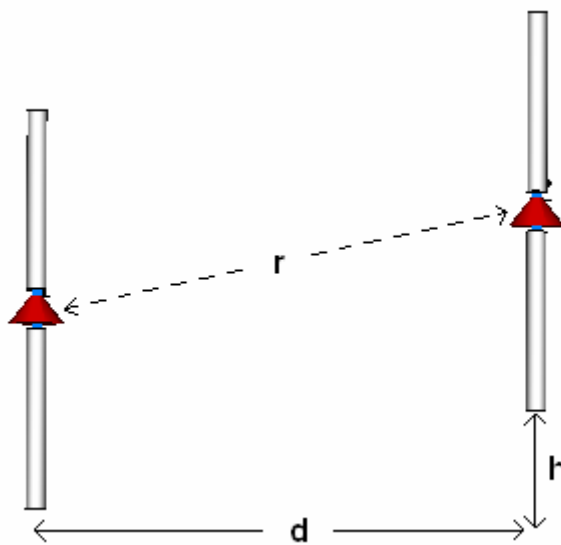


Figure 3-1 Two dipoles in free space, with distance “d” in horizontal plane, “h” in echelon

For the actual F-4 model, relative placement of antennas #6 and #10 is different from other antennas, in a sense that antennas #4, #5, #7 and #9 are placed in parallel, on the same horizontal plane; however antennas #6 and #10 are placed in echelon as compared to others. Therefore, dipoles representing #6 and #10 were moved certain amount in echelon.

### 3.2. Analysis on Hand-Made F-4 Model

In order to observe the effects of existence of geometrical details and surface variations over the aircraft fuselage, a more simple aircraft model was constructed, using shape creation tools of MWS<sup>®</sup>. This aircraft (called “hand-made” model) is composed of basic geometrical shapes such as elliptical cylinder (as the main fuselage), cones (as nose and tail) and triangles (as side wings and vertical stabilizer). All pieces, including the monopoles are made of PEC (perfect electric conductor). Since the geometry has much less details than the actual model does (such as air intake, exhaust, wingtips, stabilators, etc.), automatic mesh generator does not need to produce too many fix points, and overall mesh density, thus total number of meshes decreases considerably. By comparing the results with the ones of actual aircraft model, the differences in accuracy and computational complexity were observed. Figure 3-2 shows the side view of hand-made F-4 model, which was formed by basic geometrical shapes and equipped with identical antennas with the actual F-4 model.

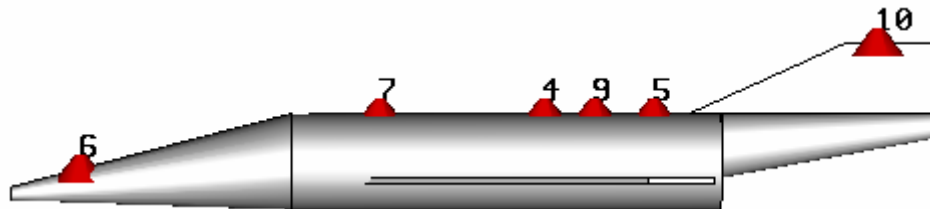


Figure 3-2 Side view of “hand-made” F-4 model

Using the same model, the effects of geometrical details on radiation characteristics were also observed. To be able to do a reasonable comparison of radiation pattern plots, special emphasis was given to mesh settings, where general mesh settings for both the actual and hand-made aircraft models were tried to be

kept as close as possible. Radiation pattern results for both hand-made and actual F-4 models were given in the following subsections of the thesis.

### 3.3. Analysis on Actual F-4 Model

As the last case of coupling analysis, similar simulations were done via actual F-4 model. The CAD model was imported from a pro-E file (\*.prt format) and it is composed of approximately 950 pieces of shells. The model was equipped with monopoles of length 250mm (quarter wavelength long at 300 MHz) with diameter of 9 mm. The antenna placement is almost identical with that of the 1:10 scale model, which is explained in detail in Chapter 4. Figure 3-3 shows the side view of actual F-4 model with desired monopoles mounted on it.

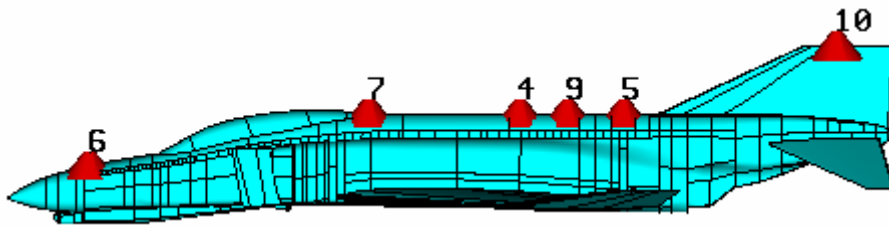


Figure 3-3 Side view of “actual” F-4 model

All surface shells (seen in figure above) forming the aircraft fuselage and monopoles are made of PEC. Along with the hand-made aircraft model, antenna-to-antenna coupling and radiation pattern analyses were done via this actual model. The results of both analyses are given in the following subsections of the thesis.

### 3.4. Comparison of Antenna-to-Antenna Coupling

For three different simulation models (dipoles in free space, monopoles on hand-made F-4 model and monopoles on actual F-4 model, respectively), antenna-to-antenna coupling values between each existing antenna and new antenna for any three alternative placement positions were calculated. For this purpose, three antennas, namely #6, #7 and #10 were assigned as “existing” antennas. A fourth “new” antenna was added on the platform, which was assumed to be likely to interfere with existing antennas. For the newly installed antenna, three different placement positions (#4, #5 and #9, respectively) on top of fuselage were assumed. Finally, antenna-to-antenna coupling values ( $S_{nm}$ ), which are listed in the table below, were calculated.

Table 3-1 Coupling scenarios between existing and new antennas

Position for new antenna	Existing antennas	S-parameters to be calculated
#4	#6, #7, #10	$S_{64}, S_{74}, S_{104}$
#5	#6, #7, #10	$S_{65}, S_{75}, S_{105}$
#9	#6, #7, #10	$S_{69}, S_{79}, S_{109}$

#### 3.4.1. Coupling between Existing Antennas and New Antenna at Position #4

S-parameters between all existing antennas (#6, #7, #10) and new antenna at position #4 were calculated, the results were compared for three different modeling cases, and given in the following figures.

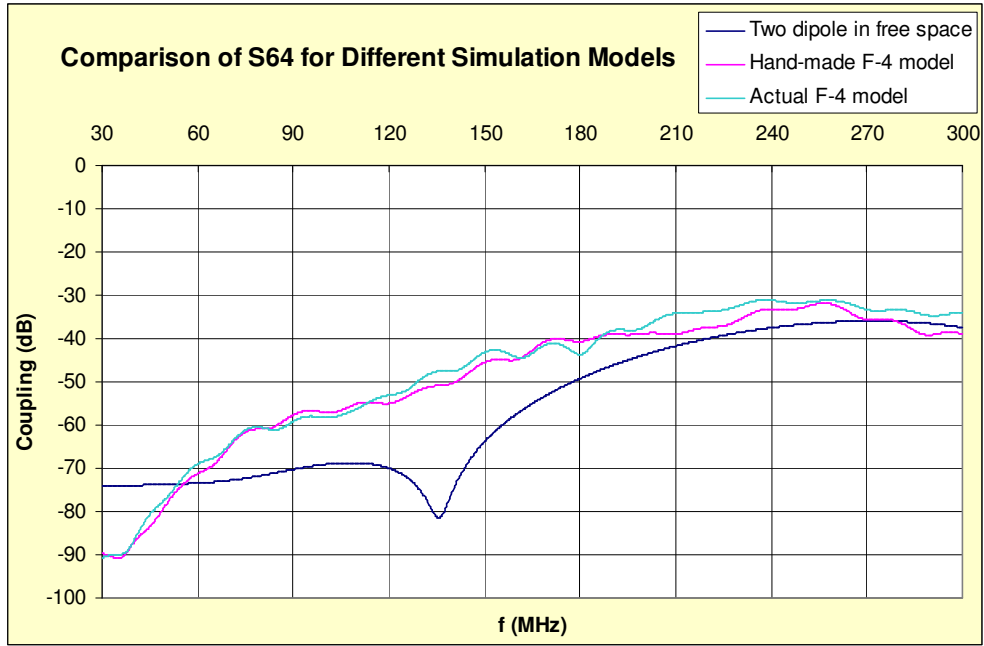


Figure 3-4 Coupling between antenna #6 and new antenna at position #4

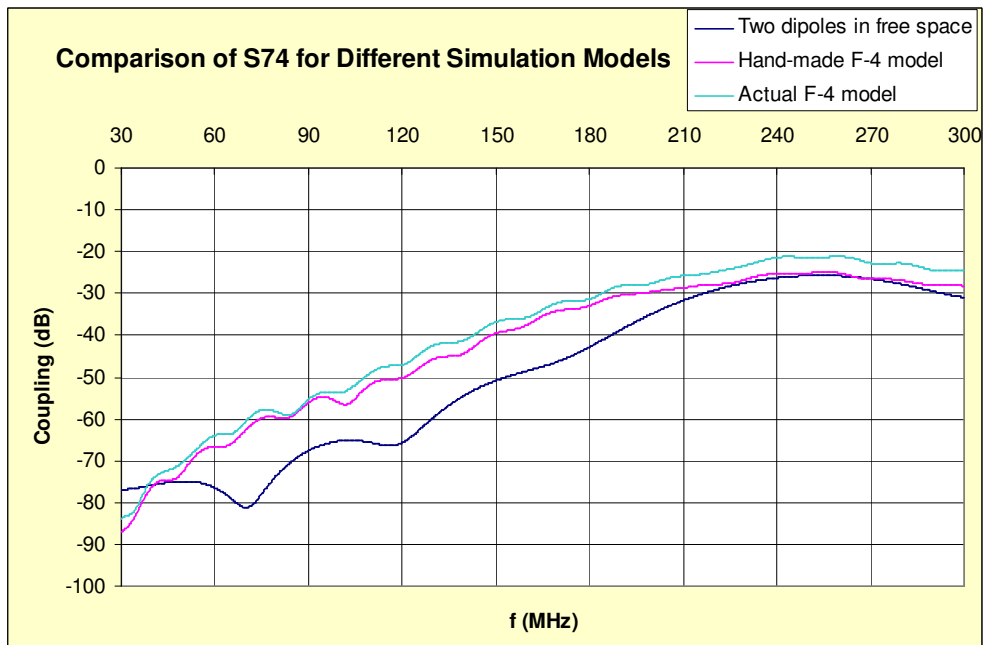


Figure 3-5 Coupling between antenna #7 and new antenna at position #4

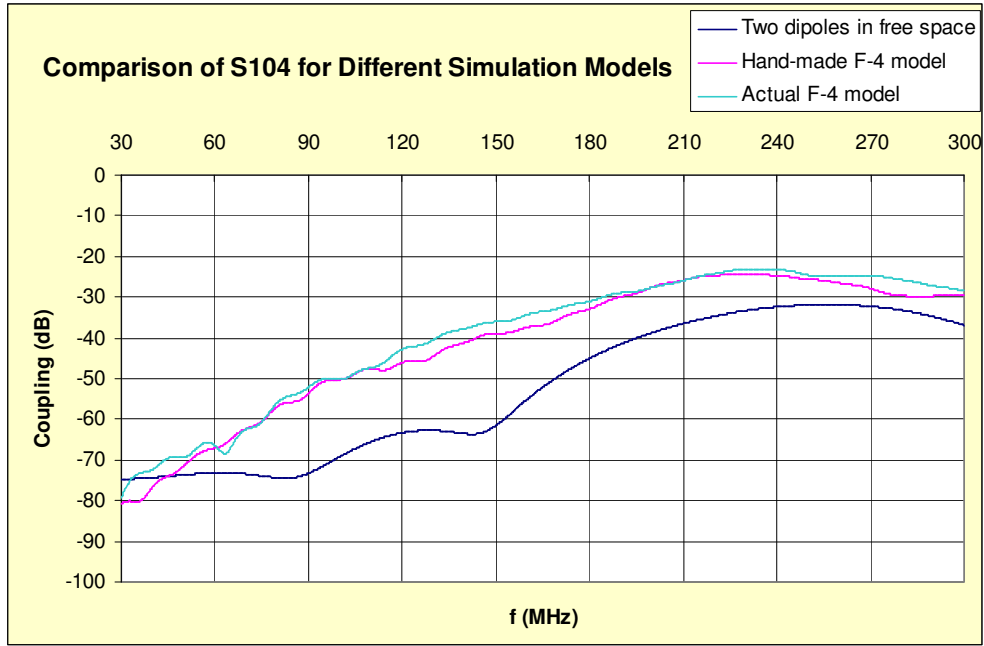


Figure 3-6 Coupling between antenna #10 and new antenna at position #4

### 3.4.2. Coupling between Existing Antennas and New Antenna at Position #5

S-parameters between all existing antennas (#6, #7, #10) and new antenna at position #5 were calculated, the results were compared for three different modeling cases, and given in the following figures.

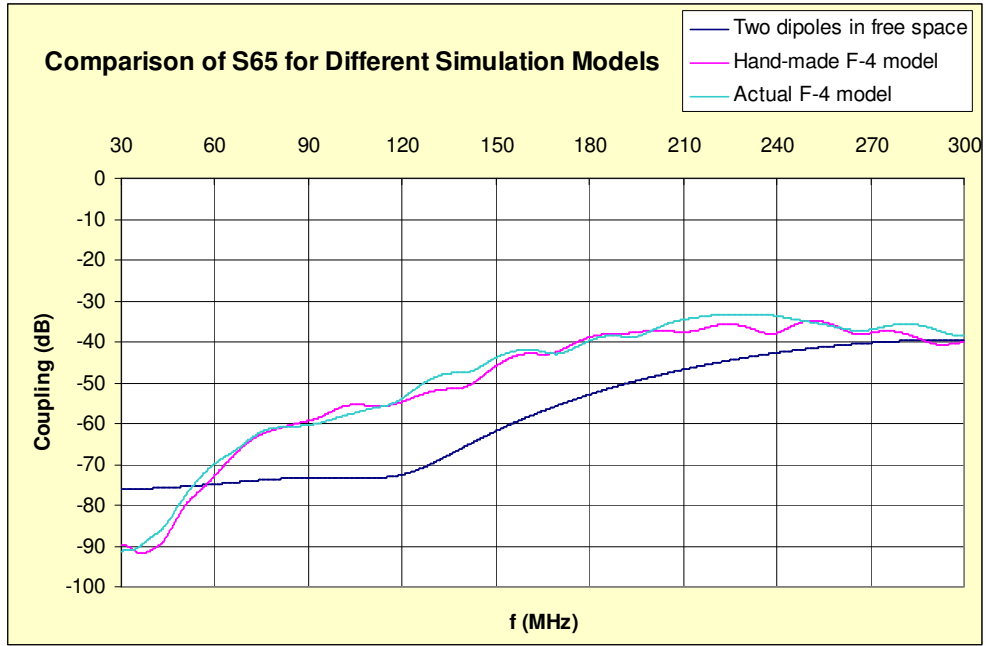


Figure 3-7 Coupling between antenna #6 and new antenna at position #5

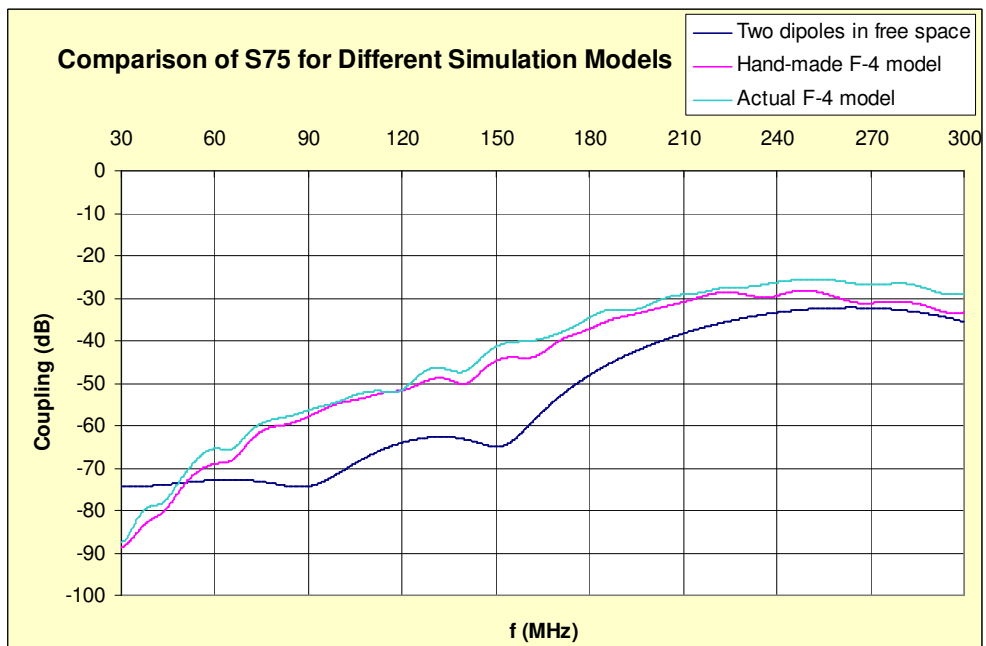


Figure 3-8 Coupling between antenna #7 and new antenna at position #5

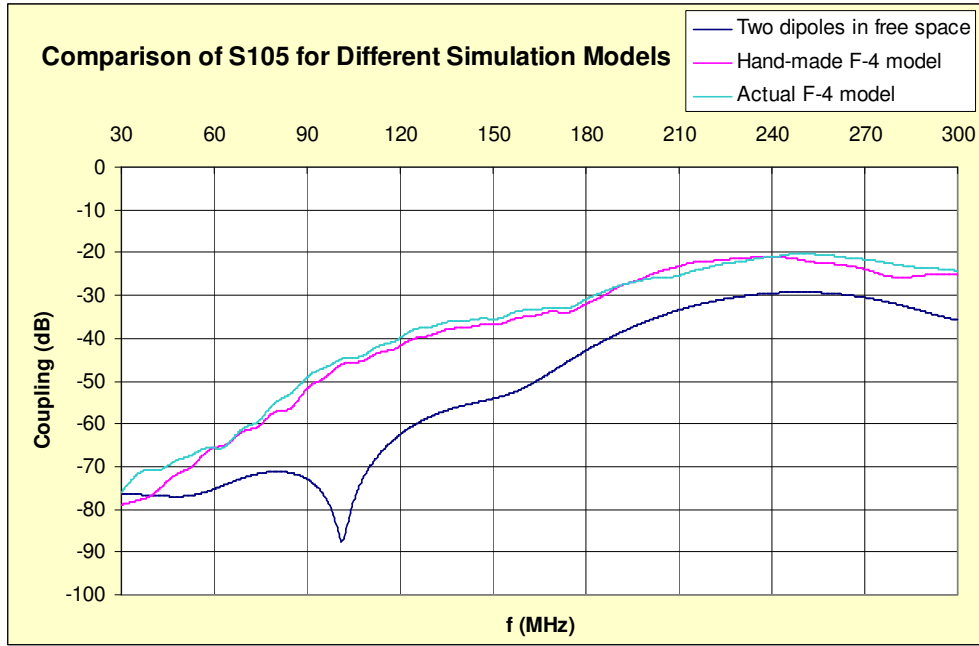


Figure 3-9 Coupling between antenna #10 and new antenna at position #5

### 3.4.3. Coupling between Existing Antennas and New Antenna at Position #5

S-parameters between all existing antennas (#6, #7, #10) and new antenna at position #9 were calculated, the results were compared for three different modeling cases, and given in the following figures.

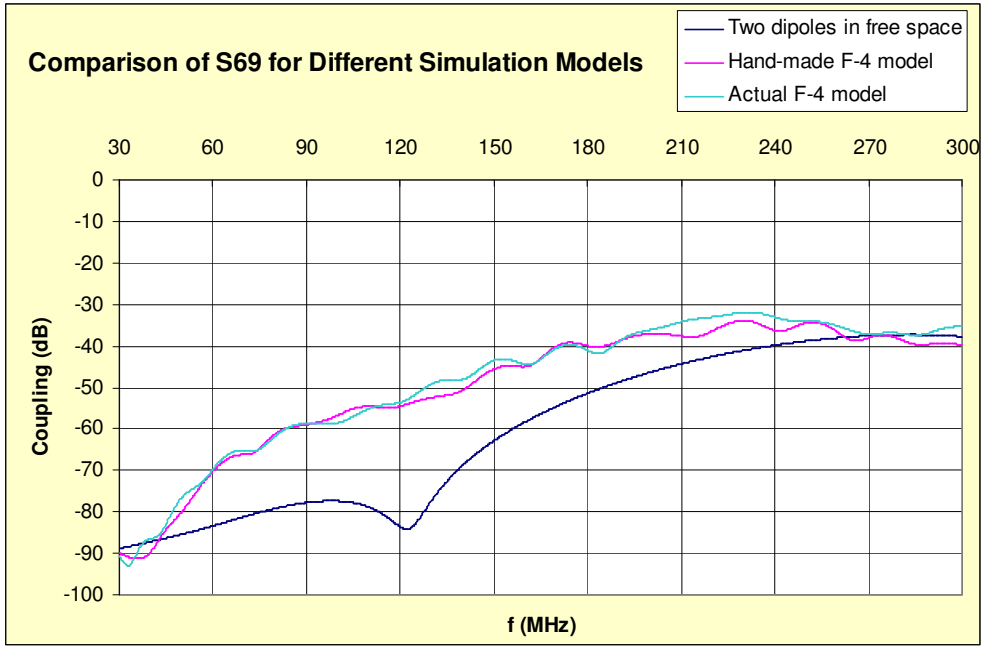


Figure 3-10 Coupling between antenna #6 and new antenna at position #9

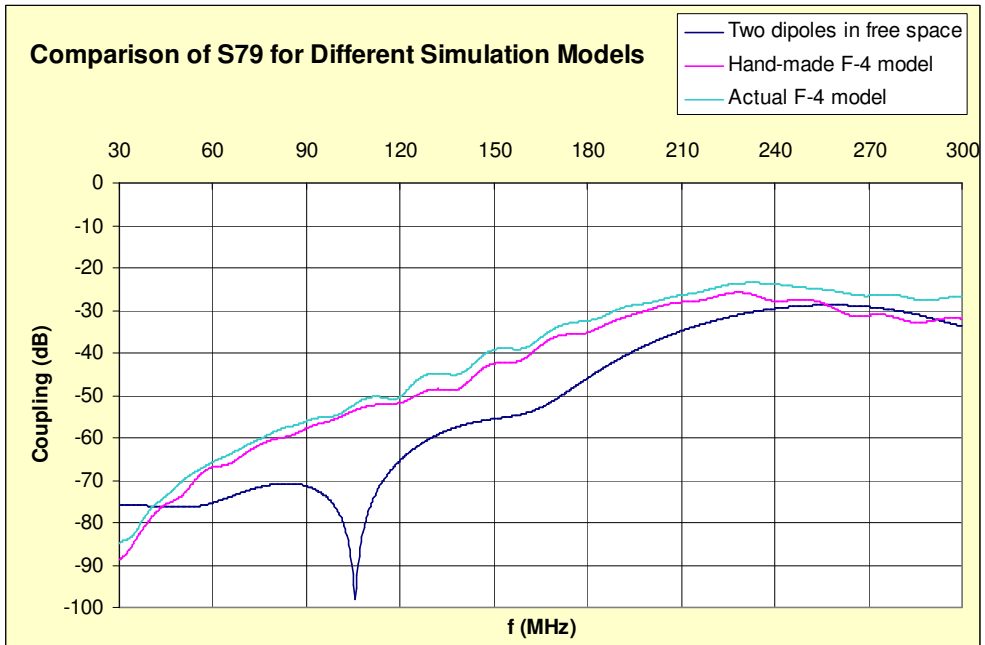


Figure 3-11 Coupling between antenna #7 and new antenna at position #9

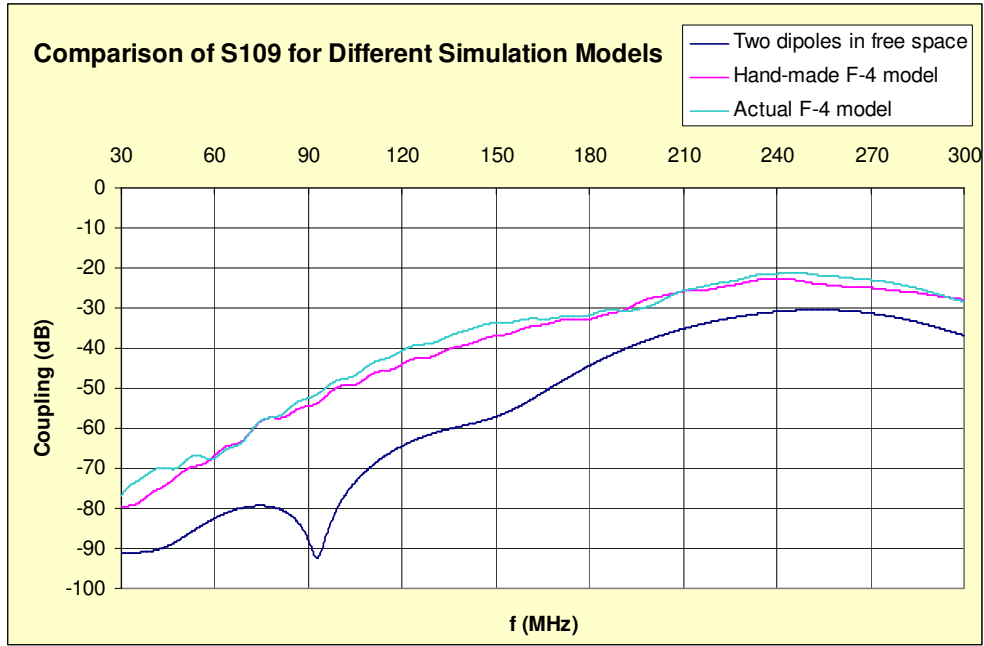


Figure 3-12 Coupling between antenna #10 and new antenna at position #9

### 3.4.4. Interpretation of Coupling Results

For each interaction scenario listed in Table 3-1, all coupling values were listed in figures above. At each figure, results obtained from three different simulation models were compared and differences between coupling values for each frequency within 30-300 MHz band were calculated. While doing this comparison, results obtained from “actual” F-4 model were used as the basis and the absolute value of coupling differences between results of three different simulation models at each frequency were averaged over frequency band of interest.

Table 3-2 Comparison of three different simulation models

S-parameters	[Actual model] – [two dipoles] (average value)	[Actual model] – [hand-made model] (average value)
S <sub>64</sub>	11,8	2,0
S <sub>74</sub>	10,6	3,0
S <sub>104</sub>	13,3	2,8
S <sub>65</sub>	13,1	1,8
S <sub>75</sub>	12,4	3,0
S <sub>105</sub>	14,3	1,8
S <sub>69</sub>	11,6	2,4
S <sub>79</sub>	11,9	3,1
S <sub>109</sub>	15,3	2,3
<b>Overall Average</b>	<b>12,7</b>	<b>2,5</b>

The results given in Table 3-2 show that, representation of monopoles over the fuselage by dipoles in free space does not yield accurate coupling results, namely the average difference between results of both models for 9 different S-parameters is about 12,7 dB, which is quite unacceptable for such a study. Considering hand-made F-4 model, the average difference between results of both models for 9 different S-parameters is about 2,5 dB. This value might be acceptable, when advantages of using a simplified geometry are taken into consideration.

Considering the results given in Table 3-2, method of representing antennas over the fuselage by dipoles in free space was discarded from the performance comparison. For the remaining two models, a comparison was done in terms of memory requirement and total simulation run time, and results were given in Table 3-3, below.

Table 3-3 Performance comparison for “actual” and “hand-made” F-4 models

	Hand-made F-4 model <sup>(1)</sup>	Actual F-4 model <sup>(2)</sup>	<b>Ratio (2)/(1)</b>
Total # of mesh cells	2.350.000	6.200.000	<b>2,6</b>
Avg. simulation run time per port (hh:mm)	01:15 hours	03:45 hours	<b>3</b>
Avg. post-processing time for a single rad.pattern plot (mm:ss)	00:45 minutes	02:25 minutes	<b>3,2</b>

As seen in Table 3-3, there is an average complexity factor of 3 between results of two simulation models. As regard to this, there is an average accuracy loss of 2,5 dB for coupling values. For a model this size, a three times more memory requirement or run time can be tolerated. However, depending on hardware configuration, a 2-3 times increase in total number of mesh cells might exceed the memory capacity of the computer, thus make the problem unsolvable. For certain cases, using such a simplified model, or sacrificing from mesh density (thus accuracy) can be preferred.

### **3.5. Comparison of Radiation Patterns**

Due to the assumed antenna placement for existing antennas and three positions of new antenna, a set of radiation pattern plots were calculated using hand-made and actual F-4 models, respectively. The results were then compared and listed in the following figures.

The radiation pattern analyses were divided into two groups. The first group covers the radiation pattern plots of each existing antenna, obtained by simulating both hand-made and actual F-4 model. The intention is to compare radiation pattern results of two different simulation models and comment on the validity of using simplified F-4 model in this sense. The second group of simulations covers

radiation pattern plots of new antenna, which are calculated for three different positions of that antenna (#4, #5 and #9). For this purpose, only results of actual F-4 model were used and equivalent pattern plots for different antenna positions were compared on each graph. All radiation patterns were plotted at 300 MHz, where all monopoles were of quarter wavelength long.

In order to limit total number of pattern plots, the study was limited only to polar directivity plots in azimuth plane ( $\theta=90^\circ$ ,  $0^\circ < \varphi < 360^\circ$ ) and elevation plane ( $\varphi=90^\circ$ ,  $0^\circ < \theta < 180^\circ$  and  $\varphi=270^\circ$ ,  $0^\circ < \theta < 180^\circ$ ). Polar patterns in azimuth plane were plotted in a regular form of directivity (in dBi) vs.  $\varphi$  (in degrees). However, since elevation patterns are defined for two different values of phi ( $\varphi=90^\circ$  and  $\varphi=270^\circ$ ), these two data sets were combined into one data set, where phi was kept fixed at  $90^\circ$  and theta was traced from  $-180^\circ$  to  $180^\circ$ , to form a complete circle over elevation plane. This manipulation helps to define elevation pattern plot for a single phi value ( $\varphi=90^\circ$  only) and plot a full elevation circle with only theta dependence. This manipulation in spherical coordinates is illustrated in Figure 3-13. All patterns were plotted with a resolution of  $1^\circ$  for both theta and phi.

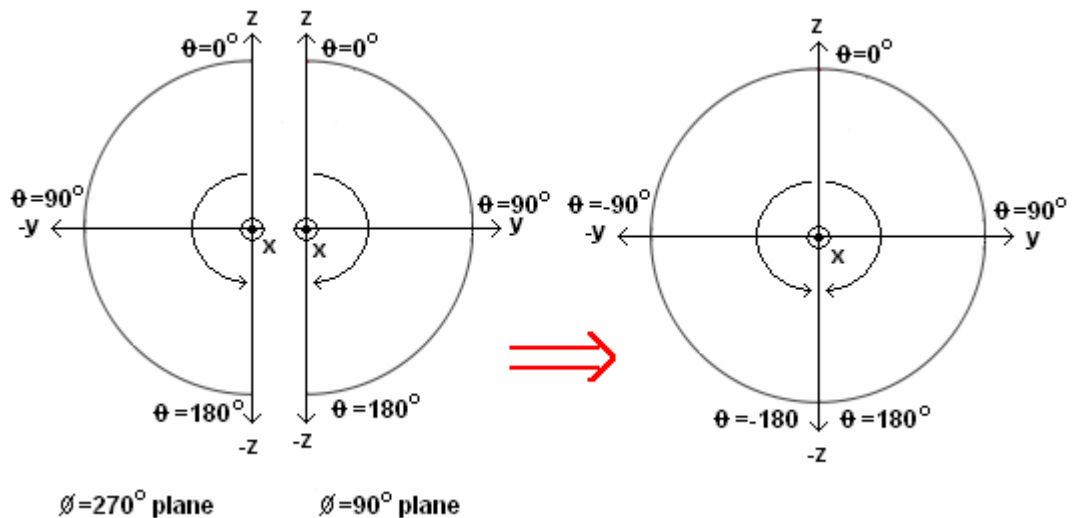


Figure 3-13 Combination of  $\varphi=90^\circ$  and  $\varphi=270^\circ$  planes for elevation plane

Additionally, Figure 3-14 shows the orientation of F-4 aircraft model both in cartesian and spherical coordinates. As seen in the figure, the aircraft lies horizontally on x-y plane; the longitudinal axis of aircraft fuselage extends in y-axis. Thus, azimuth plane ( $\theta=90^\circ$ ) corresponds to x-y plane; and “manipulated” elevation plane ( $\phi=90^\circ$  and  $\phi=270^\circ$ ) corresponds to y-z plane.

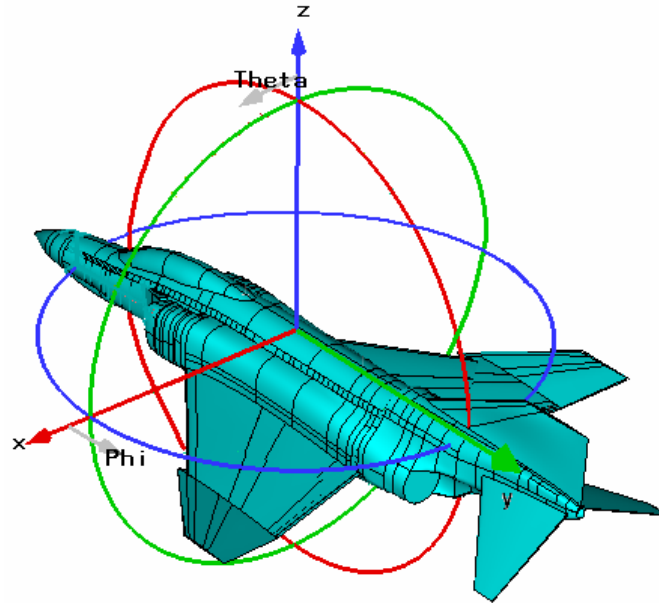


Figure 3-14 Orientation of F-4 aircraft model in cartesian & spherical coordinates

### 3.5.1. Comparison of Radiation Pattern Plots for Hand-made & Actual F-4 Model (Existing Antennas)

This part covers the radiation pattern plots of each existing antenna, obtained by simulating hand-made and actual F-4 models, respectively. For three existing antennas (#6, #7 and #10), polar patterns in azimuth and elevation planes were computed and compared for two F-4 models. The polar pattern plots of existing antennas for both azimuth and elevation planes are given in the following figures.

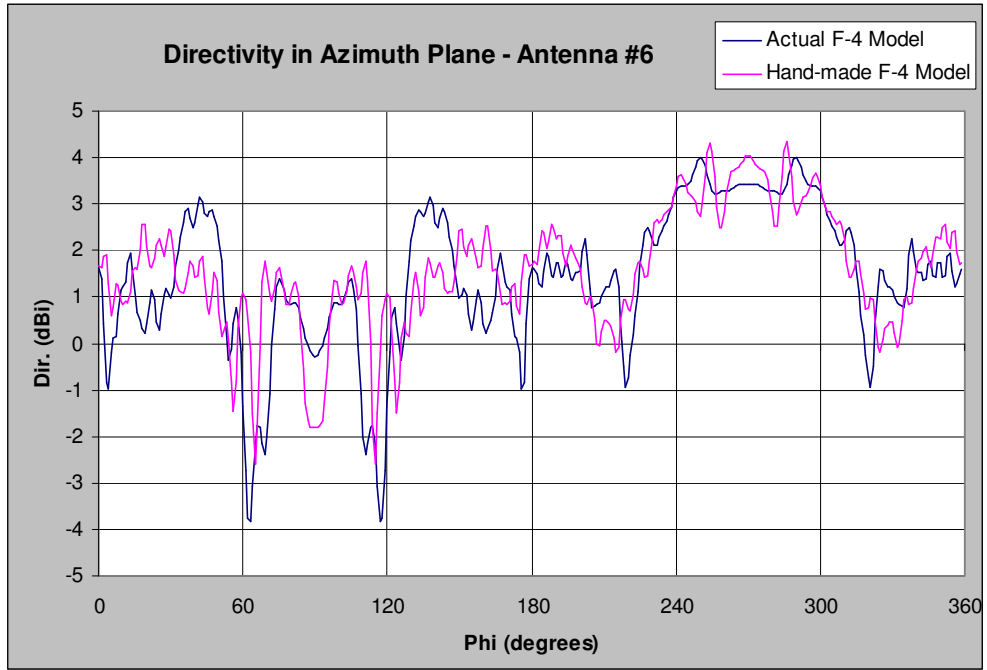


Figure 3-15 Directivity in azimuth plane - antenna #6 (actual vs. hand-made F-4)

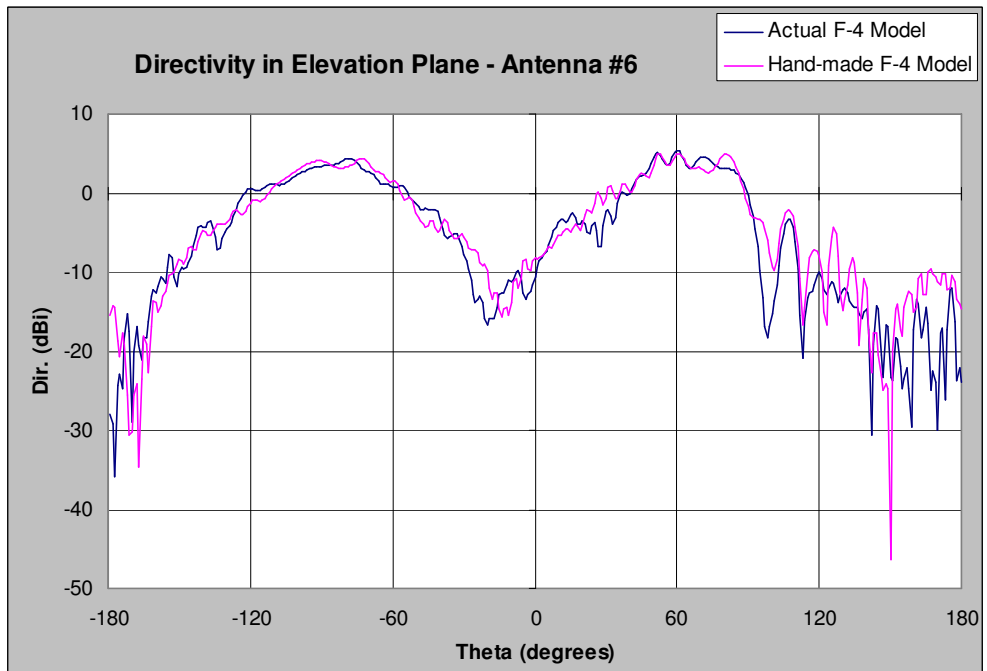


Figure 3-16 Directivity in elevation plane - antenna #6 (actual vs. hand-made F-4)

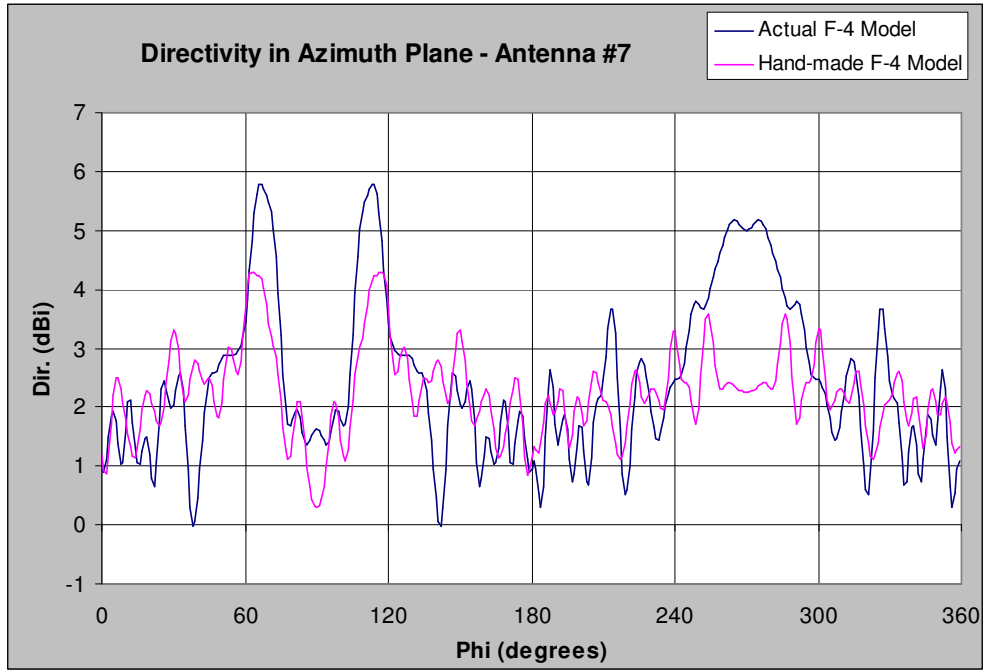


Figure 3-17 Directivity in azimuth plane - antenna #7 (actual vs. hand-made F-4)

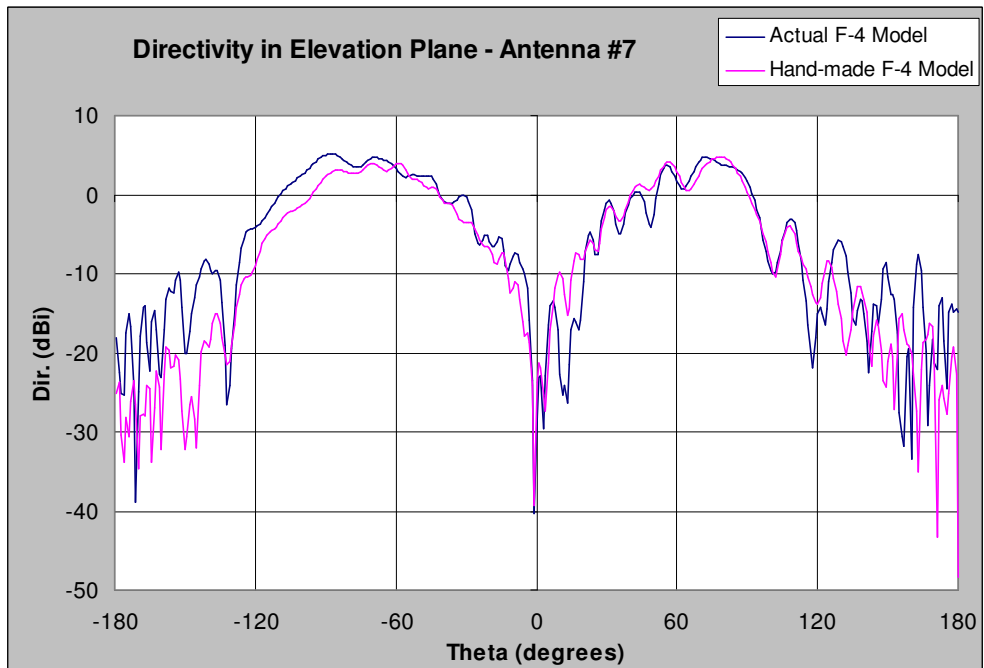


Figure 3-18 Directivity in elevation plane - antenna #7 (actual vs. hand-made F-4)

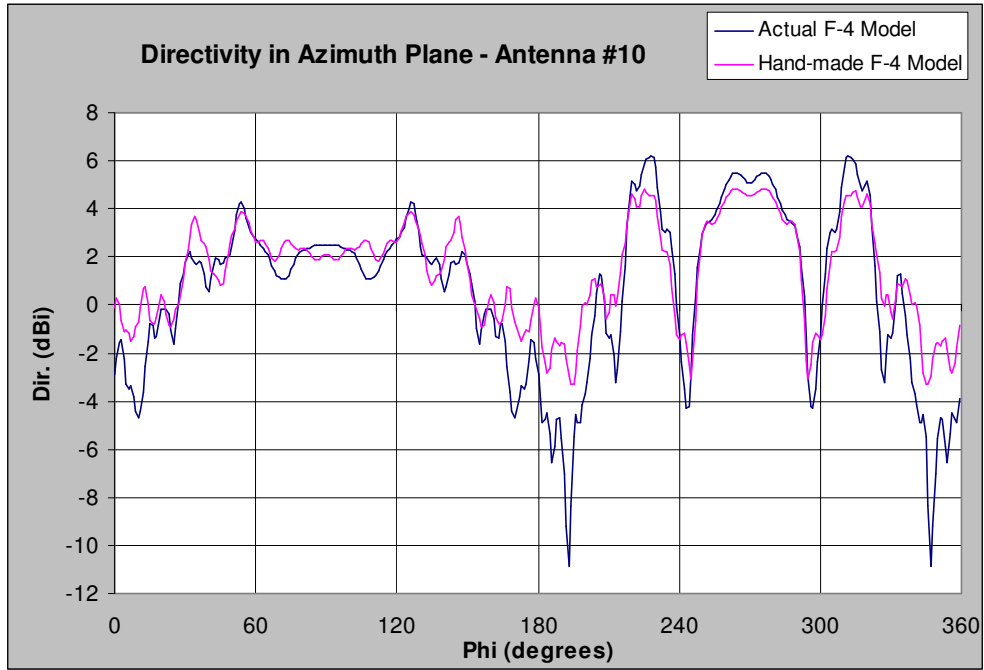


Figure 3-19 Directivity in azimuth plane - antenna #10 (actual vs. hand-made F-4)

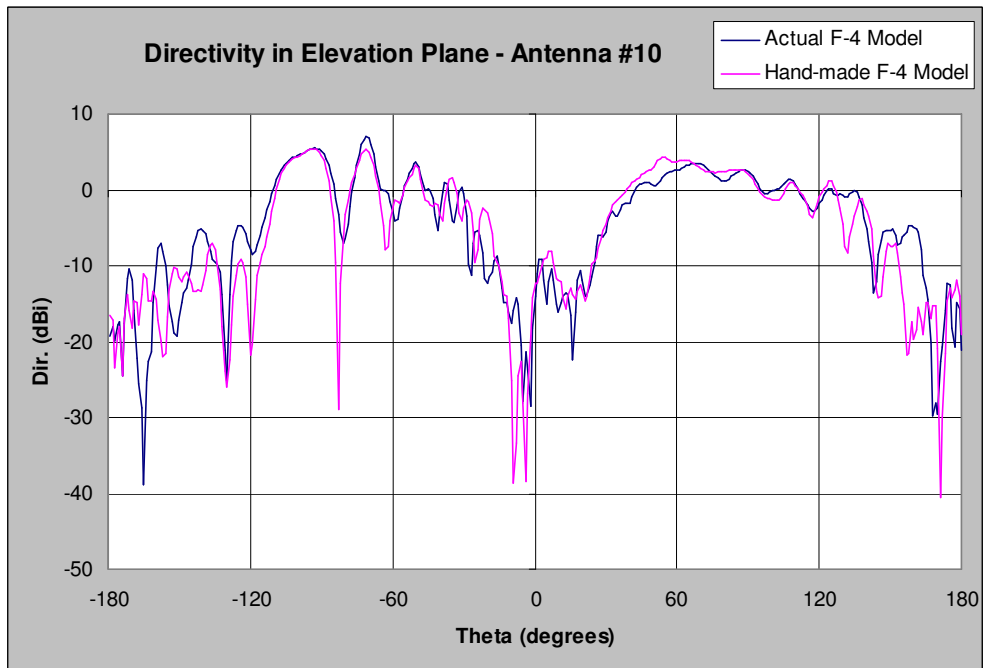


Figure 3-20 Directivity in elevation plane - antenna#10 (actual vs. hand-made F-4)

The directivities of existing antennas computed for both hand-made and actual F-4 models show that; overall patterns obtained using different models for both azimuth and elevation planes are identical. However, at certain cases, the maxima and null angles differ considerably. Therefore, it was concluded that the simplified F-4 model gives a general idea about the overall radiation behavior of the platform; but does not yield very accurate radiation results, both in terms of directivity and angle of main/side lobes.

### **3.5.2. Comparison of Radiation Pattern Plots of New Antenna at 3 Different Positions**

This part of simulations covers the radiation pattern plots of new antenna for its three placement positions on top of fuselage. For this study, the actual F-4 model was used and each set of polar plots was compared for each specific antenna location (#4, #5 and #9) of new antenna.

Similarly, polar directivity plots in azimuth and elevation planes were calculated and tabulated in the figures below.

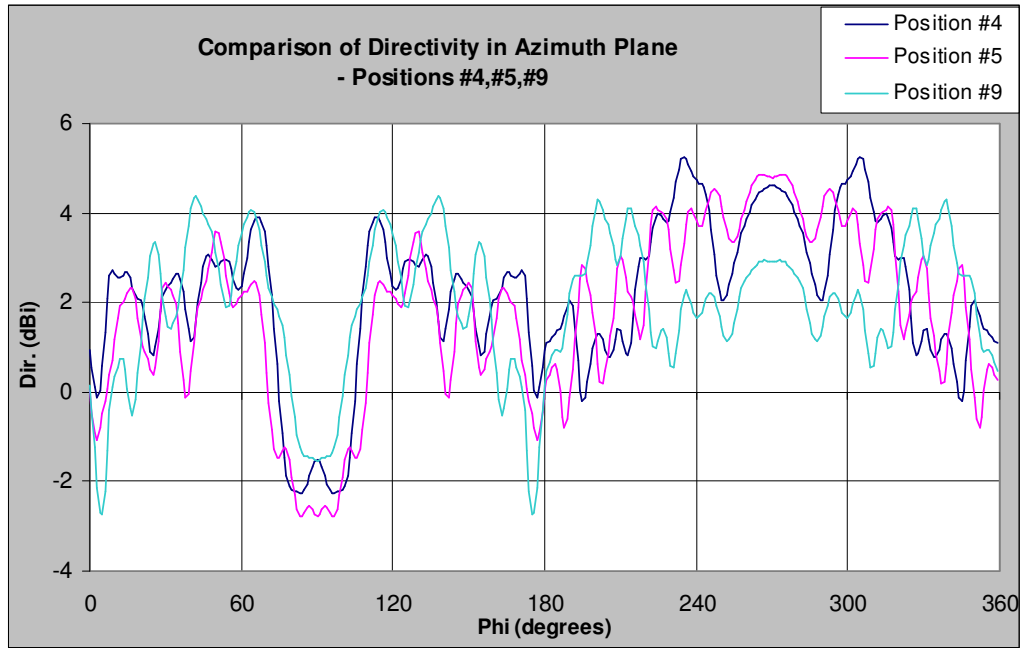


Figure 3-21 Directivity of new antenna for three positions (azimuth plane)

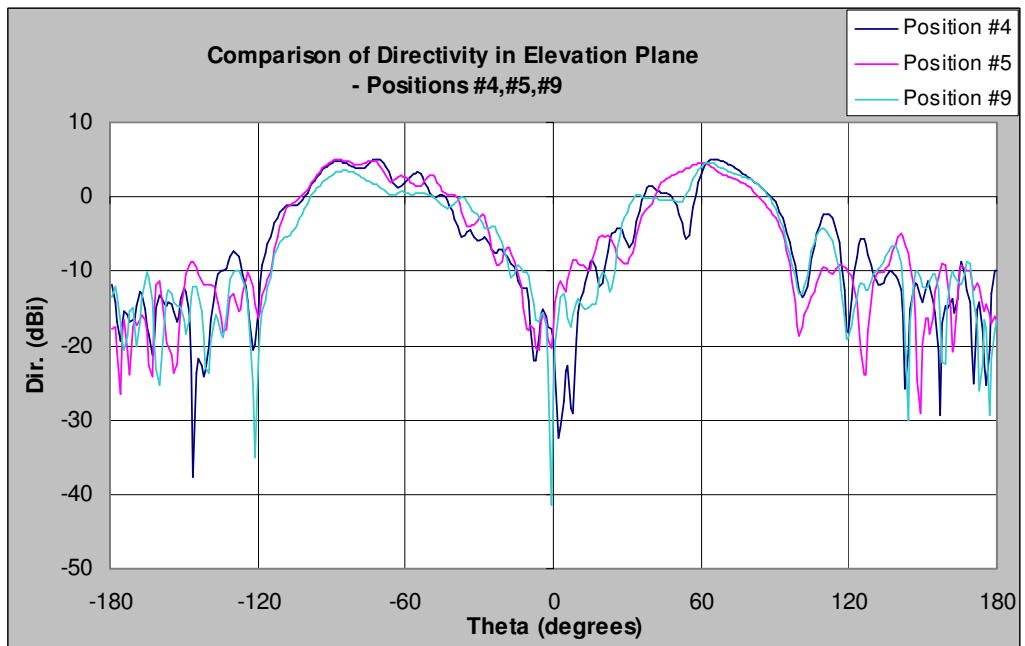


Figure 3-22 Directivity of new antenna at three positions (elevation plane)

For the directivity in azimuth plane, by observing the polar plot in Figure 3-21, the following conclusions were done;

- Since all antennas are placed vertically on top of fuselage, which acts similarly as a horizontal ground plane of finite size, the radiation pattern in azimuth plane tends to be quasi-omnidirectional. For each antenna position, directivity in azimuth plane varies within a margin of approximately 7 dB.
- For all antenna positions, maximum directivity tends to be in  $-y$  direction, towards the nose ( $\phi=270^\circ$ ) of aircraft.
- For all antenna positions, there is a null in  $+y$  direction, towards the tail ( $\phi=90^\circ$ ). The deepest null occurs for the position #5, where the monopole is at the back-most position over the fuselage. Therefore, it is concluded that, within this rough range of antenna positions, as the antenna slides back and approaches the vertical stabilizer, it is more shadowed by the stabilizer and directivity is reduced in backward direction ( $\phi=90^\circ$ ).

Similarly, by looking at Figure 3-22, the following conclusions about directivity in elevation plane were done;

- For all three antenna positions, all elevation patterns resemble well known “figure of eight” pattern of a dipole. This pattern has nulls at  $\theta=0^\circ$  and  $\theta=180^\circ$ . This figure of eight pattern is more evident and regular in the upper hemisphere ( $-90^\circ<\theta<90^\circ$ ).
- For the lower hemisphere ( $-180^\circ<\theta<-90^\circ$  plus  $90^\circ<\theta<180^\circ$ ), the shadowing effect of fuselage and side wings are more clearly observed and many side lobes of relatively small amplitudes (typically -10 to -20 dBi) are observed.
- The effect of vertical stabilizer reveals itself in a way that, the main beam is wider for negative theta values, and narrower for positive theta values. Around  $\theta=90^\circ$ , there is a null for each antenna position. Concurrently, the deepest null occurs for position #5, which is closest to vertical stabilizer.

## CHAPTER IV

### SCALE MODEL MEASUREMENTS

In this chapter, the use of scale models in antenna measurements was discussed. Firstly, reasons of using scale models in electromagnetic studies were investigated. Then, certain rules of down-scaling the geometry were stated, and the theory behind scale modeling was introduced.

Since the content of this thesis is electromagnetic analysis of certain antennas mounted on an F-4 aircraft, the construction phase of 1:10 down-scaled F-4 model was explained. Then the measurement phase was introduced, including measurement environment and equipment used during measurements.

Finally, certain S-parameter measurements were done and the results were compared with outputs of simulations done via MWS<sup>®</sup>. Reasons of any consistency and/or discrepancy were investigated and explained.

#### **4.1. Reasons for Using Scale Models in Electromagnetics**

In electromagnetics, there are certain cases where working with scale models of a problem is much preferable than working on the actual platform. This may be due to size considerations, where working on an actual platform might bring great difficulties; or it might not be possible to convert the problem to a simple canonical form, which can be approximated to previously solved problems, and that the solution can be found analytically. Therefore, scale model measurements

are preferable for cases where electrical properties of an antenna is difficult to estimate within its operational environment such as ships, aircraft, vehicles, satellites, large conducting structures, etc. [16].

The main advantage of using scale models for antenna studies is narrowing down the actual problem size. To illustrate, consider an antenna analysis done on an aircraft, which is, to some extent, studied in this thesis. An antenna-to-antenna coupling or radiation pattern measurement on such a big platform requires facilities such as huge anechoic chambers, appropriate masts and turntables for manipulating the aircraft. For such cases, scale models offer advantages over actual size measurements.

Another advantage of scale modeling is the ability of varying the environment or structure with ease. For example, a moving antenna system can be handled easily and iterative measurements for different positions/orientations can be performed.

Under the scope of this thesis, the electrical characteristics of antennas mounted on an F-4 aircraft, which is an 18 meter long military aircraft, were investigated. Ideally, the measurements have to be performed in a reflection-free and RF-silent environment. In order to achieve these conditions, the aircraft and the measurement equipment shall be put in a huge anechoic chamber, an open area test site or far field range [17]. Constructing such a facility which has proper size for an F-4 aircraft is extremely expensive and requires great labor. So, it is feasible to switch to a smaller size problem and do the necessary measurements in a moderate size model and a within a more controllable environment.

Another necessity of scaling down the problem arises from the fact that, obtaining far field condition is much more difficult for the actual size of such a problem. Thus, in order to have accurate radiation results (i.e. radiation pattern or radar cross section measurements), far field condition has to be satisfied.

There are different far field criteria, each defined for different conditions to be satisfied. For linear antennas, in order to achieve relatively small phase taper, the far field condition is as follows;

$$R > \frac{2 \cdot L^2}{\lambda} \quad (4-1)$$

where,

R: minimum distance to the antenna which satisfies far field condition

L: length of the linear antenna

$\lambda$ : wavelength

Consider two antenna systems which are placed in closed vicinity in space, and satisfying Formula 4.1. There is another concern related to inductive coupling between two antennas, resulting in interaction of moving charges on them; meaning that the existence of an antenna affects the current distribution on the other one and vice versa. Thus input impedance and radiation pattern of any antenna is affected by the other one [17]. This inductive coupling mechanism is avoided approximately at a distance of  $20\lambda$ , where, for a linear antenna with length of fraction of a wavelength, this condition imposes a much larger far field distance than the one stated in Formula 4.1, above.

A third approach in determining the far field takes the size of platform on which the antenna is mounted. This approach proposes that total distance to the antenna platform shall be  $20D$ , where  $D$  is the largest dimension of the platform on which antenna is mounted. For measuring antennas mounted on a relatively large platform, this condition is the dominating one of the three. For instance, assume a 1:10 down-scaled aircraft model of length 180 cm, equipped with communication antennas operating around 300 MHz. The frequency is up-scaled to 3 GHz, where  $\lambda$  equals 10 cm. Also assuming quarter wave monopoles of length 2,5 cm (relying on image theory, quarter wave monopole is accounted as half wave dipole),  $2L^2/\lambda$  expression requires far field distance of  $\lambda/2$ , which equals 5 cm. Considering the inductive coupling between scaled antenna and measurement

antenna, the far field condition requires a distance of  $20\lambda$ , which is 2 meters. Finally, considering not only the antenna size and frequency, but the size of platform, twenty times aircraft length (equals 36 meters) will best represent far field condition, where the overall structure would be treated as a point source [17]. Considering the actual size of the platform, this distance would be ten times greater, which would definitely be harder to satisfy.

In addition to those, working with the scale model assures a more controlled measurement environment. Actually, most antenna measurements like radiation pattern, RCS, S-parameter measurements require an RF-silent and reflection-free medium. For the platform itself, this can be achieved either by taking the measurements during flight, or, as mentioned above, putting the platform into a huge anechoic chamber. Both approaches are very expensive and laborious. From the scale model point of view, a moderate size anechoic chamber fulfills all these requirements.

## **4.2. Rules of Scale Modeling**

The theory of scale modeling has been established by Sinclair [18]. In most general sense, physical dimensions of the platform are reduced at a certain ratio and frequency is increased at the same ratio. However, other electrical parameters such as capacitance (C), inductance (H) and conductivity ( $\sigma$ ) also have to be scaled. Besides, permittivity ( $\epsilon$ ) and permeability ( $\mu$ ) have to be kept unchanged. As a result, for a perfect model, outcome of measurements such as impedance, gain, beam width, side lobe level, current distribution remain unchanged [18].

Among those parameters which have to be up/down scaled, conductivity is of special concern. Assume that the actual platform is composed of a highly conductive material like aluminum and the model has a down-scaling ratio of 10:1. Then, it is not possible to find a 10 times more conductive material than

aluminum. Silver ( $\sigma = 63 \times 10^6$  S/m) or silver plated conductors are best choice for plating the model; still they offer about twice the conductivity of aluminum ( $\sigma = 37,7 \times 10^6$  S/m) [19]. Besides, copper ( $\sigma = 59,6 \times 10^6$  S/m) is more preferably used due to its very high conductivity (second highest after silver) [19]. Although up-scaling the conductivity is not possible, it does not cause much difference for relatively highly conductive metals [18]. Another difficulty of conductivity scaling arises when dealing with antenna systems operating above ground, which has considerably low conductivity. While working on scale models of surface ships or land platforms with antennas, it is important to have good electrical representation of sea or ground; since ground plane with low conductivity affects overall electrical performance of antennas, which operate at relatively lower frequencies [18]. To be able to increase conductivity at desired degree while keeping permittivity and permeability constant, special emulsions need to be prepared. However, these kinds of applications may suffer from frequency dependence of conductivity, which causes dispersion [20]. Since this study covers a highly conductive platform which is placed in free space, such drawbacks of conductivity scaling are not a concern. Table 4-1 lists the rules of constructing scale models.

Table 4-1 Rules of modifying electrical parameters due to scaling factor “n”

Scaling factor	“n” (n>1)
Frequency (f)	Multiply by “n”
Wavelength ( $\lambda$ )	Divide by “n”
Electrical length (d/ $\lambda$ )	No change
Permittivity ( $\epsilon$ )	No change
Permeability ( $\mu$ )	No change
Capacitance (C)	Divide by “n”
Inductance (H)	Divide by “n”
Conductivity ( $\sigma$ )	Multiply by “n”

### 4.3. 1:10 Scaled F-4 Aircraft Model

Within the scope of this thesis, a 1:10 down-scaled F-4 aircraft model was constructed and equipped with certain monopole antennas. In order to verify the validity of simulation results obtained via MWS<sup>®</sup>, certain S-parameter measurements were done on this model.

During constructing the model, firstly a plastic F-4 mock-up was purchased and its cast was manufactured from fiberglass. Using this cast, a separate F-4 was molded, again from fiberglass, which has a thickness 3 to 5 mm. Fiberglass was preferred due to its relatively low weight and high strength. In order to provide rigidity, the fuselage, side wings and delta tails were molded separately, and later on, attached to each other with screws. Considering cabling for antennas, a rectangular opening was constructed on the top-center of fuselage. This opening helped to reach any point inside the fuselage, assemble RF cables-connectors and the monopoles also.

For obtaining good conductivity over fuselage, first approach was electroplating it with copper. However, electroplating non-conductive materials with copper requires special treatment. In order to achieve proper deposition of copper ions on the surface, the surface has to have certain initial conductivity and smoothness. To have an initially conductive surface, fiberglass was first coated with thin film of silver. However, this process failed due to inappropriate surface roughness of fiberglass; so it was concluded that copper electroplating was not possible. As alternative to this, copper sheets of 50  $\mu\text{m}$  thick were used to cover all over the fuselage. Whenever necessary, copper sheet was heated to get softened and patched to fuselage. Another difficulty was that, several pieces of copper sheet had to be attached for obtaining electrical continuation all over the fuselage. This was done by soldering each intersecting/overlapping face of copper sheets. This process was carefully applied especially near antenna ports, where current

distribution, thus impedance and radiation characteristics would most severely be affected by imperfect electrical continuity.

After covering all the surfaces, antenna positions were determined, being similar to those on an actual F-4 aircraft. In addition, some extra positions were determined as “alternative” locations for a “new” antenna. All antennas were modeled as monopoles, which were constructed as extensions of inner conductors of flexible coaxial cables, which feed them. Each antenna plus its cabling was constructed from a half coaxial cable assembly, one end of whom was terminated by a 4-flange SMA (female) connector, and the other end cut out and left unterminated . The bottom-center surface of F-4 model was reserved for assembling these SMA connectors, and all connectors were attached to this bottom face by screws.

Each coaxial cable was run through inside of fuselage, up to its corresponding assembling point. There, the fuselage was drilled and coaxial cable was extracted outward. Then, the cable was gently cut, dielectric layer was removed and monopole length was adjusted. The measurement equipment covers the frequency band of 10MHz-3GHz. So, an upper frequency limit of 3GHz for scale model corresponds to operating frequency of 300MHz for the real aircraft. In a parallel manner, antenna simulations (mentioned in Chapter III) had also covered the frequency band of 30-300MHz. Monopoles were selected to be quarter wavelength (near first resonant) at maximum frequency of interest (3GHz), where wavelength equals 100 mm. Length of each monopole was adjusted to be  $25 \pm 0,5$  mm. The thickness of monopoles is the same as that of coaxial cable's inner conductor, which equals 0,9 mm. Essentially, the F-4 model was equipped with relatively thick monopoles (length to radius ratio is approximately 53).

The outer conductor, which acts as ground connection of the monopole, was soldered to the copper plating all around, to form 360° metallic contact. After assembling all monopoles, the top cover of fuselage was put in place and soldered. Finally, a 1:10 down-scaled copper-plated model, which was equipped with ten

identical quarter wave monopoles over its fuselage, was achieved. The following figures depict the plating, cabling and antenna mounting phases of the model.



Figure 4-1 Overall view of model cabling (top cover removed)



Figure 4-2 Detailed view of coaxial cables inside the fuselage (top cover opened)



Figure 4-3 SMA (female) connectors assembled on bottom face



Figure 4-4 Detailed view of a monopole over the fuselage

Although scale models are assumed to be a rough representation of the actual platform, there are certain discrepancies between the model and platform itself. These discrepancies can be listed as follows:

- Sometimes, the antenna itself may be very hard to down-scale and construct with small dimensions. For such cases, an alternative solution would be using simpler antennas which have similar radiation characteristics. For instance, monopole can be used for representing any quasi-omnidirectional antenna; or an open ended waveguide can be used as an alternative to a relatively high gain antenna [1].
- In fact, actual linear antennas on real platforms have very good efficiency and VSWR performance over a much broader bandwidth as compared to a monopole. This is achieved by using electronic impedance matching units, multi-stage tuning filters or electronic switches which adjust the electrical length of that antenna [21]. In scale models, it is not possible to adopt such impedance matching devices. An alternative to this inequivalence would be

to divide the entire operation band into sub-bands and use a series of different antennas with different but complementary VSWR performances.

- Although scale model is supposed to be a smaller but exact representation of the actual platform, there might be local or global scaling errors, thus considerable differences in shape. For example, cockpit details, engine air intakes/exhausts, certain composite or dielectric coatings were omitted while constructing the scale model. However, the intention of this study is to compare the simulation results of MWS<sup>®</sup> and measurements. Thus, the main criterion is to have as much similarity between scale model and simulated geometry as possible. So, it was preferred not to deal with structural details of actual aircraft; contrarily, the scale model was kept as similar as possible to the CAD model within MWS<sup>®</sup>. Additionally, PEC surfaces within MWS<sup>®</sup> were simply represented by copper-plated surfaces.

#### **4.4. Measurement Environment**

Ideally, such scale model measurements are performed in anechoic chambers. An anechoic chamber serves for two main purposes. Firstly, it provides sufficient shielding to keep the unwanted RF signals out of the room. Reciprocally, for cases where high RF power levels are anticipated, the room arrests the high fields inside. Shielding effectiveness of a moderate type room is 60 to 120 dB, depending on the frequency, type of electromagnetic field components (whether electric or magnetic) and certain construction details of the chamber; such as the metallic junctions on the plates of the walls, RF seals (gaskets) through the doors, shape of ventilation ports, connector panels, etc. Since civil and military broadcast occupies a considerably broad portion of the RF spectrum, a shielded enclosure is required, especially for working with low RF signal levels.

Another feature of an anechoic chamber is, as its name implies; it provides an “anechoic” medium for radiating fields. An anechoic chamber without RF

absorbers is basically a big room with conductive walls, which acts like a rectangular cavity resonator. Depending on frequency and room dimensions, certain modes are excited and standing waves occur. This further introduces uncertainties to the radiated measurements. For better simulating free space condition, the inner walls of shielded room are covered with RF absorbent material to decrease reflections from the walls.

There are different types of RF absorbent materials to serve different applications. Depending on frequency, source type (whether electric or magnetic) and angle of incidence, these materials provide adequate amount of absorption and reduce the disturbing effect of reflected waves from the walls of the shielded room.

Within the scope of this thesis, measurements were conducted in a hangar, instead of an anechoic chamber. Since the hangar contains reflective metallic assemblies on its walls and ceiling, care was given to placement of the aircraft and measurement equipment. Primary precautions which were taken to overcome measurement errors due to environmental imperfections are listed below:

- The aircraft was placed on top of wooden masts and raised 1 meter above ground.
- No metallic substances near aircraft were allowed within proximity of 3 meters.
- Ceiling of hangar is high enough (~8 meters), hence no reflection from ceiling was anticipated.
- To avoid any ground reflection effects, only antennas which were mounted on top of fuselage were included in the study.
- The ambient RF signal levels were recorded within measurement frequency band (300MHz - 3GHz). It was deduced that, with absence of any nearby mobile transmitting unit (UHF transmitter, mobile phone/handset, etc.) ambient level was sufficiently low.

Figure 4-5 shows the placement of F-4 model in the hangar.



Figure 4-5 Scaled F-4 model, placed on wooden masts in hangar (side view)

#### **4.5. Measurement Setup & Procedure**

During construction of the model, ten antennas were assembled over the fuselage. Position of seven antennas out of ten was adopted from exact locations of different types of antennas mounted on a real F-4 aircraft. Remaining three antennas were placed on reasonable empty regions over the fuselage. After doing some preliminary return loss measurement on each antenna, some of them were cancelled due to unexpected impedance behavior; and some were omitted in order to eliminate ground reflections. Unexpected impedance was deemed to happen because of mechanical imperfections like antenna ground solder or bonding of copper sheets in close proximity of that antenna. Finally, six out of ten antennas

were selected and included in the study. These antennas are marked and shown in Figure 4-6.

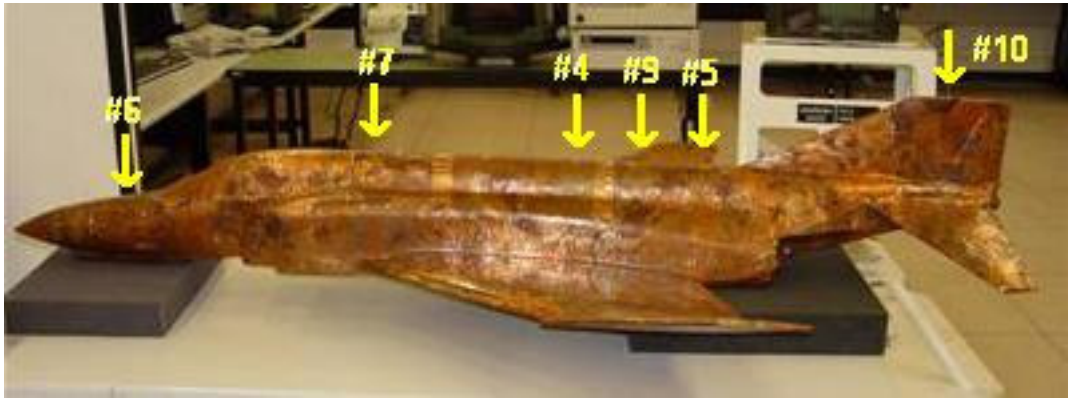


Figure 4-6 Antennas involved in S-parameter measurements

The content of measurements was derived from simulation studies and exactly same antennas were enrolled in measurements. Similarly, three antennas (namely #6, #7 and #10) were assigned as “existing” antennas. A fourth “new” antenna was added on the platform, which was assumed to be likely to interfere with existing antennas. For the newly installed antenna, three different placement positions (#4, #5 and #9, respectively) on top of fuselage were assumed. Thus, this study covered impedance measurements of each individual antenna, along with comparison of interactions between existing antennas and new antenna for its three different positions. To sum up, the measurements done are listed as follows:

- $S_{66}$ ,  $S_{77}$  and  $S_{1010}$  (return losses of existing antennas)
- $S_{44}$ ,  $S_{55}$  and  $S_{99}$  (return loss of new antenna at three different positions)
- All coupling values between new antenna and existing antennas, for three different positions of new antenna.

Measurement setup consists of a spectrum analyzer with an internal tracking generator. Main specifications of this measurement device are listed in Table 4-2.

Table 4-2 Main features of measurement equipment [22]

Brand name	Rohde&Schwarz™ FSH3
Definition	Handheld spectrum analyzer with internal preamplifier and tracking generator
Accessories	1-port VSWR bridge
	Open/short/load terminations
Measurement modes	1-port vector reflection measurement
	2-port vector transmission measurement
Frequency range	10 MHz - 3 GHz

## 4.6. Measurement Results

### 4.6.1. Return Loss Measurements

Return loss of each antenna was measured within 0,3-3 GHz band. 3-meter-long, low loss, high quality coaxial cables were used to connect the analyzer to the model. The analyzer with tracking generator and 1-port return loss measurement kit operates as a vector network analyzer; therefore, before measurements, an open/short and load calibration with VSWR Bridge was performed.

Masking effect of cable loss causes errors at return loss measurements of the system connected to cable with considerable loss [23]. As cable loss increases, return loss is measured to be lower than its actual value and antenna performance seems much better. This error is corrected with the following equation:

$$RL(antenna) = RL(measured) - 2 * L_{cable} \quad (4.1)$$

where,  $RL(antenna)$ : Actual return loss of antenna (dB)

$RL(measured)$ : Return loss measured by the equipment (dB)

$L_{cable}$ : Loss of cable connecting antenna to measurement equipment (dB)

Return loss measurements for both “existing” and “new” antennas were tabulated in following figures, below. For easy comparison, simulation results were also given on same plots. Since there is 1:10 ratio between frequency band of simulations and measurements, frequencies of simulation results were up-scaled by factor of 10.

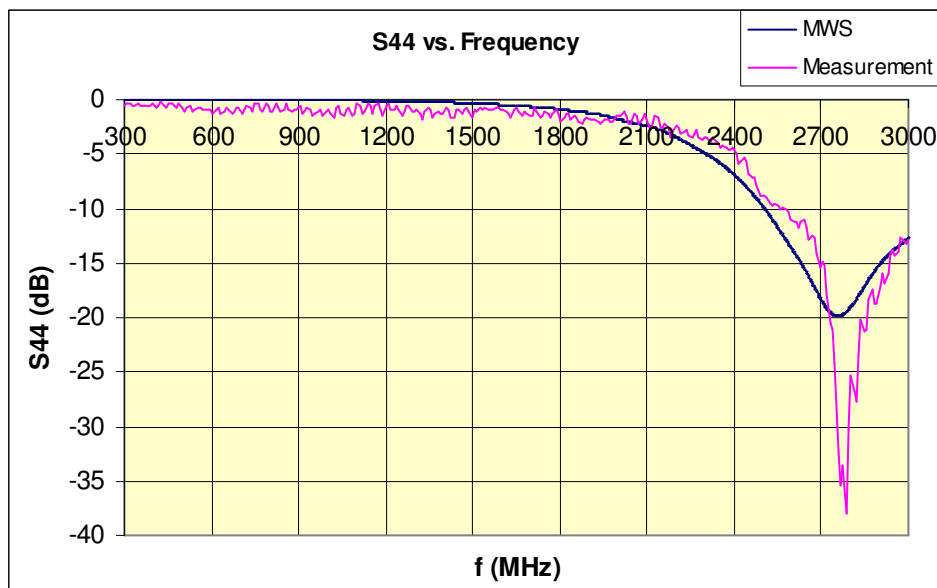


Figure 4-7 Return loss (dB) vs. frequency (MHz) for antenna #4

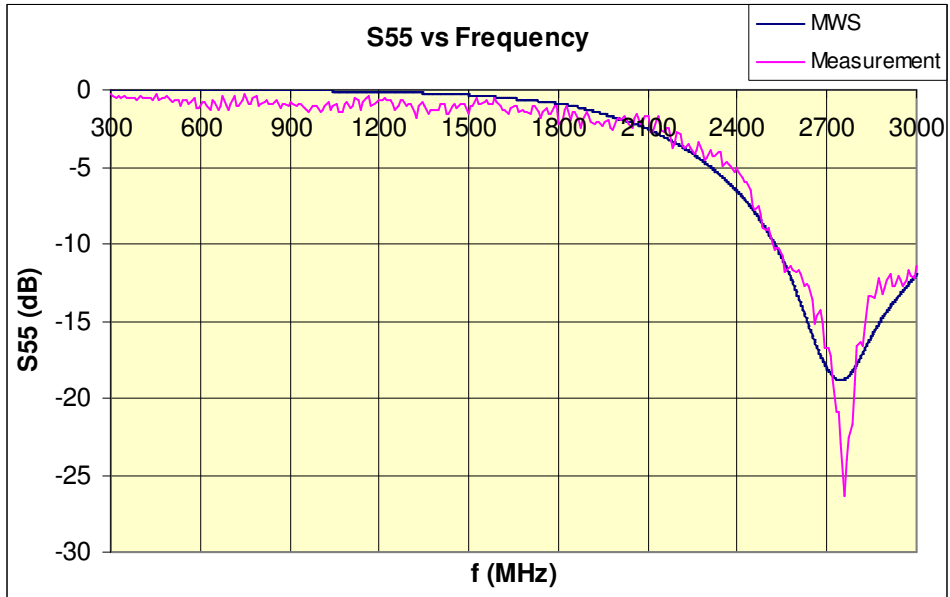


Figure 4-8 Return loss (dB) vs. frequency (MHz) for antenna #5

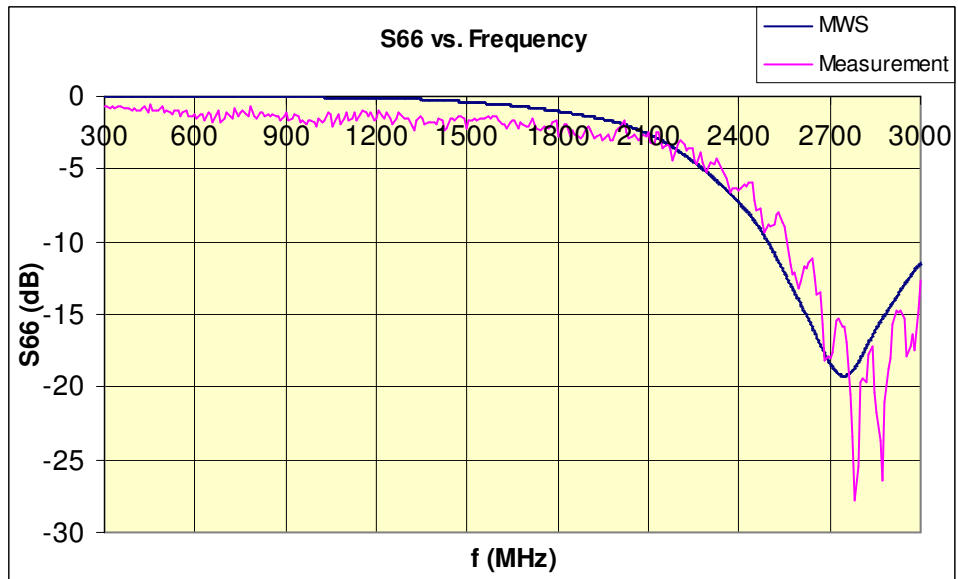


Figure 4-9 Return loss (dB) vs. frequency (MHz) for antenna #6

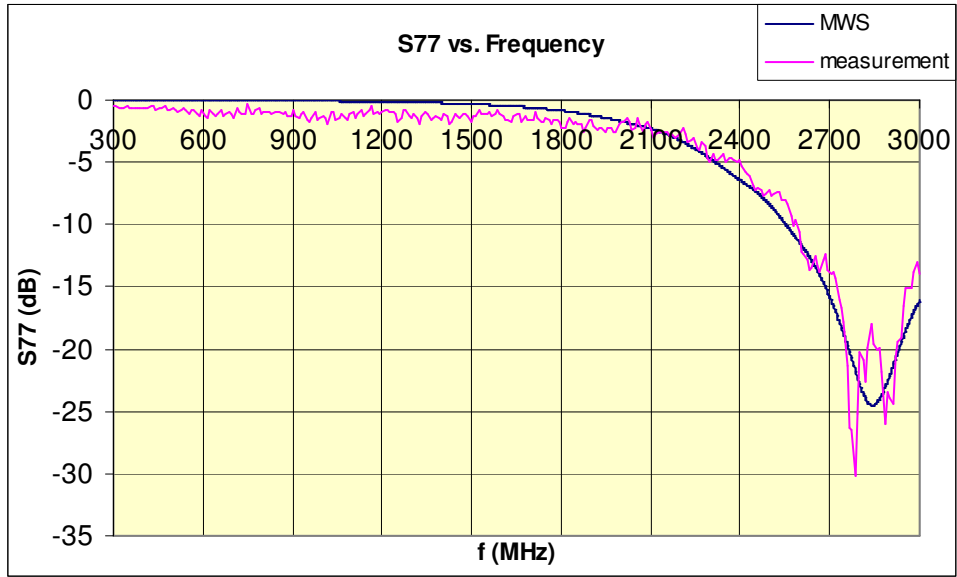


Figure 4-10 Return loss (dB) vs. frequency (MHz) for antenna #7

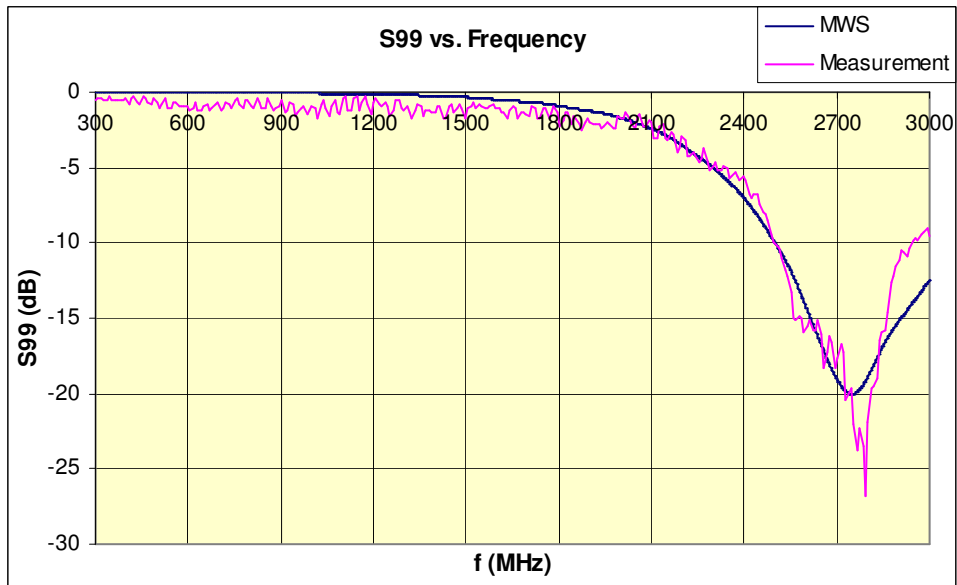


Figure 4-11 Return loss (dB) vs. frequency (MHz) for antenna #9

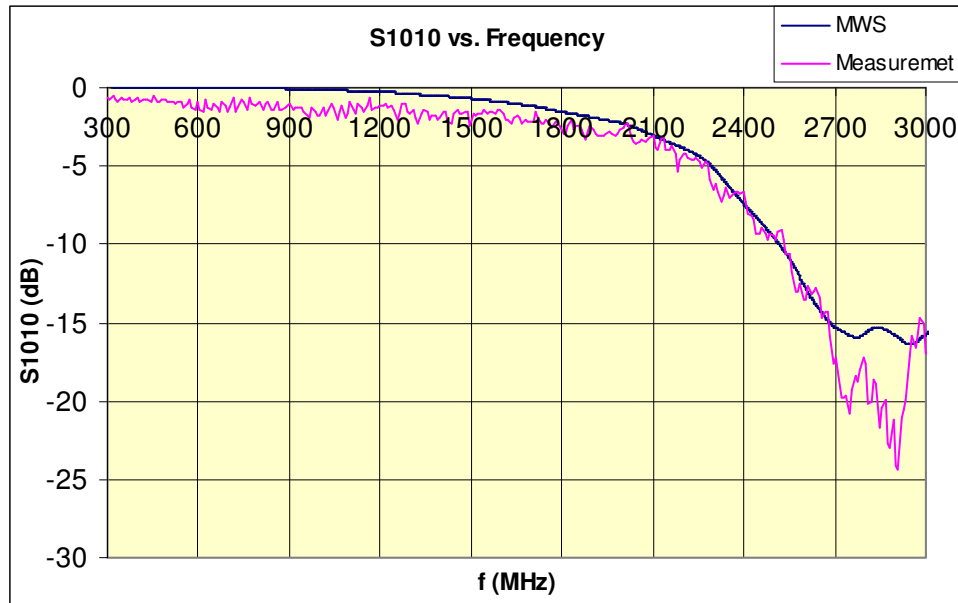


Figure 4-12 Return loss (dB) vs. frequency (MHz) for antenna #10

#### 4.6.2. Transmission Loss (Coupling) Measurements

After measuring return losses of each antenna, antenna-to-antenna coupling levels were measured with spectrum analyzer and its built-in tracking generator. Similarly, in 0,3-3 GHz band, 2-port vector transmission calibration was done, using a “through” component and “load”. In order not to deal with calculation of cable losses, all cable losses were initially introduced within “through” calibration cycle. The RF output power of tracking generator was fixed at 0 dBm (1 mW). Dynamic range at vector transmission measurement mode is -80 dB between 10MHz and 2,2GHz, and -65 dB between 2,2-3 GHz [22]. Therefore, considering typical coupling values achieved within frequency band of interest, it was claimed that all coupling values down to -80 dB remain within measurable range of the analyzer.

Measurements were grouped as interactions between each “new” antenna with all other “existing” antennas, for three predefined positions of the new antenna. Therefore, three sets of measurements were done. Reciprocal measurements ( $S_{xy}$  -  $S_{yx}$ ) were omitted, i.e. all coupling values were measured one way only. The table below shows pairs of antennas to be measured:

Table 4-3 List of S-parameters to be measured

New antenna	Existing antennas	S-parameters to be measured
#4	#6, #7, #10	$S_{64}$ , $S_{74}$ , $S_{104}$
#5	#6, #7, #10	$S_{65}$ , $S_{75}$ , $S_{105}$
#9	#6, #7, #10	$S_{69}$ , $S_{79}$ , $S_{109}$

#### 4.6.2.1. Antenna #4 vs. Existing Antennas

The following plots show results of coupling values measured between antenna #4 and other existing antennas. Again for ease of comparison, simulation results are also given on same plots.

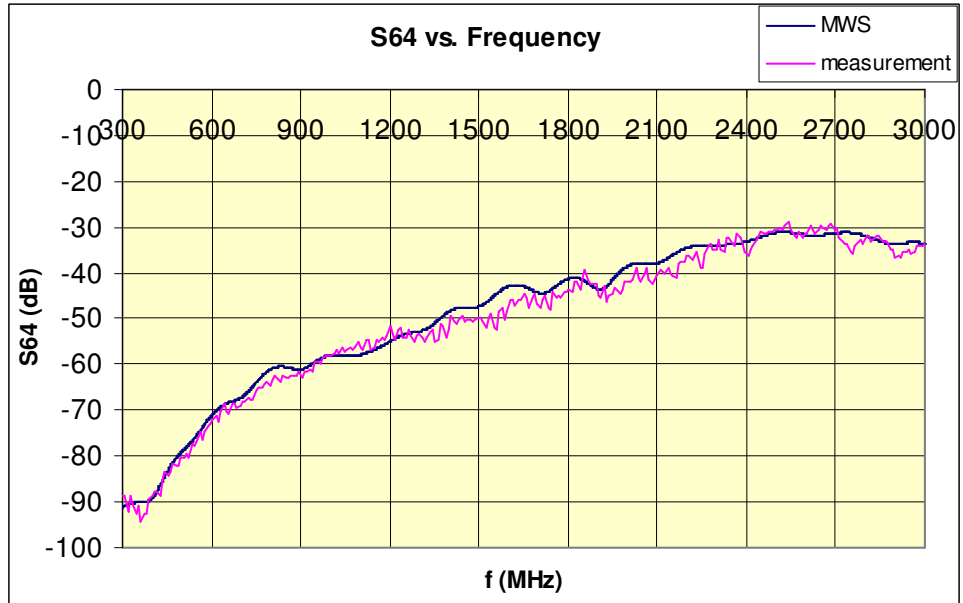


Figure 4-13  $S_{64}$  vs. Frequency

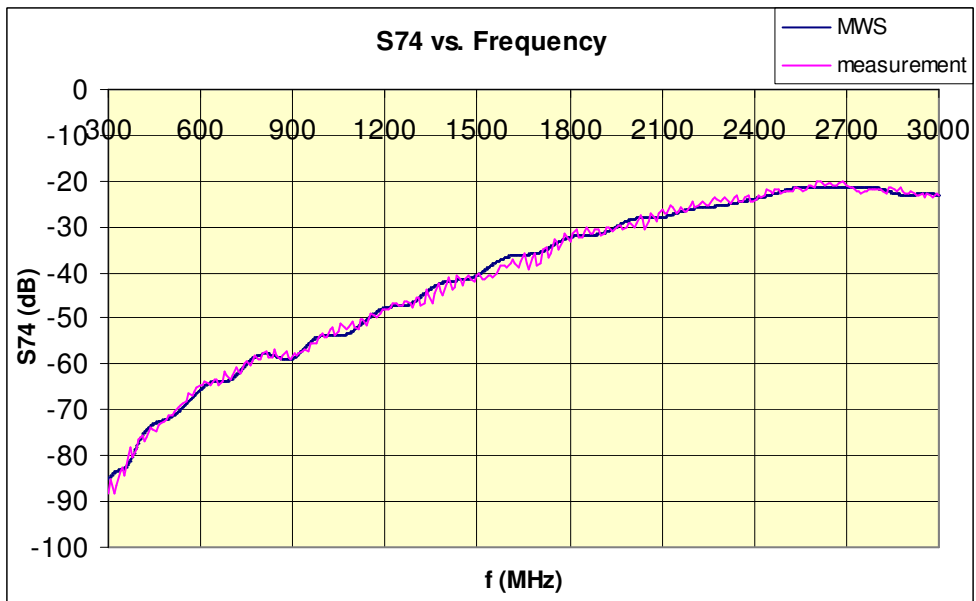


Figure 4-14  $S_{74}$  vs. Frequency

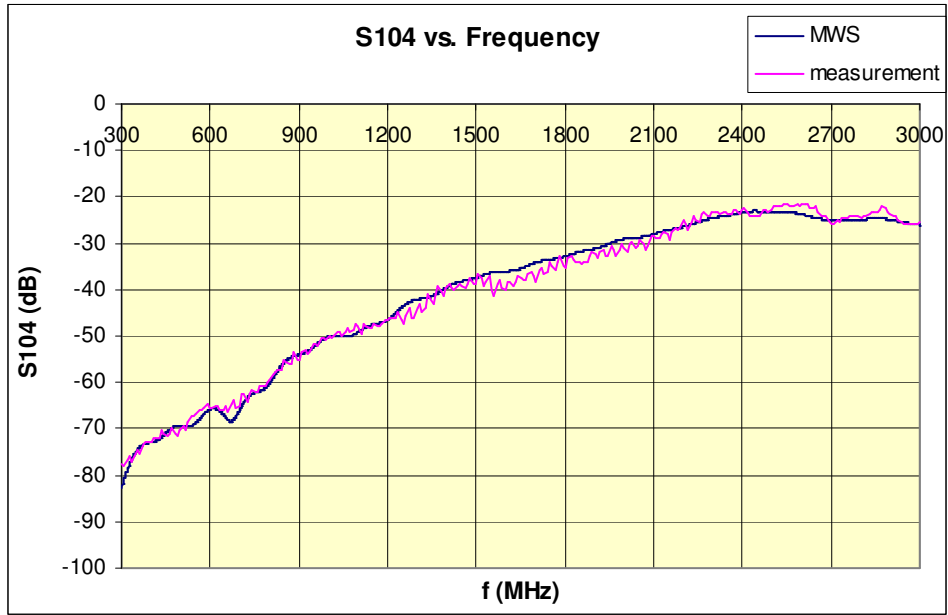


Figure 4-15  $S_{104}$  vs. Frequency

#### 4.6.2.2. Antenna #5 vs. Existing Antennas

The following plots show results of coupling values measured between antenna #5 and other existing antennas. Again for easy comparison, simulation results are also given on same plots.

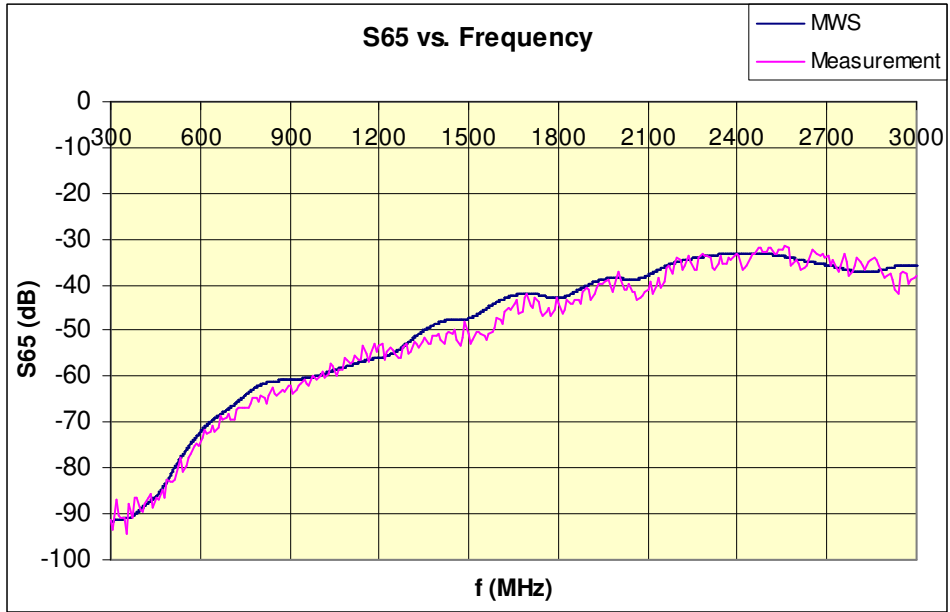


Figure 4-16  $S_{65}$  vs. Frequency

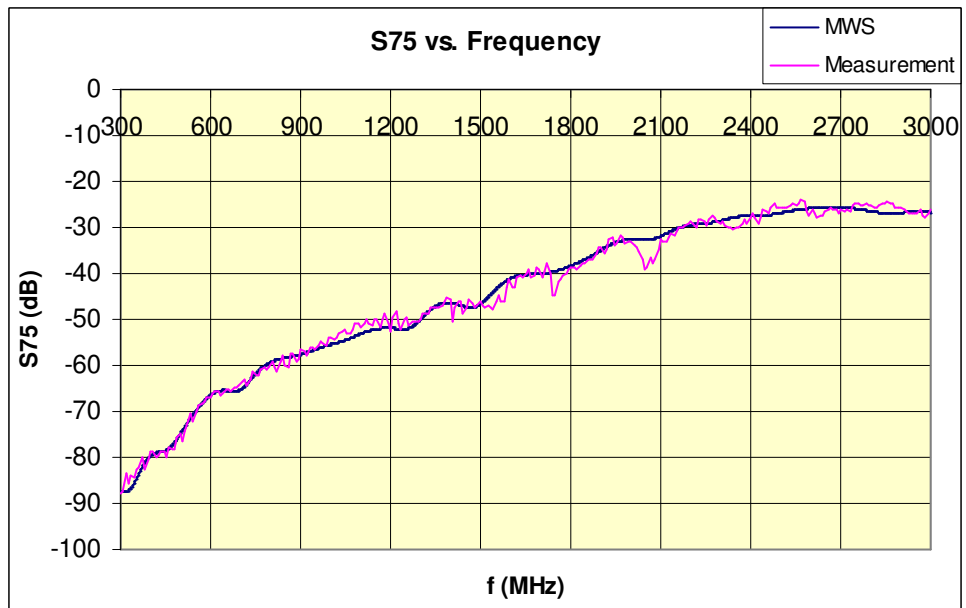


Figure 4-17  $S_{75}$  vs. Frequency

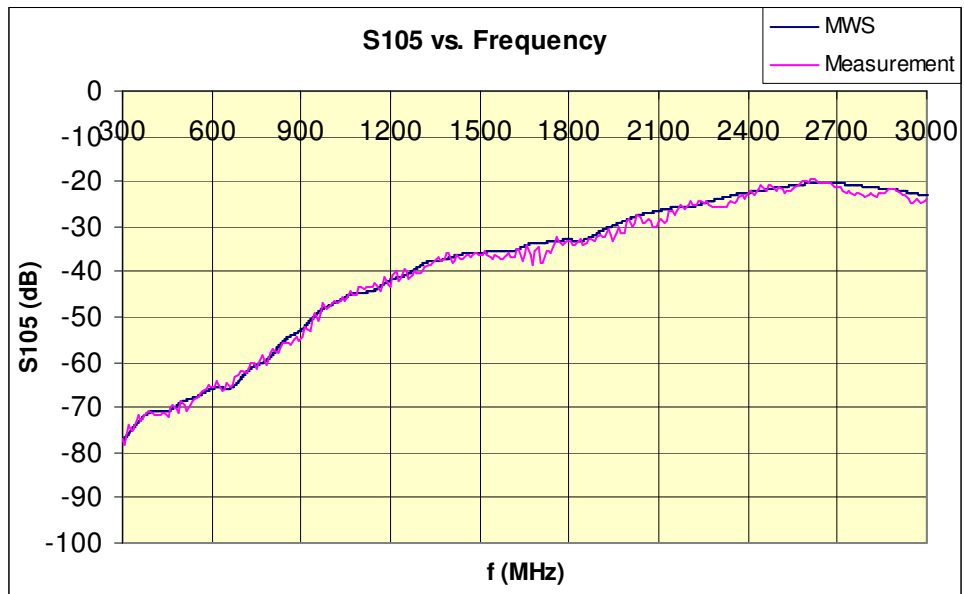


Figure 4-18  $S_{105}$  vs. Frequency

#### 4.6.2.3. Antenna #9 vs. Existing Antennas

The following plots show results of coupling values measured between antenna #9 and other existing antennas. Again for easy comparison, simulation results are also given on same plots.

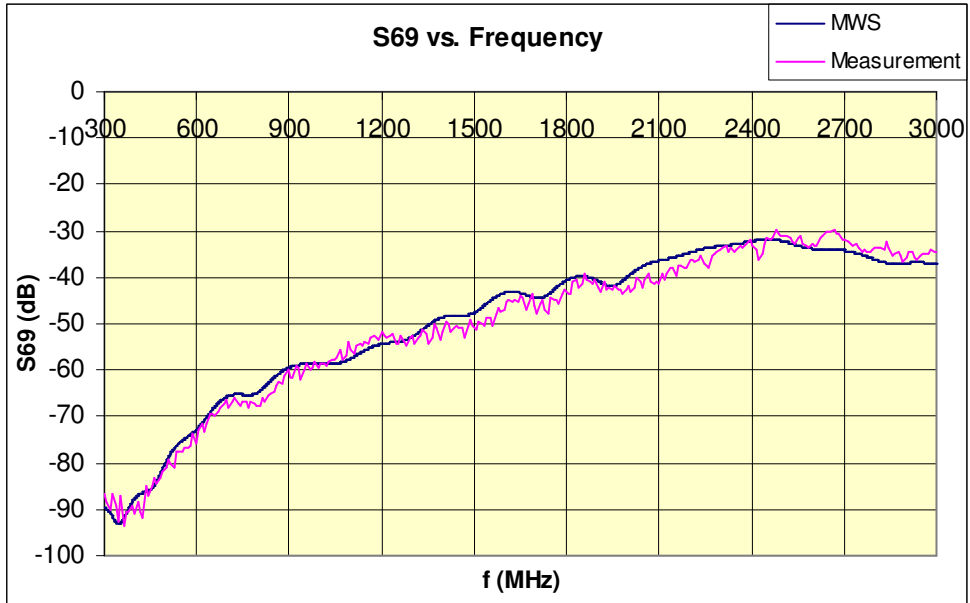


Figure 4-19  $S_{69}$  vs. Frequency

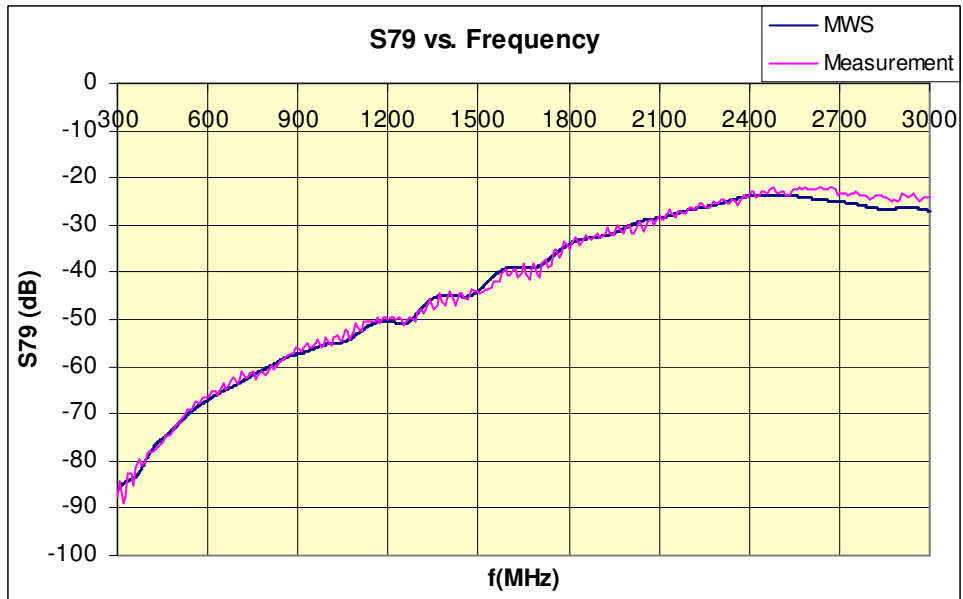


Figure 4-20  $S_{79}$  vs. Frequency

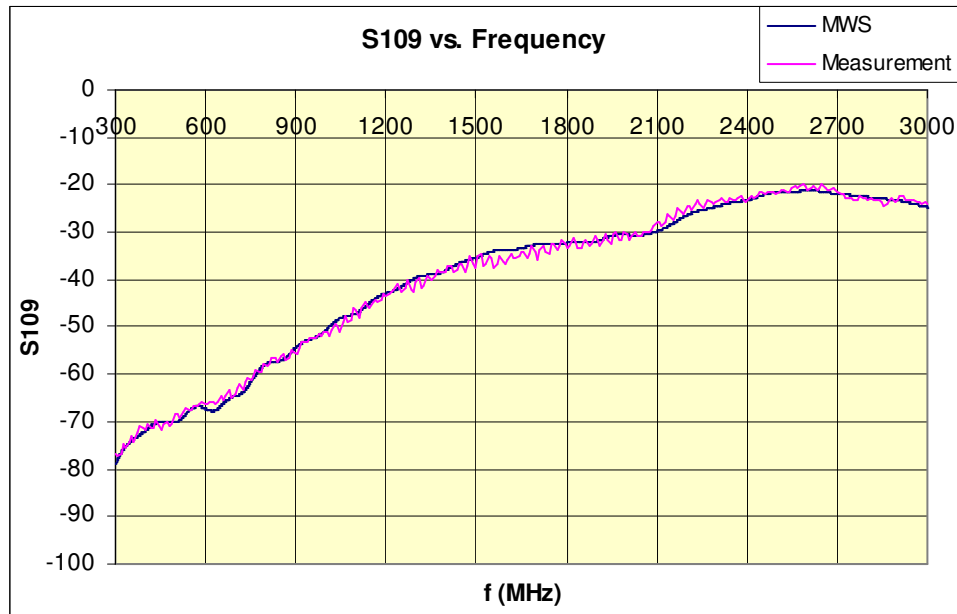


Figure 4-21  $S_{109}$  vs. Frequency

#### 4.6.3. Comparison of Antenna-to-Antenna Interactions for Different Positions of “New” Antenna

In this subsection of the thesis, antenna-to-antenna coupling values for three different positions (named as #4, #5 and #9) of the “newly installed” antenna were investigated. Antenna-to-antenna interaction between each one of existing antennas and “new” antenna for three alternative placement positions were compared. For all of these cases, simulation and measurement results were tabulated separately. Hence, three different cases of coupling comparison were done via using measurement and simulation results, respectively. Six different interaction scenarios were listed as follows;

- Coupling between existing antenna #6 and new antenna, placed at positions #4, #5 and #9 (simulation & measurement)

- Coupling between existing antenna #7 and new antenna, placed at positions #4, #5 and #9 (simulation & measurement)
- Coupling between existing antenna #10 and new antenna, placed at positions #4, #5 and #9 (simulation & measurement)

While comparing the results measured for all six cases, coupling values were investigated within frequency band of 2,4-3 GHz only. The frequency band was narrowed down due to the fact that, these monopole antennas are well-matched only at frequencies where their electrical length varies around (but slightly shorter than) quarter wavelength. Therefore, for the anticipated frequency band of 2,4 to 3 GHz, all monopoles have electrical length of  $0,2\lambda$  to  $0,25\lambda$ . Return loss measurement and simulation results also show that, within this frequency band, all monopoles have return loss values of at least -6 dB within 2,4-2,7 GHz, and that of at least -12 dB within 2,7-3 GHz. Investigating coupling values within a narrower frequency band also helps to more easily compare coupling values obtained for three different antenna positions. Coupling comparisons of both simulation and measurement results are given in the following figures.

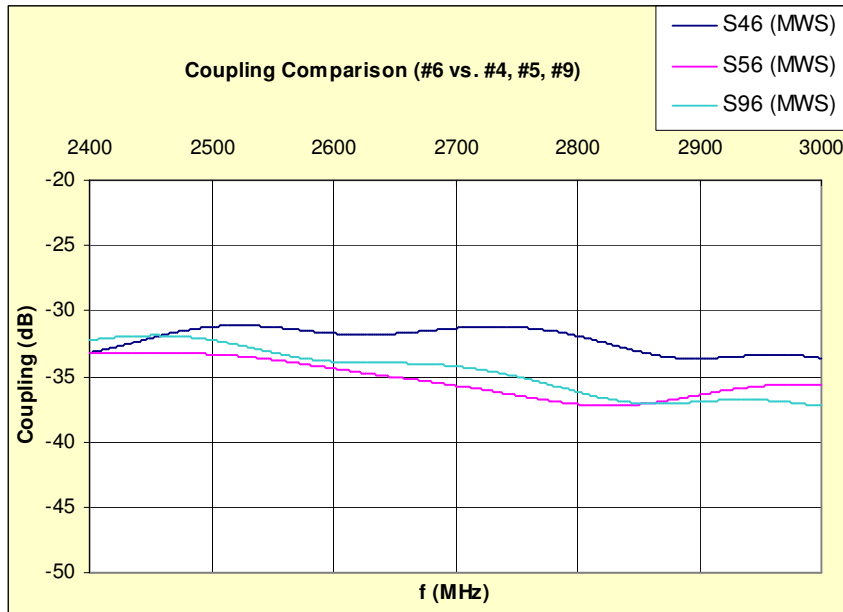


Figure 4-22 Comparison of coupling values between “antenna #6” and “new” antenna, for three different positions – simulation

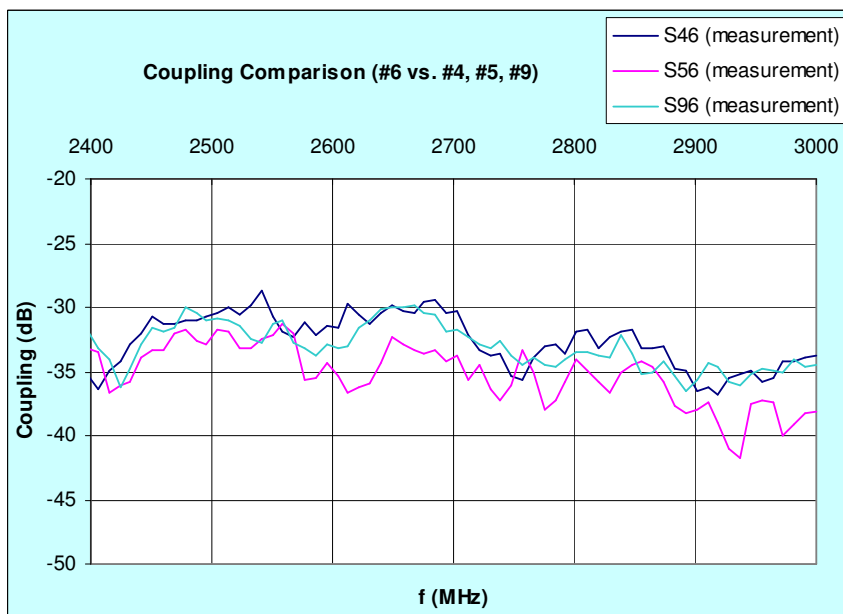


Figure 4-23 Comparison of coupling values between “antenna #6” and “new” antenna, for three different positions – measurement

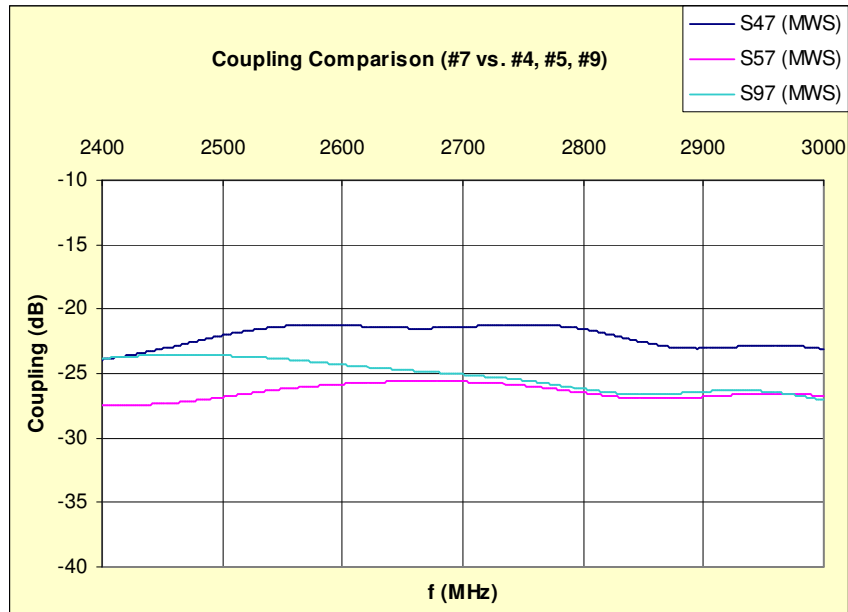


Figure 4-24 Comparison of coupling values between “antenna #7” and “new” antenna, for three different positions – simulation

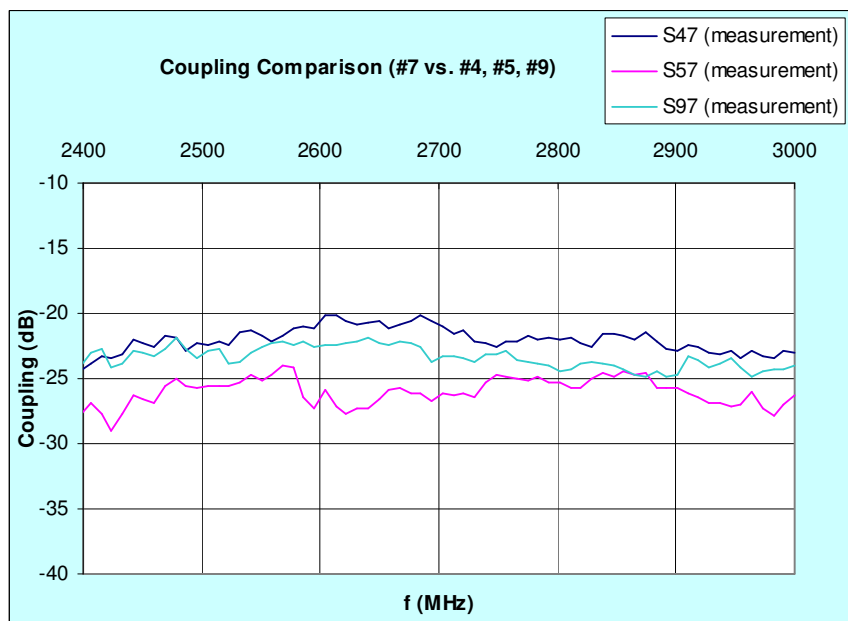


Figure 4-25 Comparison of coupling values between “antenna #7” and “new” antenna, for three different positions – measurement

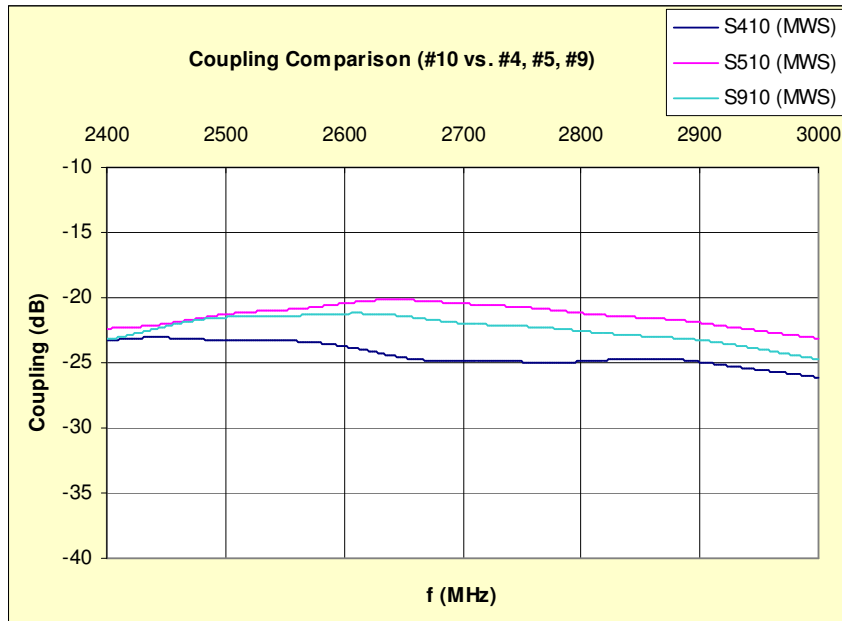


Figure 4-26 Comparison of coupling values between “antenna #10” and “new” antenna, for three different positions – simulation

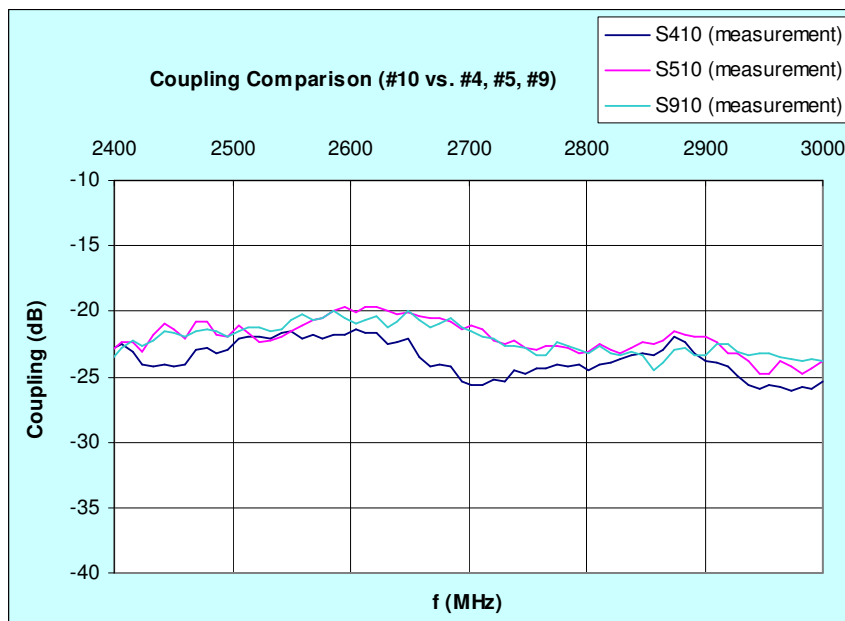


Figure 4-27 Comparison of coupling values between “antenna #10” and “new” antenna, for three different positions – measurement

#### 4.6.4. Interpretation of Results

The outcome of scale model measurements and simulations are listed, below:

- For some antennas, return loss measurement results have strong ripples around frequencies where return loss has its minimum value. These ripples occur because of mechanical imperfections of feed section, monopole itself and roughness of aircraft's surface. However, the overall return loss pattern well agrees with simulation results. In simulation, none of those imperfections are present; therefore the return loss plots are quite smooth and regular.
- For three different antenna positions (#4, #5 and #9) of new antenna, measurement and simulation results of coupling with existing antennas are in very good agreement. Ripples existing on coupling measurement traces are due to mechanical imperfections, plus sample detection feature of measuring device, which is used in transmission loss measurement mode. Also, it was concluded that any defect on contacts of copper sheets would deteriorate ground currents, thus yield ripples on coupling and return loss results, as well.
- Considering the interaction between "new" antenna and "existing" antennas #6 and #7, both for simulation and measurement results, it was observed that, as the distance between two antennas increase, coupling decreases gradually, almost all over the frequency band of interest (2,4-3 GHz). Within the frequency band of interest, physical separation between "new" antenna for its three positions and antenna #6 is approximately  $8\lambda$ ; and that of antenna #7 is approximately  $4\lambda$ . The gradual decay of coupling as the "new" antenna gets apart from any of antennas #6 and #7 indicates that, the fuselage acts as a "regular" ground plane (in sense of its dimensions and smoothness).

- Considering the interaction between “new” antenna and “existing” antenna #10, a slight different coupling pattern is observed as compared to the case in previous item. Here, antenna #10 and “new” antenna at its any position are not in line of sight, on the same plane. On the contrary, they are positioned in echelon. Therefore, coupling values are not strictly inversely proportional to separation between antennas. Both simulation and measurement results show that, within frequency band of interest, level of signals coupled from antenna #10 to “new” antenna when located at positions #5 and #9 are close to each other. On the other hand, signals coupled to new antenna when located at position #4 are smaller in magnitude, as compared to the ones at positions #5 and #9. Therefore, it was deduced that, for monopoles, any of which are mounted on geometrically varying sections of fuselage, variation of coupling cannot directly be estimated by considering physical separation between antennas.
- Within 2,4-3 GHz band, the average difference of coupling between existing antennas and “new” antenna for three different positions are listed in table below, both for simulation and measurement results.

Table 4-4 Comparison of average coupling differences between simulation and measurement results in 2,4-3 GHz band

Existing Antenna	Avg. Coupling Differences	Simulation Result (dB)	Measurement Result (dB)	Mean difference   [sim.]-[meas.]   (dB)
Antenna #6	$S_{96} - S_{46}$	-2,5	-0,5	2
	$S_{96} - S_{56}$	0,6	2,2	1,4
	$S_{46} - S_{56}$	3,1	2,6	0,5
Antenna #7	$S_{97} - S_{47}$	-3,0	-1,4	1,6
	$S_{97} - S_{57}$	1,3	2,6	1,3
	$S_{47} - S_{57}$	4,3	4,0	0,3
Antenna #10	$S_{910} - S_{410}$	2,0	1,5	0,5
	$S_{910} - S_{510}$	-1,0	-0,2	0,8
	$S_{410} - S_{510}$	-3,0	-1,6	1,4
<b>Average (dB) =</b>				<b>1,1</b>

- It was observed that, while comparing coupling between existing antennas and new antenna at three positions, simulation and measurement results follow each other within an average difference of 1,1 dB (which was calculated from arithmetic averages of mean differences of simulation and measurement data, given in right-most column of Table 4-4).

## CHAPTER V

### CONCLUSION AND FUTURE WORK

The work presented in this thesis includes

- Brief information about using electromagnetic simulation tools for doing antenna analyses was given.
- Basic theory of Finite Integration Technique, the numerical method which MWS<sup>®</sup> uses, was introduced.
- An electromagnetic simulation tool, named CST Microwave Studio<sup>®</sup> was analyzed and verified by examining and applying previously done simulation and measurement studies which cover monopoles mounted on ground planes of finite size [8]. Due to accuracy considerations, minimum requirements of simulation settings were determined and used throughout subsequent simulations.
- Antenna-to-antenna coupling and radiation pattern analyses were done on an F-4 aircraft, both for simplified and exact geometrical models. Also accuracy and performance comparison between results of these two models were done.
- A 1:10 down-scaled F-4 model was constructed, its fuselage was plated with copper and the model was equipped with identical antennas which had been used at simulations.
- Brief information about scale model antenna measurements was given. Principles of scaling certain electrical properties of model were also discussed.

- Identical to simulations, antenna-to-antenna coupling measurements were done on the scale model. Results obtained from simulations and measurements were compared and the validity of simulation results was investigated.
- Finally, a good agreement of antenna-to-antenna coupling values between measurement and simulation results was observed.

Future studies which can be done within this concept are listed as follows:

- Using the same scale model, a similar antenna analysis with different monopole lengths, tuned to different frequencies can be done. Variation of antenna-to-antenna coupling for different antenna lengths can be observed.
- This thesis covers antenna measurements which operate in VHF band (30-300 MHz). Similarly, studies covering HF band (3-30 MHz) antennas can be done. Since these antennas operate at lower frequencies, the electrical length of aircraft would be comparable to wavelength, and shape of fuselage would be much more effective on impedance and radiation characteristics.
- For varying antenna positions and dimensions, radiation pattern measurements can be done with the scale model, and be compared with simulation results.
- By omitting antennas on the scale model and improving surface roughness, radar cross section measurements can be done.

## REFERENCES

- [1] M. J. Sidford, "Influences of the Airframe on the Performance of Antennas for Avionics", AGARD Lecture Series, No.131, pp. 6-1, 1983.
- [2] T. Weiland, "A Discretization Method for the Solution of Maxwell's Equations for Six-Component Fields", *Electronics and Communication*, Vol.31, pp.116-120, 1977.
- [3] M.Clemens and T.Weiland, "Discrete Electromagnetism with The Finite Integration Technique", *Progress In Electromagnetics Research*, PIER 32, 65-87, 2001
- [4] R. Marklein, "The Finite Integration Technique as a General Tool to Compute Acoustic, Electromagnetic, Elastodynamic, and Coupled Wave Fields", p.209, University of Kassel, Germany
- [5] R. Courant, K. Friedrichs, and H. Lewy, "Über die partiellen Differenzgleichungen der mathematischen Physik," *Mathematische Annalen*, 100, pp. 32-74, 1928
- [6] CST Studio Suite™ 2006, "Getting Started Tutorial, Choose the Right Port", pp.119-120, 2005
- [7] CST Studio Suite™ 2006, "Advanced Topics Tutorial, Performance Improvements", pp. 49-54, 2005
- [8] Melvin M.Weiner, "Monopole Element at the Center of a Circular Ground Plane Whose Radius is Small or Comparable to a Wavelength", *IEEE Transactions on Antennas and Propagation*, Vol.AP-35, no.5, May 1987.
- [9] R.W.P. King, "Theory of Linear Antennas", Harvard University Press, fig.30.7a, 1956.
- [10] CST Studio Suite™ 2006, "Antenna Tutorial", pp.115-163, 2005
- [11] E.Hallen, "Theoretical Investigations into the Transmitting and Receiving Qualities of Antennae", *Nova Acta Regiae Soc. Sci. Upsaliensis*, Ser. IV, No.4, 1-44, 1938

- [12] J.D. Kraus, "Antennas", McGraw-Hill, 2<sup>nd</sup> Edition, pp 379, 1988.
- [13] CST Studio Suite™ 2006, "Getting Started", Discrete Ports, pp 122, 2005
- [14] E. Hallén, "Admittance Diagrams for Antennas and the Relation between Antenna Theories", Cruft Laboratory Tech. Rept. 46, Harvard University, 1948
- [15] A. Dorne, "Very High Frequency Techniques" Radio Research Laboratory Staff, McGraw-Hill, chapter 4, New York, 1947
- [16] G. Sinclair, "Theory of Models of Electromagnetic Systems, Proc. IRE, 36, 1948, p.1364.
- [17] E. Joy, Lecture Notes on "Far-Field, Anechoic Chamber, Compact and Near-Field Antenna Measurements", Georgia Institute of Technology, Chapter 2, 2007
- [18] J.S. Belrose, "Scale Modeling and Full Scale Measurement Techniques with Particular Reference to Antennas in their Operational Environments", AGARD Lecture Series No.131, pp.2-1, 1983.
- [19] Environment Chemistry,  
["http://www.environmentchemistry.com/yogi/periodic/electrical.html/"](http://www.environmentchemistry.com/yogi/periodic/electrical.html/),  
 date of last access: 22.11.2007.
- [20] D.L. Moffat & J.R. Puskar, "A Subsurface Electromagnetic Pulse Radar", Geophysics, vol.41, pp 506-518, June 1976.
- [21] M. J. Sidford, "Influences of the Airframe on the Performance of Antennas for Avionics", AGARD Lecture Series, No.131, pp. 6-4, 1983.
- [22] Rohde & Schwarz GmbH, "R&S™ FSH Handheld Spectrum Analyzer Datasheet", 4<sup>th</sup> edition, pp.11-21, March 2007.
- [23] J. Norton, "Masking Effect of Cable Loss on Antenna VSWR and Return Loss Measurements, Application Note", Bird Technologies Group, pp.1-5.